UNIVERSIDAD DE VALLADOLID

ESCUELA DE INGENIERIAS INDUSTRIALES

Grado en Ingeniería Mecánica

# Hydrogen safety

Autor:

Sánchez Gallardo, Javier

Responsable de Intercambio en la UVa
María Ángeles Pérez Rueda

University of South-Eastern Norway

Valladolid, junio 2020.

TFG REALIZADO EN PROGRAMA DE INTERCAMBIO

TÍTULO:      Hydrogen safety

ALUMNO:      Javier Sánchez Gallardo

FECHA:       28 de mayo de 2020

CENTRO:      University of South-Eastern Norway

TUTOR:       André Vagner Gaathaug

# Resumen

Este estudio tiene dos objetivos principales que se pueden dividir de la siguiente manera.

En primer lugar, la planificación y construcción de un sistema de llenado de hidrogeno a alta presión, donde, además se realizan simulaciones de la perdida de presión del sistema y de las condiciones en el interior del tanque durante el proceso de purga y llenado del mismo.

Por otro lado, se procederá a estudiar la integridad estructural de un espacio cerrado cuando sucede una fuga inesperada de hidrogeno, procedente de un tanque a alta presión. Para ello se diseñan dos tipos diferentes de garajes usando el software Solidworks. Las sobrepresiones que se producen cuando esta fuga sucede han sido calculadas mediante simulaciones en MATLAB. Combinando los resultados obtenidos en MATLAB con el diseño en Solidworks, se puede obtener resultados de cómo afecta la sobrepresión a la estructura del garaje.
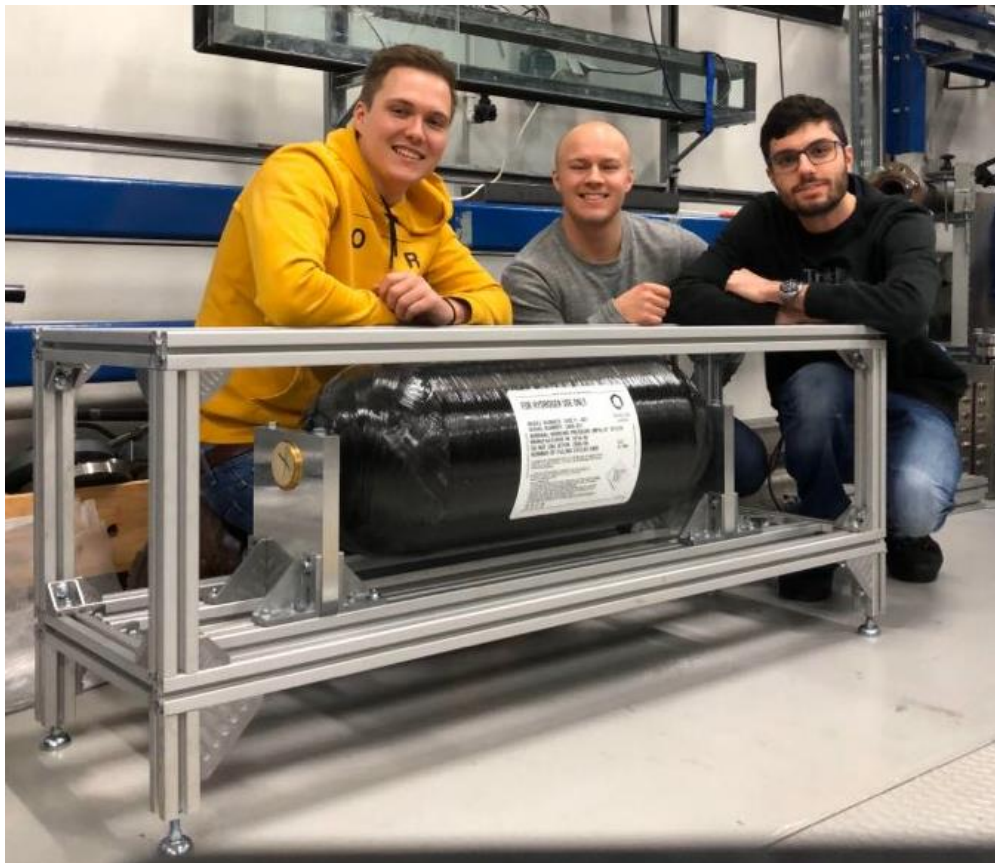
# Palabras clave

Hidrogeno, seguridad, fuga, sobrepresión, garaje.

# University of South-Eastern Norway

PRH612-1 20V Bachelor thesis

# Hydrogen safety

MA-07-2020



# Faculty of Technology, Natural Sciences and Maritime Sciences
Campus Porsgrunn

www.usn.no

# University of
# South-Eastern Norway

**Course**:     PRH612-Bachelor thesis, 2020
**Title**:     Hydrogen safety

This report forms part of the basis for assessing the student's performance in the course.

**Project group:** MA-07-2020          **Availability:** Open

**Group participants:**          Nils Jørgen Aavik

Magnus Egerdahl

Javier Sánchez Gallardo

**Supervisor:**          André Vagner Gaathaug

**Project partner:**          **HyTunnel-CS**

**Approved for archiving:**          _____

(supervisor signature)

**Summary:**

This report is the final bachelors project for the mechanical engineering degree at USN Porsgrunn.

Due to the corona situation the project will be referred to as two parts in the summary for clarity.

Part one: This part is about the planning and construction of a high-pressure hydrogen filling system. This system will later be used in experiments studying the pressure peaking phenomenon. Due to the corona virus the filling system could not be finished. Part one also includes the mathematical approach used to calculate the pressure loss in the system as well as the number of purges needed to store hydrogen safely in the tank.

Part two: The aim of part two is to investigate the structural integrity of a garage enclosure when an unscheduled release occurs. The enclosure is made of leca and wood respectively. This is done by simulating the garages in Solidworks. The overpressures used are made in a MATLAB simulation. Furthermore, the report investigates the relationship between the vent size and TPRD diameter. In order to store hydrogen vehicles safely inside an enclosure, sufficient venting and small enough TPRD diameter is important. The results from the Solidworks- and MATLAB simulations are presented in the report.

# Preface

Due to the ongoing situation with the Corona virus the thesis has changed somewhat during the semester. The original plan was to make a hydrogen filling system and participate in experiments on the pressure peaking phenomenon using this system. This has not been feasible due to the shutdown of the school, the given restrictions on gatherings of people and the 1-meter distance rule. Therefore, the bachelor thesis had to change. The focus was shifted towards structural analysis of a garage enclosure during a release of hydrogen.

Because some of the work towards construction and operating a hydrogen filling system was done before the Corona situation the report may seem "divided". Some work was already been done, and some was ongoing when the lockdown was a fact. The work that was ongoing has been finished and everything done prior to the lockdown is included in the report. Hopefully this will make the report easier to understand.

This bachelor thesis partakes in the Horizon 2020 project financed by the HyTunnel project group and is a part of the mechanical engineer bachelor's degree at USN Porsgrunn. This bachelor's degree awards 20 study points. The work has been done between January 12 and May 19.

We would like to direct a thank you to our supervisor André Vagner Gaathaug for many helpful conversations during this project. We would also like to thank Magne Bratland and Mladen Jecmenica for help and guidance. Agnieszka Lach has provided us with helpful literature during the semester, which has been very useful.

Finally, we would like to thank Geir Egil Aavik for proof reading the report.

Porsgrunn, 12/05/2020

# Nomenclature

| | |
|---|---|
| $a_f$ | heat transfer coefficient between nitrogen and ambient fluid, W/m$^2$/K |
| $A$ | inlet area, m$^2$ |
| $A_s$ | internal surface area of tank, m$^2$ |
| $ASTM$ | American society for testing and materials |
| $BOM$ | Bill of materials |
| $c_p$ | constant-pressure specific heat, J/kg/K |
| $c_v$ | constant-volume specific heat, J/kg/K |
| $c_w$ | constant-tank wall specific heat, J/kg/K |
| $g$ | gravity acceleration, m/s$^2$ |
| $h_{in}$ | specific enthalpy of nitrogen, J/kg |
| $h_i$ | heat transfer coefficient inside the tank, W/(m$^2$K) |
| $h_o$ | heat transfer coefficient outside the tank, W/(m$^2$K) |
| $k$ | Thermal conductivity coefficient, W/(m K) |
| $LFL$ | Lower flammability limit |
| $LOC$ | Limiting oxygen concentration |
| $m$ | mass of nitrogen inside the tank, kg |
| $m_0$ | initial nitrogen mass, kg |
| $m_n$ | actual nitrogen mass in the tank, kg |
| $m_{n-1}$ | previous step nitrogen mass. kg |
| $m_w$ | tank wall mass, kg |
| $\dot{m}_{in}$ | inlet mass flow, kg/s |
| $\dot{n}$ | Molar flow rate, mol/s |
| $P$ | general properties |
| $Pa$ | Pascal, N/m$^2$ |
| $P_{amb}$ | ambient pressure, bar |
| $ppm$ | Parts per million |
| $p_{in}$ | inlet pressure, MPa |
| $p_n$ | actual pressure in tank, MPa |
| $p_{n-1}$ | previous step pressure in tank, MPa |
| $\dot{Q}$ | heat inflow rate, $\dot{Q} = a_f A_s (T_f - T)$ |

| | |
|---|---|
| $R$ | nitrogen gas constant, J/kg/K |
| $t$ | time variable, s |
| $t^*$ | characteristic time, $t^* = m_0/\dot{m}$, s |
| $T$ | temperature of the nitrogen in tank, K |
| $T_{in}$ | inflow temperature, K |
| $T_{amb}$ | temperature of ambient fluid, K |
| $T_{n-1}$ | previous step temperature of the nitrogen in tank, K |
| $T_w$ | temperature of tank wall, K |
| $T_{w0}$ | initial temperature of tank wall, K |
| $TPRD$ | thermally activated pressure relief device |
| $u$ | specific internal energy inside the tank, J/kg |
| $u_1$ | specific internal energy of the inflow, J/kg |
| $v$ | nitrogen speed inside tank, m/s |
| $v_1$ | inflow speed, m/s |
| $V$ | tank volume, m$^3$ |
| $\dot{W}$ | work applied inside the tank, J |
| $z$ | height variation of the fluid inside the tank, m |
| $z_1$ | height variation of the inlet, m |
| $\Delta t$ | time step, s |
| $\alpha$ | dimensionless heat transfer coefficient, $\alpha = \dfrac{a_f A_s}{C_v \dot{m}}$ |
| $\beta$ | thermal expansion coefficient of air, K$^{-1}$ |
| $\gamma$ | ratio of specific heats, $\gamma = \dfrac{C_p}{C_v}$ |
| $\mu$ | fraction of initial mass over total mass of nitrogen, $\mu = m_0/m$ |
| $\rho$ | density inside the tank, kg/m$^3$ |
| $\rho_1$ | inflow density, kg/m$^3$ |
| $\nu$ | kinematic viscosity of air, m$^2$/s |
| $\tau$ | dimensionless time, $\tau = t/t^*$ |

# Contents

# 1 Introduction

The use of hydrogen fuel cells will be an important part of the green shift going forward. It is clear that a change from using fossil fuel to using greener alternatives is needed to battle climate change. Hydrogen can be used as a fuel for cars, trucks, ships or even planes, and there has been a commercial growth in these types of vehicles. Together with the increase of demand of use of hydrogen as a fuel, the need for safety standards regarding hydrogen storage increases. It's important to understand the potential hazards with indoor storage of hydrogen as it poses great risks of both structural damage and the loss of human lives, if an unscheduled release were to occur. In this report the release of hydrogen in a confined space will be investigated further.

The goal of this bachelor thesis is to present the hazards and risks associated with hydrogen operations. The structural integrity of residential garages is analysed in order to conclude a safe configuration. To attain these goals, the following objectives are addressed:

- Experiment design
- Purging and filling process
- MATLAB simulation
- Structural analysis

To purge the tank of oxygen before experimental use, the method described in ASTM G-124 has been used to calculate the number of purges needed. To compute the conditions inside the tank during hydrogen filling an overall heat transfer coefficient has been applied. Furthermore, an adiabatic source model has been utilized to calculate the pressure loss in the experiment. Moreover, a thermodynamic model to calculate the overpressures generated by the ignited and unignited release of hydrogen. The overpressures are then used in several Solidworks simulations to analyse the garage structures base on the finite element method.
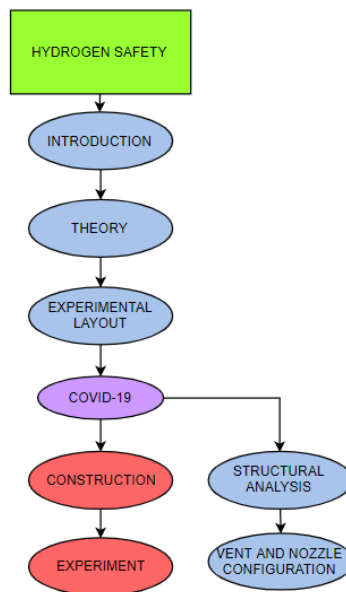


Figure 1 Report structure

## 1.1 Hydrogen properties

Hydrogen makes up 75% of the mass of all visible matter in the universe. Hydrogen consists of a central nucleus and a single orbiting electron. The proton has a positive charge and the electron has a negative charge, making the individual hydrogen atoms neutral. With a single electron orbiting the nucleus, individual hydrogen atoms become highly reactive, therefore atoms naturally combine into pairs of $H_2$. [1]

Hydrogen is a solid at -262°C with a density of 70.6 kg/m$^3$. In gas form hydrogen has a density of 0.0899 kg/m$^3$ at 0$^0$C and 1 bar making it the lightest gas on earth. [2] Hydrogen is environmentally friendly and is regenerative making it a perfect alternative for fuel cell technology. The most common way of hydrogen storage is under high pressure. Though this storage method comes with great risk if hazards are not validated correctly. Research states that at 25 MPa hydrogen has an expansion ratio of 240, capable of severe structural damage if released in a confined space. [1]

Overpressure in a garage from hydrogen release can be regulated using proper ventilation. With the low density of hydrogen, the gas rapidly mixes with ambient air and has great ability to flow out of release area. The great buoyancy helps lower concentrations below LFL quickly. The lower flammability limit of percent hydrogen in air is 4% and upper flammability limit is 75%. [3] With a minimum ignition energy of only 0.017 mJ, unignited hydrogen in a confined space with such a wide flammability limit can easily ignite. [4]

Another safety hazard regarding the wide flammability limit of hydrogen is during hydrogen filling. Filling with compressed hydrogen requires control of specified operating windows such as tank temperature, pressure, and fuel concentration. To ensure safe operating limits a tank must be purged to diminish oxygen before the filling can proceed. Gaseous behaviour during filling can be calculated using the following properties at 1bar of pressure and 20ºC temperature. [5] [6]:

Table 1 Thermal properties of hydrogen

| Thermal properties of hydrogen | |
| --- | --- |
| K (W/(k·m)) | 0,1815 |
| Cp (J/kg·K) | 14319,3 |
| γ | 1,405 |
| R (J/kg*K) | 4124,18 |
| Cv (J/kg·K) | 10191,9 |

The fact that hydrogen is odourless, colourless and tasteless makes hydrogen hard to detect if a hydrogen leak would occur. The compounds that usually give scent to natural gases such as thiophanes and mercaptans cannot be added to the hydrogen fuel, due to sulphur in the compounds poisoning the hydrogen. Hydrogen itself is not poisonous, but at high concentrations hydrogen acts as an asphyxiant due to displacement of oxygen causing hypoxia. [1]

## 1.2 Hydrogen safety

In all applications with hydrogen, safety is a main focus. Due to the explosive nature of hydrogen-air mixtures it is important to assess the hazards and risks, as well as to implement safety features. This thesis focuses mainly on hydrogen release in confined spaces, so this chapter will revolve around the hazards, risks and safety features related to this.

### 1.2.1 Main hazards

Unignited release of hydrogen in a confined space is an important part of the risk assessment. In a confined space, the release of hydrogen can lead to a build-up of a flammable hydrogen-air mixture, which in turn can cause major damage to structures and endanger human lives, if an ignition source is present. The release of hydrogen and the formation of such a flammable cloud depends highly on the confined space, the internal diameter of the pipe and how the space is ventilated. For this report the focus will mainly be unignited and ignited release in a garage enclosure.

### 1.2.2 Enclosed release

A main hazard for hydrogen release in an enclosure is the following overpressure if an ignition source is present. Due to the flammability limits of hydrogen (4-75% vol.), it is important to have good venting inside the enclosure. In a residential garage this will typically be a vent, whose size and the diameter of the TPRD (thermally activated pressure relief device) on the vessel are two of the most important factors considering the release of hydrogen at a given pressure.

Numerous studies over the last years has been conducted to investigate hydrogen release in an enclosure. Hussein et al. [7] considered the ignited release of hydrogen from a 700-bar tank fitted with (TPRD) in terms of numerical simulations. In their study two volumes were considered; a laboratory enclosure and a real scale garage with a single vent. The volumes of the enclosures were 1 $m^3$ and 30,42 $m^3$ respectively. Multiple tests were carried out using different diameter of the TPRD and vent sizes. It is important to emphasise that this study focuses on the pressure peaking phenomenon with immediate ignition and non-premixed combustion.

Five scenarios are considered in the work from Hussein et al. Below is a table showing the different configurations;

Table 2 The 5 cases from Hussein et al. [7]

|  | Vent size | TPRD diameter |
|---|---|---|
| Case 1 | 0.35 x 0.55 m | 3.34 mm |
| Case 2 | 0.95 x 0.90 m | 3.34 mm |
| Case 3 | 0.65 x 0.90 m | 3.34 mm |
| Case 4 | 0.35 x 0.55 m | 2 mm |
| Case 5 | 0.05 x 0.25 m | 0.5 mm |

Figure 2 displays the overpressure vs time for case 1.
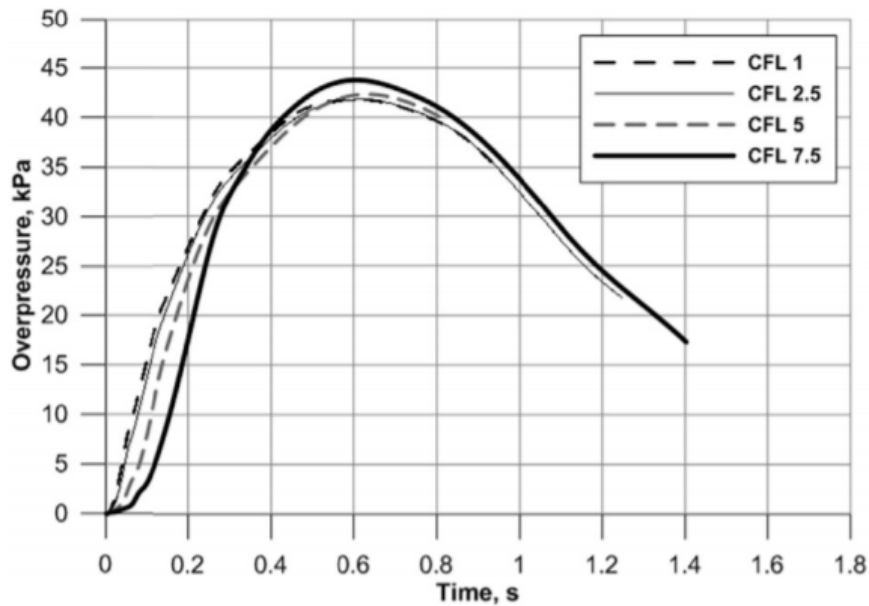


Figure 2 Overpressure versus time, case 1 [7]

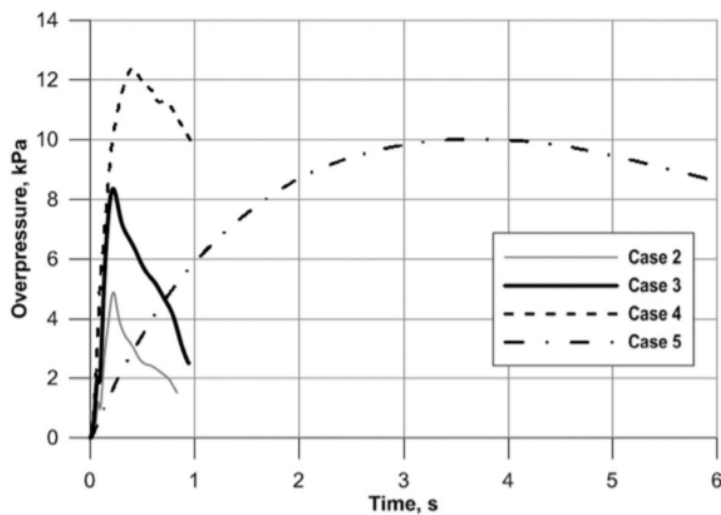Figure 3 displays the overpressure vs time for cases 2 through 5.



Figure 3 Overpressure versus time for case 2-5 [7]

Figure 3 shows that the resulting overpressure decreases with increasing TPRD diameter. Comparing case 1 in Figure 2 to case 2 in Figure 3 the overpressure is 8,6 times [7] lower. Case 2 has the largest vent (0,95 x 0,90 m) which, realistically, is too big for a garage.

The work from Hussein et. al. concludes that the relationship between vent size and TPRD diameter is non-linear and that a reduction of the TPRD diameter leads to a reduction in both overpressure and duration of the pressure peaking [7].

Similar findings to Hussein et al. case 1 has been found by Brennan et. al. [8]. Brennan et. al. performed numerical simulations for both ignited and unignited releases considering overpressure. They also used a 700-bar hydrogen vessel, a TPRD office diameter of 3.34 mm and a vent size of 0.35 x 0.55 m. For the ignited release Brennan et. al. found that already within 1 second of ignition the overpressure reaches over 55 kPa. This could potentially cause destruction to the garage structure.
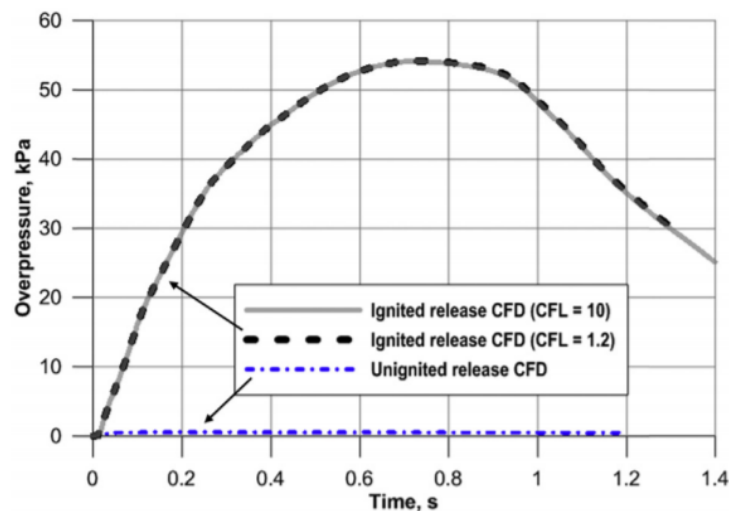


Figure 4 "Predicted overpressure in a garage, for both an unignited and ignited release of 0.299 kg/s" [8]

In their study they found that with an unignited release, the overpressure will be in the region of 0.55 kPa. This will not likely cause any damage to the garage structure. However, there exists a potential hazard in the form of oxygen depletion. This can cause asphyxiation if a human was to enter the garage. An unignited release can also be dangerous if an ignition source was introduced to the flammable hydrogen-air mixture already present.

### 1.2.2.1 Garage vent hazards

In the events of an ignited release in a garage enclosure an external flame will develop in the vent. This could potentially be dangerous for the surrounding buildings, vegetation or people. Brennan et. al. did some work on this in their numerical study of ignited and unignited release in a garage enclosure [8]. They found that the external flame reaches a maximum length of 3 m in around 1.56 seconds. This has obvious implications for the surrounding buildings and vegetation. It is worth noting that the area beyond the maximum flame length is not considered safe. Brennen et al. found that with a safe temperature of 70˚C, for humans the safe distance from the vent would be in the region of 9 meters. [8]

### 1.2.2.2 Garage windows

This sub-chapter will support the assumption that PPP (pressure peaking phenomenon) will not be critical in garages containing windows, as windows will shatter at lower pressures and act as natural ventilation. Typical Norwegian windows have an area of 0.5 m² which will

add to the total area of ventilation in the garage. This will lower the overpressure in the enclosure and ensure minimal structural damage, as windows will typically shatter at 1.03 kPa [9]. If a window were to shatter in the events of a release, it will be a hazard in itself with shattered glass being blown out. This bachelor thesis do not consider garages with windows.

# 1.3 Pressure peaking phenomenon

Pressure peaking is a phenomenon that applies only to gasses lighter than air and is most distinct for hydrogen. The phenomenon was defined by Shentsov et al. as "a transient process of pressure change with pronounced peak in an enclosure with ventilation." [10]. If an unscheduled release from a hydrogen vessel were to occur in an enclosure a peak in pressure would present itself shortly after. It was shown by Shentsov et al. that a release from a 35 MPa vessel with a PRD diameter of 5.08 mm in an enclosure of 30.4 m$^3$ and a vent size of 25x5 cm the peak overpressure would be significantly above 10-20 kPa. This would greatly damage civil structures and might cause collapse in a matter of seconds [10].

The pressure peaking phenomenon poses a great hazard in terms of storing hydrogen vehicles in enclosures. If a release were to happen the possibility of damage to the structure, car and potentially humans is of great magnitude. This phenomenon has been studied in great detail and it seems that the correlation between the TPRD diameter and vent size is the determining factors for the overpressure in the enclosure. This correlation will be investigated further in this report using a MATLAB model.

## 1.3.1 Ignited and unignited release

For an unignited release the pressure can reach as high as 20 kPa, as shown in the experiment by Shentsov et al. [10]. If this flammable hydrogen-air mixture were to ignite, the pressure would far exceed 20 kPa. As seen in chapter 1.2.2 Figure 4 the overpressure from the ignited release can reach as high as 55 kPa [8]. This is with a TPRD diameter and vent size that are considered "safe" for an unignited release (3.34 mm diameter and 19.25 cm$^2$ vent). This shows that the correlation between TPRD diameter and vent size is an important aspect to consider when storing hydrogen in enclosures.

# 2 **Experiment**

This chapter will present the components that will be used in the experiments as well as explain precautions considered while the experimental layout was created.

## 2.1 Components

### 2.1.1 Haskel AGT-152

A Haskel AGT-152 gas booster pump will be used in the experiments to pressurize the hydrogen in the tank. The booster pump has a 2-way piston and uses a supply of air to generate the pressure needed. The air will be supplied by a diesel compressor. This booster comes in a premade frame from Proserv and already has the pump installed with measuring instruments, valves and tubing.

### 2.1.2 Coriolis meter

For measuring of mass flow rate in the tubes a Coriolis meter is used. A Coriolis meter is based on motion mechanics in the sense that when a fluid moves through a vibrating pipe, it will accelerate towards the point of peak amplitude vibration. When the fluid has passed this point, it decelerates. The acceleration and deceleration over this point causes the pipe to oscillate. These oscillations generate voltage signals that are measured and corresponds to mass flow. A Coriolis meter will give a very accurate reading on mass flow. [11]

### 2.1.3 Hydrogen Tank

The primary component in the experiment is the hydrogen vessel. This vessel manufactured by Hexagon Composites subsidiary Hexagon Lincoln, is a type 4 vessel capable of hydrogen storage at 70 MPa. 70 MPa and a capacity of 36.8 litre makes for a strong candidate towards traditional powered vehicles with about 250 km of range. [12] The vessel is constructed using HDPE plastic liner with a carbon fibre-reinforced epoxy on the outer shell for endurance towards fatigue situations. (Appendix A)

## 2.2 Layout

In this sub-chapter the disposition of the elements to be used during the experiment will be presented. The basic operation of the system is as follows. First, the hydrogen goes from a commercial tank at about 200 bar to the pressure booster, where it increases its pressure to 700 bar with help from an air compressor. Then, the hydrogen is directed to the tank with a constant mass inflow until the tank reaches 700 bar (around 2kg of hydrogen). The stored hydrogen can then be released in the experiment passing through the Coriolis meter for measurements. The P&ID is presented below:
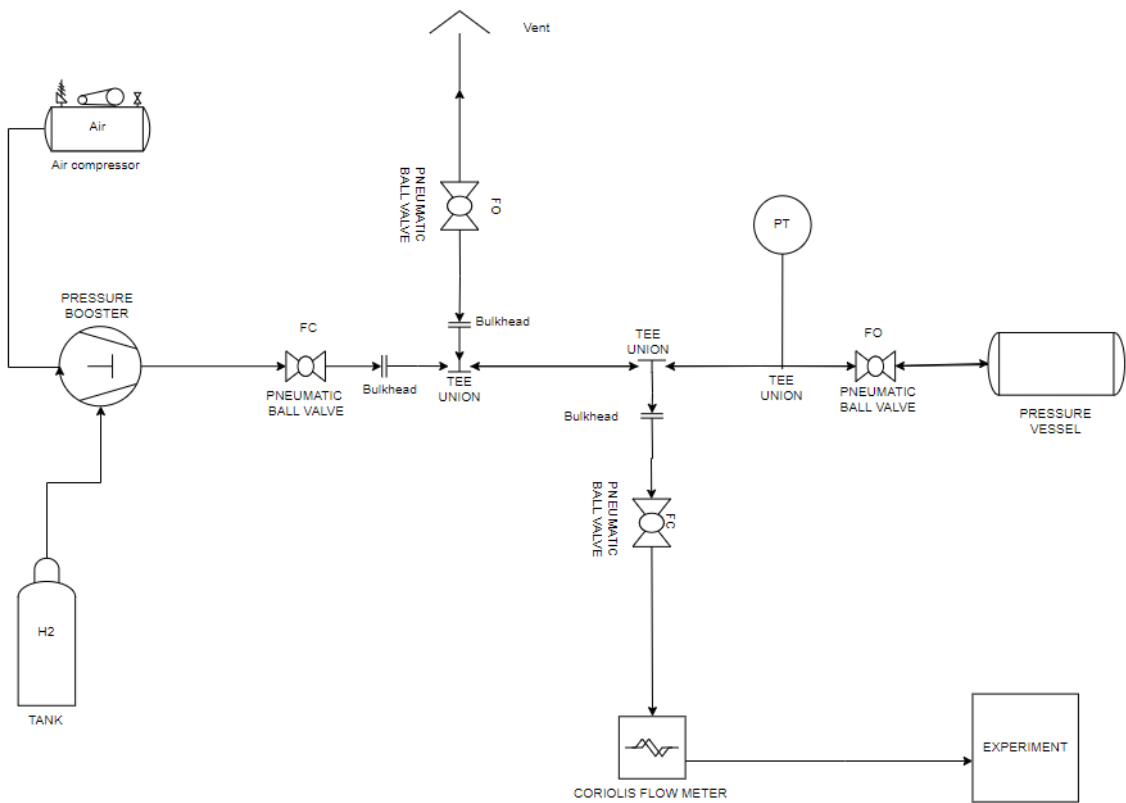
Figure 5 Layout (Appendix F)

The actual experiment will be held inside a 40ft container placed outside. The container will act as a safety barrier from the high-pressure hydrogen vessel. Tubing and fittings from Swagelok will be used for the whole system. As shown below will the main stretch of tubing go from the pressure-booster to the vessel. This stretch of tubing will have supports every 60 cm along the container and will be mounted at a height of about 1 meter. Safety venting mentioned in sub-chapter 2.5 explains the importance of vent placement. The vent will therefore go along the wall of the container pointing towards the sky, preventing injury from hydrogen jet or heat radiation.



Figure 6 Layout components

## 2.2.1 Valve setup
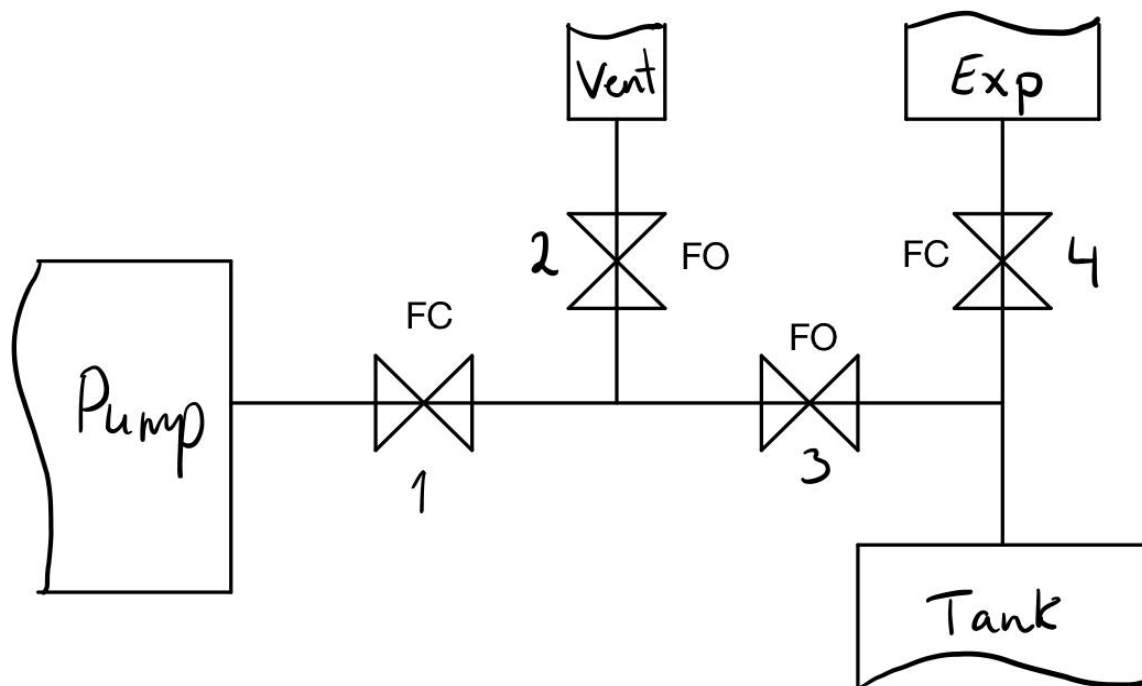


Figure 7 Valve setup

The high-pressure filling system needs a valve system for flow control. In Figure 6 a chart of the system is shown. A valve system is necessary to control the filling and emptying of the tank, as well as flow to the experiment. To ensure the safe use of the system, the valves will be pneumatically controlled so they can be operated at a safe distance. The valves used are gate valves.

**Procedure for filling the tank**

In this setup, to fill the tank with hydrogen, valve number 1 and 3 will be open while 2 and 4 are closed. After the tank is filled, there are still leftover hydrogen in the pipes that needs to be vented out. This is done by closing valve 1 while valve 4 is still closed. By opening valve 2 the leftover hydrogen will be vented out. When used for experiments, only valve 4 will be open.

## 2.3 Swagelok

Swagelok is a privately held company with expertise within oil and gas industries. With experience from outer space to hundreds of different project facilities, Swagelok is a well trusted company. Swagelok is chosen as the main supplier of tubing and fittings that will be used in the experiment.

A formal meeting was arranged with Swagelok, where an introduction to safe use and operation of Swagelok products was presented by Knut Marker, the sales project manager. The meeting also presents the different possibilities available with the products Swagelok offer.

With the given information from the meeting, two alternative layouts were created consisting of a mixture of 6x1.5mm and 3/8 tubing or 3/8 tubing for the whole system. The alternatives were presented in a follow up meeting. The meeting concludes that the combination of metric 6x1.5mm tubing and 3/8 tubing will be the most appropriate layout for the experiment, as the university already have 6mm tubing in house. 3/8 tubing will also have a bigger diameter than 6mm tubing, therefore less pressure loss will arise during release in the experiment.

Due to coronavirus pandemic, complications arise with the 6mm and 3/8 combination where the accessibility of 3/8 tubing is limited. Therefore, it is concluded to use 6mm tubing and fittings for the whole system. BOM is presented in Appendix G and the final P&ID (Piping and instrumentation diagram) in Figure 8.
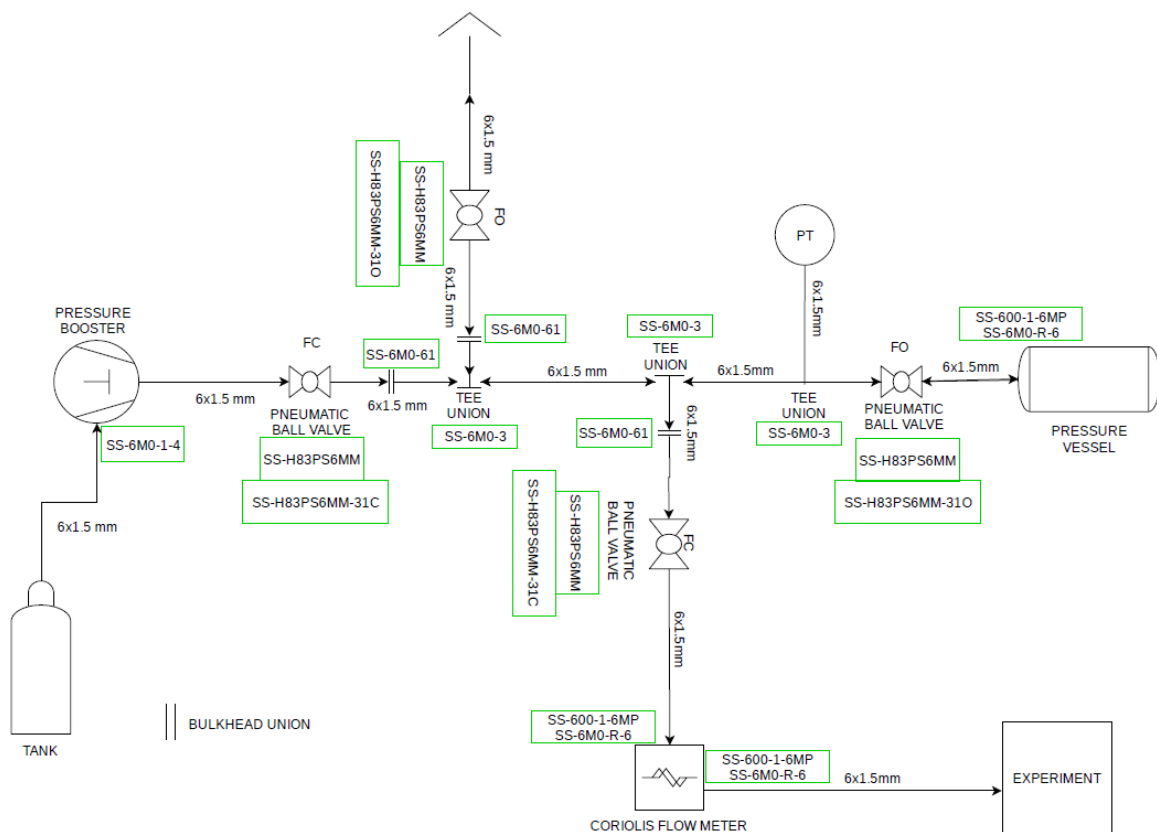


Figure 8 Final P&ID with Swagelok references

## 2.4 Pressure loss

To calculate the pressure loss in the experiment an adiabatic source model from the book Chemical Process Safety [9] has been applied. It is important to know the pressure loss in the experiment because the pressure at the end nozzle will determine the mass flow in the outlet. Below is a brief walk-through of the adiabatic source model used.

The mechanical energy balance applied to this case is written in the form

$$\frac{dP}{\rho} + \frac{\bar{u}d\bar{u}}{\alpha g_c} + \frac{g}{g_c}dz + dF = -\frac{\delta W_s}{m} \tag{1}$$

For this case one can assume that $\frac{g}{g_c}dz \approx 0$ for gases. Assuming straight pipes with no valves or fittings, the equations for frictional loss in a pipe, $F = K_f \left(\frac{u^2}{2g_c}\right)$, and excess head loss, $K_f = \frac{4fL}{d}$, can be combined and differentiated to result in

$$dF = \frac{2f\bar{u}^2 \, dL}{g_c d} \tag{2}$$

A constant Fanning friction factor across the pipe is an important assumption that is only valid for high Reynolds numbers. Furthermore, due to no mechanical work on the gas one can assume that $\delta W_s = 0$. To describe the changes in temperature of the gas, a total energy balance is given by

$$dh + \frac{\bar{u}d\bar{u}}{\alpha g_c} + \frac{g}{g_c}dz = \delta q - \frac{\delta W_s}{m} \tag{3}$$

Using the following assumptions

$$dh = C_p dT, \qquad \delta q = 0, \qquad \frac{g}{g_c}dz \approx 0, \qquad \delta W_s = 0$$

And combining, integrating and manipulating the mechanical- and total energy equations, the following equations are presented [9]

$$\frac{T_2}{T_1} = \frac{Y_1}{Y_2}, where \ Y_i = 1 + \frac{\gamma - 1}{2}Ma_i^2 \tag{4}$$

$$\frac{P_2}{P_1} = \frac{Ma_1}{Ma_2}\sqrt{\frac{Y_1}{Y_2}} \tag{5}$$

$$\frac{\rho_2}{\rho_1} = \frac{Ma_1}{Ma_2}\sqrt{\frac{Y_2}{Y_1}} \tag{6}$$

$$G = \rho\bar{u} = Ma_1 P_1 \sqrt{\frac{\gamma g_c M}{R_g T_1}} = Ma_2 P_2 \sqrt{\frac{\gamma g_c M}{R_g T_2}} \qquad (7)$$

$$\frac{\gamma + 1}{2} \ln\left(\frac{Ma_2^2 Y_1}{Ma_1^2 Y_2}\right) - \left(\frac{1}{Ma_1^2} - \frac{1}{Ma_2^2}\right) + \gamma\left(\frac{4fL}{d}\right) = 0 \qquad (8)$$

Equations (7) and (8) above are converted to a more useful way by replacing the Mach numbers by temperatures and pressures using equations (4), (5) and (6). This results in the following equations used to calculate the pressure loss

$$\frac{\gamma + 1}{\gamma} \ln\frac{P_1 T_2}{P_2 T_1} - \frac{\gamma - 1}{2\gamma}\left(\frac{P_1^2 T_2^2 - P_2^2 T_1^2}{T_2 - T_1}\right)\left(\frac{1}{P_1^2 T_2} - \frac{1}{P_2^2 T_1}\right) + \frac{4fL}{d} = 0, \qquad (9)$$

$$G = \sqrt{\frac{2g_c M}{R_g}\frac{\gamma}{\gamma - 1}\frac{T_2 - T_1}{\left(T_1/P_1\right)^2 - \left(T_2/P_2\right)^2}} \qquad (10)$$

Equations (9) and (10) are set equal to each other in order to find $P_2$ and $T_2$ using a MATLAB model (Appendix K) with a programmed iterative method. The model is made by André Vagner Gaathaug.

## 2.5 Safety venting

The hydrogen system is equipped with 4 actuator valves and during an emergency the valves connected to the pressure booster and experiment will fail safe close. In a case of emergency, the valves from the pressurized hydrogen vessel fail safe open, as well for the valve regulating the venting of the system.

Through a fail-safe ventilation of pressurized hydrogen at 70MPa, certain precautions need to be taken. In experiments conducted with pressures at this level, the placement of such fail-safe ventilation is critical to prevent structural damage and of course maintain human safety, as well as prevent explosion scenarios. In this sub-chapter, the necessary precautions during safety venting will be explained with the respect to behaviour of pressurized hydrogen.

### 2.5.1 Hydrogen Jet

Fail-safe ventilation of a 70 MPa pressurized vessel will lead to high-pressure hydrogen jets. These jets are capable of structural damage and inflicting critical harm to humans. Gas pressurized at as low as 20 MPa has the capability to penetrate clothes and working gloves. Penetration of skin will also occur at only 0.7 MPa from a few centimetres from the release point. [13] This leads to the conclusion that ventilation of pressurized gas needs to be directed away from humans as well as other fragile objects.

## 2.5.2 Spontaneous ignition

The release of 70 MPa into the open atmosphere leads to the formation of a highly under-expanded jet capable of self-ignition without any ignition sources. Self-ignition occurs when high-pressure hydrogen is discharged into the atmosphere. During discharge through venting tube, a shock wave compresses the air causing mixture of hydrogen and air along tube contact surfaces, causing temperature rise of mixture. Temperature rises due to compression of the mixture, and the mixture ignites when temperature of spontaneous ignition is exceeded.

The temperature of the mixture is key factor during self-ignition. Spontaneous ignition also called autoignition occurs at about 833.15 kelvin for hydrogen, this means that autoignition only occurs when the shock heated mixture between the leading shock wave and jet front reach these temperatures. [14] [15] [16]

A self-ignition like this is found to be dependent on variables such as pressure of release, diameter and length of tubing as well as the geometry of the eventual nozzles. The possibility of spontaneous ignition occurring increases with the increase of both tube length as well as pressure. Since the hydrogen tank operates at such high pressures as well as relatively long venting tube lengths, the likelihood of spontaneous ignition is high. [14] Molkov et al. explains that the probability of spontaneous ignition from high-pressure equipment is high. Control of such scenarios is one of the challenges in hydrogen safety today, as there is little fundamental explanation to why it happens. [4]

During spontaneous ignition jets flames will occur. It is then necessary to predict the safety distance to minimize individual and environmental risk.

### 2.5.2.1 Hazard distance jet flames

The model "Novel dimensionless flame length correlation" developed by Vladimir Molkov and Jean-Bernard Saffers is a dimensionless model based on the function of Froude number (Fr), Reynolds number (Re), and Mach number (M) to calculate the flame length of high-pressure hydrogen release. Based on the model presented in the article will the release of hydrogen at 70 MPa with nozzle size of 3mm have a flame length of 9.91 meters. With a flame length of almost 10 meters, Molkov and Saffers conclude that 35 meters is a safe distance where no harm from the jet flame will occur. First, second- or third-degree burns can be a consequence of jet flame exposure. This study define 70ºC as a no harm criterion, limiting level of consequence to a degree where no injuries may occur. [17] The vent environment shall thereby be an open atmosphere and the vent should be pointed up toward the sky for safer circumstances.

## 2.5.3 Buoyancy

Hydrogen with only a density of 0.0899 kg/m$^3$ makes for an extremely buoyant gas. The buoyancy of this gas is an advantage for most cases as the gas can quickly mix with ambient air and lower hydrogen-air concentration below LFL of 4%. In this case the experiment will be outside making accidental release of hydrogen a lot less dangerous as natural wind will quickly create turbulence and lower dangerous concentrations. [1]

# 3 **Design**

In this chapter the different supports for the components used in the experiment will be presented. For the hydrogen tank and the Coriolis meter, frames have been constructed as supports. Furthermore, a special tank mount was ordered to hold the tank itself. A finite element analysis is included in this chapter to verify the strains on the mounts.

## 3.1 Hydrogen tank frame

Using Rexroth profiles an aluminium frame was designed and constructed to ensure safe operation and transportation of the hydrogen tank. The flexibility of Rexroth technology allows for easy adjustments and simple mounting possibilities.

The frame was designed using Solidworks 2019, which allows for the use of Rexroth profiles to get a realistic illustration of the finished product. When designing the frame, necessary dimensions for complete cover of the tank is based on tank dimensions. (see Appendix A)
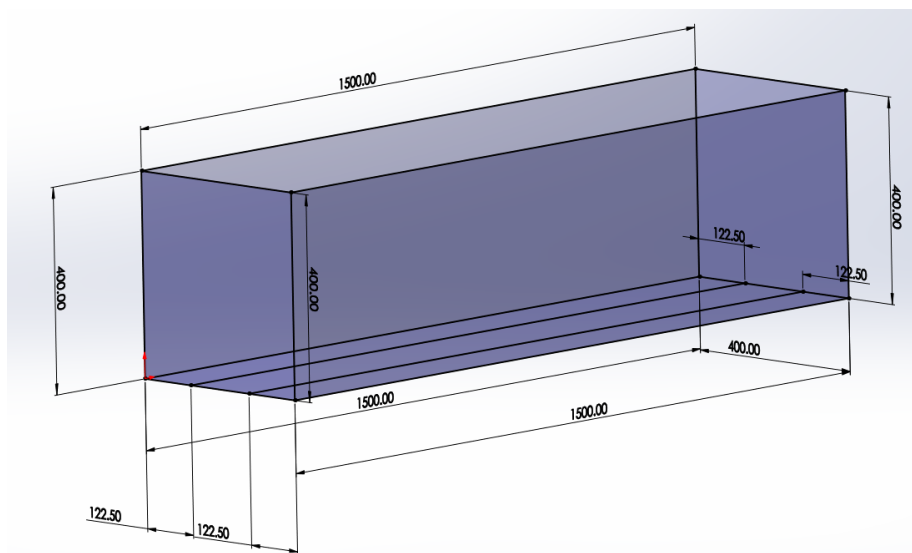


Figure 9 Dimensions

The frame has a length of 1500mm as the total length of the tank is 910.3mm which allows room for eventual valves or other instruments to be mounted inside the frame. The tank has a diameter of 320.8mm, so to allow easy accessibility of the tank the width and height of the frame is 400mm. The Rexroth profile used is 45x45mm. Rexroth profiles is therefore cut in the following lengths:

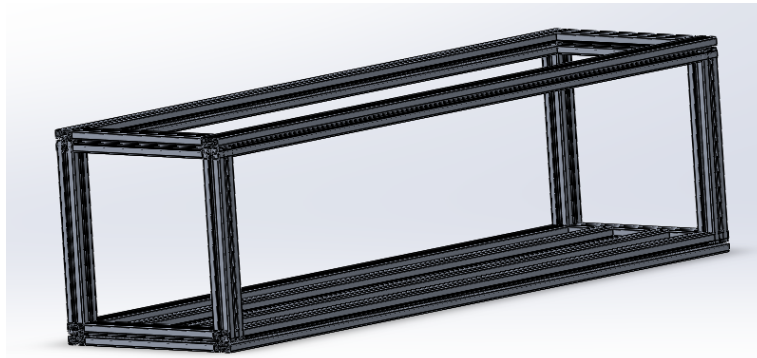- 4 x 1500mm
- 2 x 1410mm
- 8 x 355mm

Figure 10 Rexroth structural member

### 3.1.1 Construction

The Rexroth profiles was cut using a circular saw and assembled using Rexroth corner brackets shown in Figure 16. Threaded legs were also mounted to the frame for height adjustability.

## 3.2 Coriolis frame

When placing each element of the system in its corresponding place, it is necessary that they are protected and can be transported easily. To do this, it was decided to build a small frame to fix the measuring elements of the system: Coriolis meter and Coriolis transmitter. Also, within this frame the corresponding electronics would have to be located to operate these systems. Next, we will discuss how the design and subsequent construction of this frame has been carried out.

### 3.2.1 Method

In order to carry out the least possible work, aluminium bars left over from the construction of the tank frame was used to construct Coriolis frame. The available material is as follows:

- 9 aluminium bars of 900 mm length
- 4 aluminium bars of 630 mm length
- 5 aluminium bars of 750 mm length

Before starting to make the design, it is necessary to think about the conditions that the design must comply with, for safety or operational reasons. These requirements are:

1. All the elements must be inside the frame, including the connections and the electronics. In addition, the ground clearance must be as large as possible to avoid damaging the material when transporting.
2. The hydrogen stream will flow through the Coriolis meter while the experiment is running. To prevent condensation from occurring inside it, it is necessary to use gravity to avoid this phenomenon, so the position that this device must have within the frame is shown in the Figure 11.

Figure 11 Coriolis meter operating position [18]

3. The Coriolis meter has a safety vent, which must be in an easily accessible position, so it should be located on one of the edges of the frame.
4. Coriolis transmitter has a screen where it displays useful information, so it should be in a position where it can be easily seen. Although, this device can be remotely operated and can store the data and send it to a computer.

Another important aspect is deciding how the devices will be fixed to the frame. Any type of glue or permanent fixation should be avoided, as this could avoid their subsequent use in other projects. To mount the Coriolis meter, it has been decided to use the type of fixing shown in Figure 12. It consists of a flange covered with rubber inside to prevent slipping and to be able to fix the device with the pressure it exerts. In turn, this flange will be fixed to the frame by using a screw compatible with the rail of the Rexroth bar and immobilized by using a nut.



Figure 12 Coriolis meter fixing elements [19] [20]

The Coriolis transmitter is mounted to the frame using equipment provided by Emerson displayed below.



Figure 13 Coriolis transmitter fixing elements

As mentioned, the design of the frame is based on the remaining Rexroth profiles. Somewhat similar design as the tank frame allow for horizontal and vertical movement of the inner bar for desired fittings.
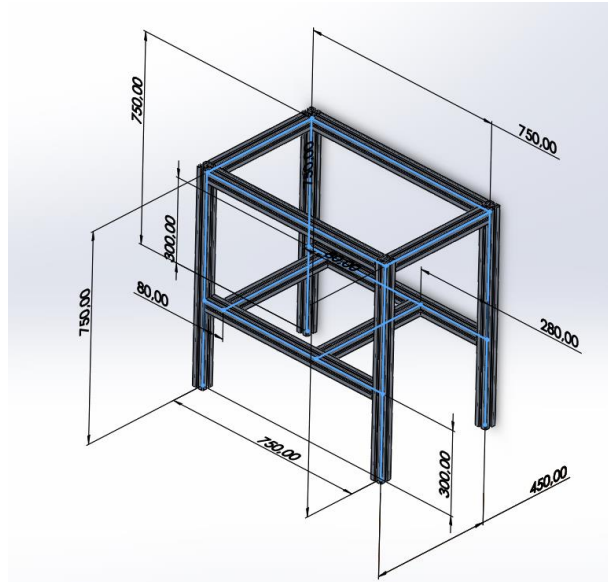


Figure 14 Coriolis meter frame design

Figure 15 displays the distribution of the components. The Coriolis meter safety valve is located towards the outside of the frame and the Coriolis transmitter screen is placed in a position where it can be easily seen.

To construct the following design, Rexroth profiles are cut using a circular saw:
- 8 aluminium bars of 750 mm length
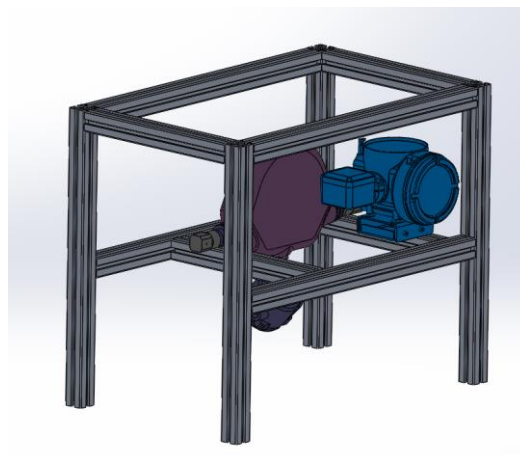- 4 aluminium bars of 450 mm length



Figure 15 Coriolis meter frame device placement

### 3.2.2 Construction

After cutting the bars in the measurements explained above, they are assembled using the brackets provided by Rexroth. (Figure 16).



Figure 16 Bosch Rexroth Bracket (standard) 43x42 [21]

Finally, both the Coriolis meter and the Coriolis transmitter are fixed using the methods explained, obtaining condition requirement while still reserving room for necessary electronics. The final result is shown in Figure 17.
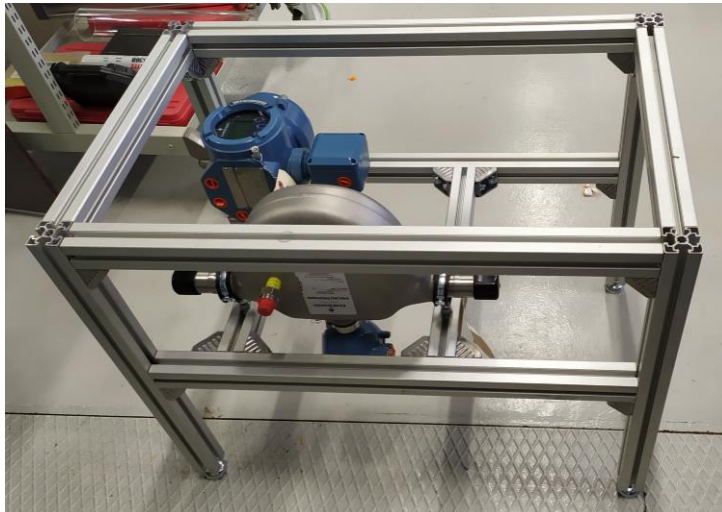


Figure 17 Coriolis frame final construction

## 3.3 Tank mounts

The hydrogen tank provided by Hexagon Lincoln has a carbon fibre reinforced epoxy outer shell, a design and material considered to withstand high pressure as well as external forces. That being said, it is still important to stay clear of all unwanted scenarios and it is essential to provide good support of the vessel both during operation as well as transportation. High quality aluminium mounts have been designed and machined to ensure enough support.

### 3.3.1 Design

The hydrogen tank is designed for either boss mounting or strap mounting. As listed in appendix A, shall all customer bracket kits made for strap mounting be approved by Hexagon Lincoln. Boss mounting shall therefore be used to secure the tank, as this method does not

require to be approved by Hexagon Lincoln. Boss mounting also secures the vessel from axial movement where strap mounting might not be as reliable. The boss mount must be suitable under certain conditions listed below:

- Hardware shall encompass full circumference of boss neck.
- Hardware shall be capable of restraining container from operation and crash loads.
- Hardware shall allow container to move along centreline axis of container without damage or wear of boss neck surface, movement required to accommodate axial growth of container under pressure.
- Hardware shall be suitably located to prevent hardware from disengaging with boss neck under container length changes and deflection of vehicle mounting frame and from applying load to the boss neck radius or stepped surface.

(Appendix A)

The purpose of this mount is to secure the hydrogen tank to the frame. The design is made for easy installation of the hydrogen tank as well as flexibility to adjust the mounts horizontally as desired. Key features considered is the thickness of the mounts, the diameter of the boss, holes for Rexroth corner brackets, as well as threads for the top piece. The mounts are also designed in considerations of the conditions listed above.

## 3.3.1.1 Dimensions

As pressure rises in the tank, horizontal expansion of the tank occurs. According to appendix A the total expansion of the tank at operating pressures is 3.7 mm. Mount thickness is therefore important to consider preventing external forces on the boss mount.
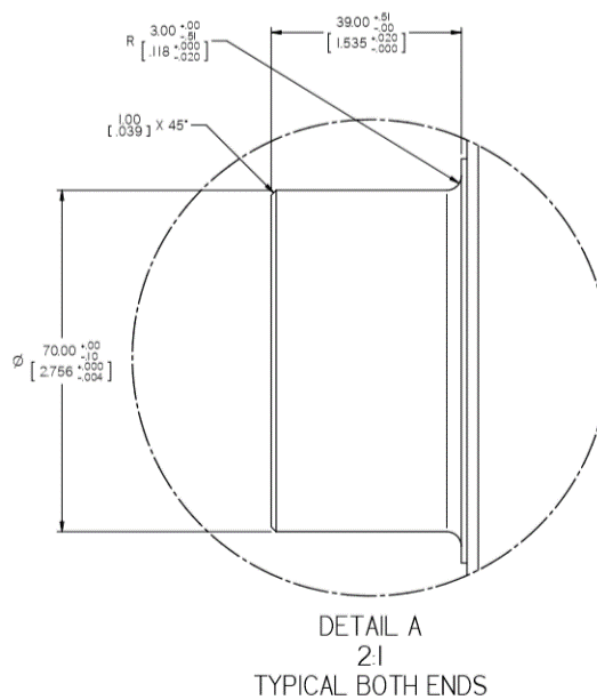


Figure 18 (Appendix A)

Taking into account the filets of the boss as well as total expansion, the maximum thickness of the mount should be roughly 33mm. The thickness of the mount is set to 27mm which allows free movement of tank without disengaging the mount. As shown above, the diameter of the boss is 70mm. The diameter of the mounts are set to 71mm for a conservative clearance to allow for free axial movement of the tank. Friction tape or a thin liner can then later be applied to the boss to reduce movement if desired. To encompass full circumference of the boss, a top piece is created and mounted using 2 M10 x 100mm bolts.
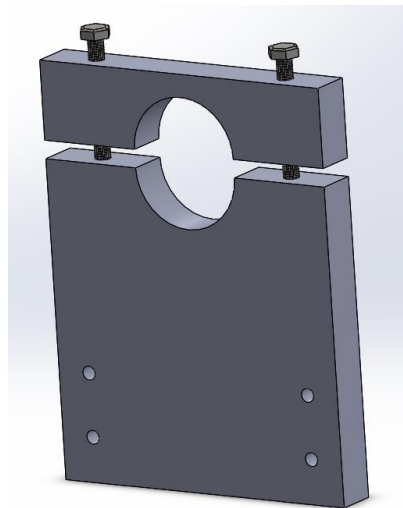


Figure 19 Illustration of mounts

With the convenience of Rexroth profiles allows for the use of Rexroth corner pieces to secure the mounts to the tank frame. The brilliance of these corner pieces is the fact that the whole tank can be moved around in the tank frame to best position the necessary instrument along with the tank. Rexroth 45/90mm corner pieces will be used.



Figure 20 45/90 Rexroth [58]

M8 x 50mm bolts are used to secure the corner pieces to the mount. Holes will therefore be necessary in the mounts. The finished results are shown below.
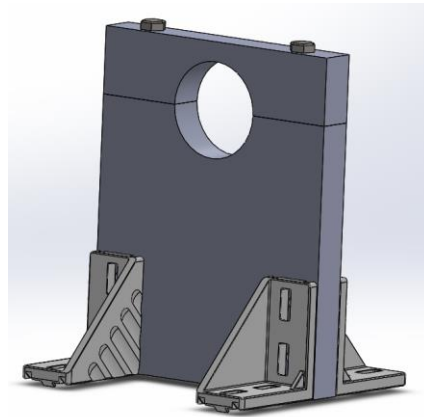


Figure 21 Assembled mounts
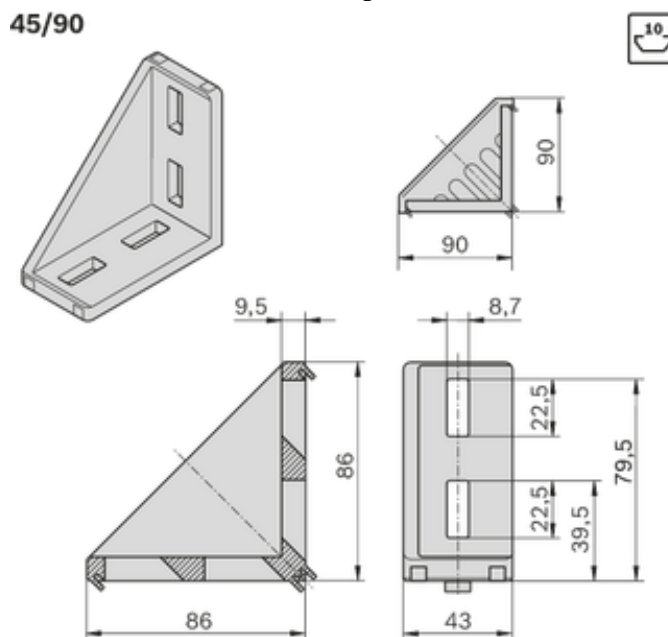
### 3.3.2 Construction drawings

According to data explained in section 3.3.1, construction drawings of the designed parts have been created. Separate drawings have been made for each part. These drawings were sent to the Karlsen & Solbakken Maskinering to machine the parts.

The construction drawings follow the international organization for standardization, the following standards used is listed below:

- ISO 128-33:2018 to marking, designation, placing and orientation of views, sections and cuts, and the position of text in relation to figures on construction drawings. [21]
- ISO 129-1:2018 for presentation of dimensions and associated tolerances that apply to 2D technical drawings in all disciplines. [21]
- ISO 6410 for the representation of threaded parts. [21]

Construction drawings is shown in Appendix I

### 3.3.3 Stress test

#### 3.3.3.1 Total Force

The total weight on the tank mounts consist of the hydrogen tank itself as well as the total weight of hydrogen at 70 MPa. The tank weighs 33 kg and has a total volume of 0.0368 m$^3$. (See appendix A) The weight of compressed hydrogen at 70 MPa is calculated below based on the ideal gas law [22]:

$$\rho = \frac{P}{R * K} = \frac{700 * 10^5 \, Pa}{4124.2 \, \frac{J}{kgK} * 294 \, K} = 57.73 \, \frac{kg}{m3}$$

$$M = \rho * V = 57.73 \, \frac{kg}{m^3} * (0.0368 \, m^3) = 2.12 kg$$

To be conservative the total weight of compressed hydrogen is 2.5 kg, this makes for a total of 35.5 kg including the tank.

$$F = mg$$
$$F = 35.5 \, kg * 9.81 \frac{m}{s^2}$$
$$F = 348.25 \, N$$

### 3.3.3.2 Finite element method

FEM is a numerical technique based on partial differential equations, also known as PDE's. PDE's are calculated to get an estimation on certain component behaviours under given structural loads. [23]

Static simulation was performed on the hydrogen tank boss mounts to ensure that the mounts where adequate to withstand the total force. The stress test simulation was performed using Solidworks.

Table 3 Simulation properties

| Properties: |
| --- |
| Material – 6061 Aluminium alloy |
| Fixtures – Fixed geometry Rexroth connection points |
| External loads – 174.125 N |
| Mesh – Standard mesh 4-point Jacobian |

The simulation estimates a total stress of 0.198 MPa on the boss mounts. This only constitutes for about 0.0036 % of the total capacity of the mounts, without a doubt satisfies the necessary strength required.
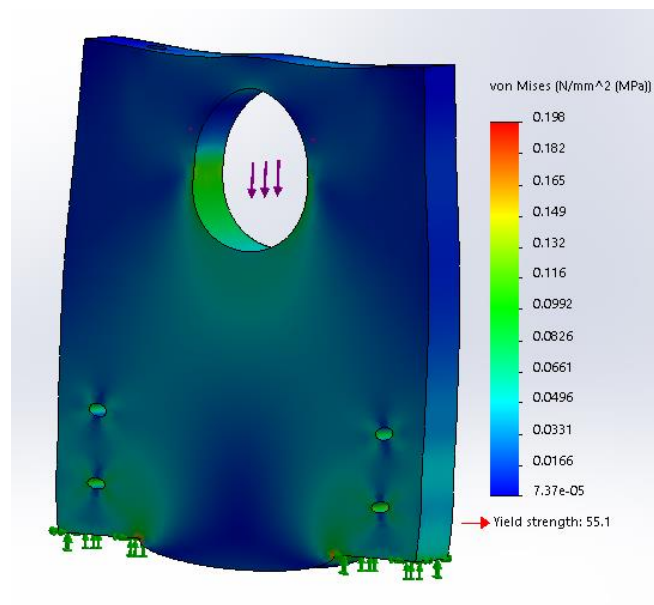


Figure 22 Solidworks simulation (Appendix J)

# 3.4 Pressure booster legs

When all components are connected, it was concluded that it would be much easier to have all the inputs and outputs of the elements at the same height. This allows the use of straight tubes, thus avoiding having to bend them, saving a reasonable amount of time. In addition, straight tubes avoid additional pressure loss due to the variation in height.

This solution is not a problem in the case of the tank frame and in the Coriolis meter frame, since, as previously stated, its construction was carried out with adjustable supports at the base of the legs, which allow modifying its height up to about 6 centimetres.

Due to safety reasons, it was considered more convenient to raise the components as much as possible, to increase their distance from the ground. This was a drawback in the case of the booster pump since it is a commercial model, whose support does not allow height adjustment.



Figure 23 Booster pump HASKEL AGT-62/152H

To solve this problem, it was decided to manufacture plastic supports to raise the booster pump to the required height. For this, a 3D printer model RAISE3D Pro2 and Cura slicer has been used.



Figure 24 Raise3D Pro2 and Cura Slicer

## 3.4.1 Method

Due to the heights of the tank frame and the Coriolis meter frame, it has been decided to place all the elements at a height of 41cm above the ground. The height of the initial booster pump is 36 cm, so it will be necessary to raise it about 5cm, opting for the following design.
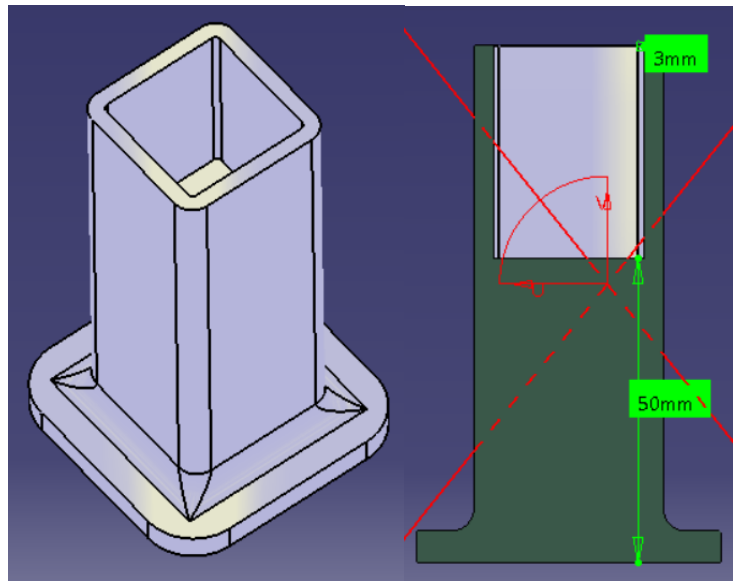
Figure 25 Support design

As the booster pump can be heavy, it has been decided to make a somewhat larger base to better distribute the weight towards the ground and improve stability. Also, a better adhesion to the printer bed is achieved.

Another important factor to consider is how the supports are fixed to the legs of the booster pump. It has been decided not to use any type of adhesive product. Therefore, the supports fitted with a sliding fit.

To solve this problem, test prototypes have been designed to simulate the size of the hole where the leg is housed, using different measurements around 25mm, which is the nominal measurement of the booster pump leg.
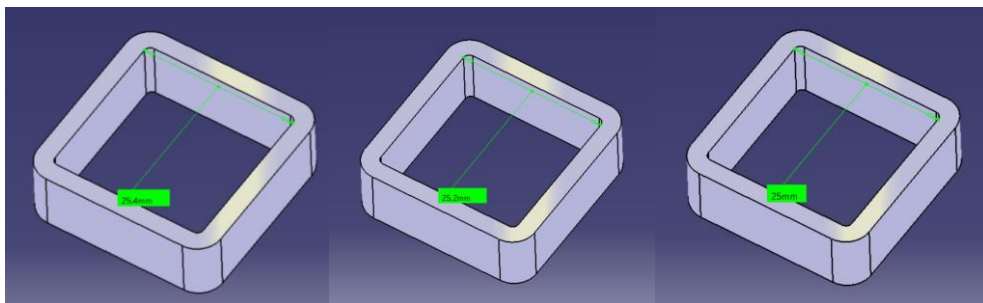


Figure 26 Prototypes made before final design

Once the prototypes are made, the necessary G-code is generated to print them. For this, the Cura software is used.

After testing the different prototypes on the legs of the booster pump we see that the one that best fit is the one with an internal measurement of 25mm on each side. This is due to the fact that the filament wire has a thickness of 0.4mm, which implies that 0.2mm, which gives us a final measurement of 24.6mm. However, during cooling PLA shrinks assuming that this measurement is around 24.8mm. This explains why it is the nominal size of 25mm that best adjusts to a tight tolerance.
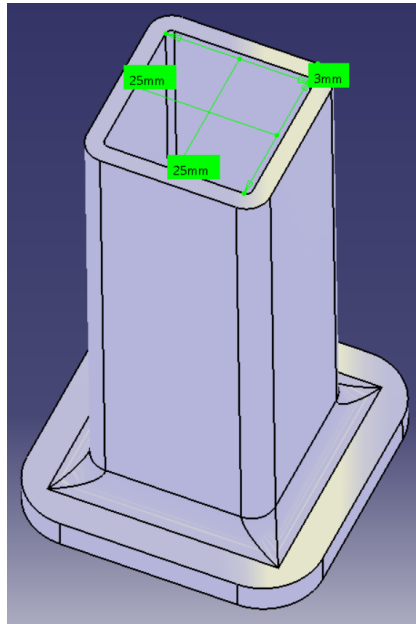
Figure 27 Final support design

As in the case of prototypes, we proceed to generate the G-Code with Cura Slicer. In this case we are going to increase the infill up to 50% to make the base of the support more resistant, due to the high weight of the booster pump, although this involves more printing time and more material used.

The printing time is almost 5 hours, which is somewhat high, because it has been used some conservative settings, but that will make the supports more resistant and durable. The material used is 51 grams per support, which hardly costs 16kr per support. In any case, much more economical than machining them in any type of metal.

## 3.4.2 Results

After a few hours of printing, the result being the one shown in Figure 28 and Figure 29.



Figure 28 Support fitted in the leg



Figure 29 Elevated booster pump

# 4 **Purging**

Purging is based on the process of applying an inert gas to a combustible mixture to reduce the oxygen concentration below LOC, to prevent deflagration of the mixture. LOC is the limiting oxygen concentration, basically the limit of quantity oxygen needed for a mixture to be combustible. The LOC is typically around 10% for most gases, applying a control point of 4% below LOC. [9]

The purging gas which in this case is nitrogen should be both applied and exhausted to ensure effective mixing. The exhaust gas must be vented safely, preferably through pipe leading to higher altitudes preventing plumes of exhaust gas at purge site. Multiple purges or cycles is necessary to ensure acceptable oxidant concentrations. [24]

The use of nitrogen during purging creates an inert atmosphere inside the vessel which is essential to prevent combustion during hydrogen applications. Nitrogen is also a good purging gas due to its properties resulting in a very dry gas. Bottled nitrogen, which in this case will be used is typically dryer than 2 ppm, resulting in a dew point of only $-70^0$C. [25] A dry atmosphere is essential to eliminate all access water vapor. Remaining water vapor during pressure increase can cause problems as water vapor turns to liquid.

During purging, for safety reasons the temperature inside the tank must not reach above 358K (Appendix A), so an approximate estimation of the conditions inside the tank during the purging process has been established.

This tank is designed for filling pressures up to 875 bar (Appendix A), so filling it with nitrogen at much lower pressures should not be a problem. However, by repeating the filling and emptying process several times, it is possible that the temperature reaches high values if an adequate waiting time between cycles is not respected.

This chapter also describes an approximation of the amount of heat that the tank walls can store and how it affects the temperature inside.

## 4.1 Pressure purging

Pressure purging is the process of adding an inert gas to a pressurized vessel, then venting the gas to the atmosphere until atmospheric pressure is achieved. This procedure is completed until acceptable LOC. During the pressurization, the number of moles oxygen remains constant, although the mole fraction decreases. As the vessel is filled with inert gas, we now have a new composition of the mixture. During release the composition remains constant, thus the total number of mole oxygen is decreased. During release, the oxygen mole fraction remains constant assuming we have a full mix of fluids. [9]

American society for testing and materials (ASTM) has created a standard (ASTM G-124) determining the combustion behaviour of metallic materials. The same equation can be used to calculate total purge cycles necessary to satisfy safe hydrogen and oxygen compositions. The equation is valid under a certain assumption. The assumption being that the purge gases behave ideally and compress ideally. As oxygen and nitrogen behave much like ideal gases, the assumption made is acceptable and ASTM G-124 is valid. [26]

## 4.1.1 ASTM G-124

In the first purge the tank increases the pressure up to the selected purge pressure (Ph), then it is vented until reaching the atmospheric pressure ($P_{amb}$). To calculate the molarity of air after this process the following formula is used. [26]

$$X_1 = \frac{P_{amb}}{Ph} \tag{11}$$

In addition, to calculate the remaining air moles the following expression can be used.

$$n_1 = n_0 * X_1 \tag{12}$$

In the following purges the process is the same. However, the equation that provides the air molarity now considers the molarity of the previous blowdown, so it is written as follows.

$$X_2 = \frac{X_1 * P_{amb}}{Ph} = \left(\frac{P_{amb}}{Ph}\right)^2 \tag{13}$$

To calculate the number of moles remaining, equation (12) can be used, substituting the molarity of this step.

$$n_2 = n_0 * X_2 \tag{14}$$

In general, for a number $N$ of purges, these equations can be written as follows.

$$X_N = \left(\frac{P_{amb}}{Ph}\right)^N \tag{15}$$

$$n_N = n0 * X_N \tag{16}$$

In many cases the purge pressure and atmospheric pressure are known, therefore, to obtain the number N of necessary purges, it can be solved as follows starting from equation (15).

$$\log(X_N) = log\left(\left(\frac{P_{amb}}{Ph}\right)^N\right) = N \cdot log\left(\frac{P_{amb}}{Ph}\right) \tag{17}$$

Clearing the number of purges is finally obtained.

$$N = \frac{Log(X_N)}{Log\left(\frac{P_{amb}}{Ph}\right)} \tag{18}$$

For example, if a concentration of 0.01% air is taken as safe, which means a concentration of 0.0001 per unit, the equation would look like this.

$$N = -\frac{4}{log\left(\frac{P_{amb}}{Ph}\right)} \tag{19}$$

## 4.1.2 Purging Excel

See appendix B

Table 4 ASTM G-124 purging method

| Purging | | | |
|---|---|---|---|
| **Pressure conditions** | | | |
| $P_{amb} =$ | 1,01325 | bar | Xn - Molar ratio of initial gas |
| Ph= | 10 | bar | Pa - Initial pressure |
| **Number of purges:** | | | Ph - purge pressure |
| Xn= | 0,1 | | N - purges required |
| N= | 1,006 | | |
| | | | |
| **Purges when Xn=0.0001** | | **Proportion of air remaining** | |
| Xn= | 0.0001 | N'th purge= | 4 |
| N= | 4,023 | Xn= | 0,000105 |

The purge equation does not conclude the exact number of cycles required, however the number acquired is almost always within one purge of the exact theoretical number. This makes for a good tool to estimate the number of purges required. The equation itself calculates the nitrogen percentage within 0.2% of the actual nitrogen percentage per cycle.

That being said, one can conclude that the equation will be accurate enough for this experiment. Keep in mind that higher purging pressure will be favoured to decrease number of cycles required, and to ensure a more accurate calculation. [26]

## 4.2 Conditions inside the tank during the purge process

In this chapter, three different ways of calculating the temperature inside the tank have been used. The two first methods do not consider the walls in the control volume. Later, in a third section, a method is presented to estimate how the heat capacity of the walls affects the temperature inside the tank.

The starting point of the three methods begins by proposing an energy balance and a mass balance at a control volume, which in this case will be the tank.

The main difference between the first two methods is that in the first one it is assumed, among other things, that the control volume is completely adiabatic, while on the contrary, in the second method this hypothesis is not carried out. In this way, in the results section, a comparison can be made between both methods, observing how the adiabatic control volume hypothesis affects the temperature inside.

Considering these results, an approximation of the real temperature inside the tank is calculated by using a tool called the general rule of mixtures. Which allows us, without using any type of software or simulation, to approximate a temperature value that can be similar to the real one, taking into account the capacity of the tank walls to store heat.

This last section has been made based on an article called: *Estimation of final hydrogen temperature from refuelling parameters* [27] written by Jinsheng Xiao, Pierre Bénard, Richard Chahine. Substituting the properties of hydrogen with the properties of nitrogen and applying the material, mass and volume data of the type IV tank that is being used in this project.

Finally, using all these results and graphs, a safe pressure can be established at which to purge. In addition, an excel program [Appendix B] has been made, in which both the initial and environmental conditions can be modified. In this program, properties can also be set for the inlet mass flow and see how all these changes affect pressure and temperature as a function of time.

To validate the theoretical method, thermocouples could be installed inside the tank during the purging process. In this way it would be possible to compare the results obtained theoretically with a very simple method, to the real ones.

In this way, it is possible to establish the validity or not of this method and see to what extent they affect all the hypotheses made, which will be presented at the beginning of each method.

### 4.2.1 Method

#### 4.2.1.1 Adiabatic case

In this case an assumption has been made that the nitrogen does not lose any heat, the conduction transmission coefficient "k" of the gas is so small.

Furthermore, the following assumptions have been made:

- Kinetic energy of the gas is despised against internal $\qquad$ $v = 0$
- No shaft work on the air in the tank $\qquad$ $\dot{W} = 0$
- Properties of the mass flow remains constant $\qquad$ $T_{in}, \dot{m}_{in}, p_{in} = cte$
- When working with a gas, the term of potential energy can be considered zero
- The whole tank is made of carbon fibre composite (disregarding the parts made of steel)

These last five assumptions will hold for all calculations made during this chapter.

The positive normal vector will also be considered as the one that leaves the control surface (Figure 30), so in this case the term corresponding to the mass inflow will be negative, since it is entering the control volume.
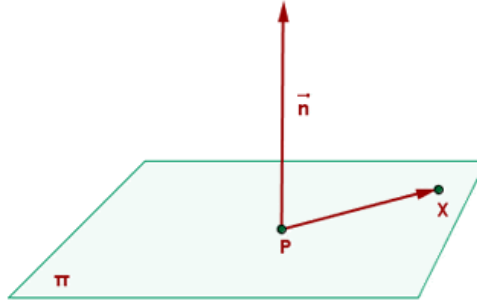


Figure 30 Normal vector direction with respect to a surface

To begin, the equation of the energy balance is proposed at a control volume, which in this case is the tank, with an input that will be the nitrogen mass inflow from a commercial cylinder, whose conditions are known [28].

$$\frac{d}{dt} \iiint \left( \frac{v^2}{2} + gz + u \right) \rho dV - \iint \dot{m}_{in} \left( h_{in} + gz_{in} + \frac{v_1^2}{2} \right) \cdot \vec{n} dA = \dot{Q} + \dot{W} \qquad (20)$$

In the case of the term mass inflow, enthalpy can be related to internal energy through the following equality: $h_{in} = p_{in}/\rho_{in} + u_{in}$, which will facilitate the calculations in the following steps. Applying the steps explained above and all the proposed assumptions, the energy balance is as follows:

$$\frac{d}{dt} \iiint u \rho dV - \dot{m}_{in} \left( \frac{p_{in}}{\rho_{in}} + u_{in} \right) = 0 \qquad (21)$$

The volume of the tank is always going to be constant, so it can come out of the integral. Moreover, we can write that: $\rho = m/V$, so the volume would be simplified in this term, remaining:

$$\frac{d}{dt}(um) - \dot{m}_{in}\left(\frac{p_{in}}{\rho_{in}} + u_{in}\right) = 0 \tag{22}$$

Considering that it is an ideal gas, it can be said that: $p_1/\rho_1 = RT_1$, in addition, the internal energy can be written as a function of the specific heat at constant volume and the temperature differential: $du = CvdT$.

$$\frac{d}{dt}((CvdT)m) - \dot{m}_{in}(RT_{in} + CvdT) = 0 \tag{23}$$

Grouping terms and leaving the differentials on the left side of the equation this result is obtained:

$$\frac{dT}{dt} = \frac{\dot{m}_{in}\left[RT_{in} + Cv(T_{in} - T)\right]}{mCv} \tag{24}$$

The time differential passes by multiplying to the right side of the equation, so now both sides of the equality can be integrated to eliminate the differentials.

$$\int_{T_0}^{T_n} dT = \frac{\dot{m}_{in}\left[RT_{in} + Cv(T_{in} - T)\right]}{mCv}\int_{t_0}^{t_n} dt \tag{25}$$

The selected integration limits allow the calculation of the temperature inside the tank, based on initial conditions that must be known and a time that must be imposed. Solving the integrals leads to the result:

$$T_n - T_0 = \frac{\dot{m}_{in}\left[RT_{in} + Cv(T_{in} - T_0)\right]}{m_0 Cv}\Delta t \tag{26}$$

As this formula is going to be implemented in an excel sheet to solve it in intervals of one tenth of a second, in the interval following the initial one, the equation will be written as follows:

$$T_n = T_{n-1} + \frac{\dot{m}_{in}\left[RT_{in} + Cv(T_{in} - T_{n-1})\right]}{m_{n-1} Cv}\Delta t \tag{27}$$

In the equation, it can be seen that the required terms are properties of the gas, in this case nitrogen, and the properties of the mass inflow. However, the term of the mass inside the tank also varies as it is filling, so it is necessary to look for another equation, that allows to know the evolution of the mass inside the tank as a function of time.

For this, the conservation equation of the mass applied to a control volume can be used, which in this case, as for the energy balance, will be the tank. [29]

$$\frac{d}{dt} \iiint \rho dV + \iint \rho \, (\vec{v} \cdot \vec{n}) \, dA = 0 \tag{28}$$

Using the same procedure as in the energy balance, the density can be written as $\rho = m/V$. In addition, the second term can also be replaced by this equality $\dot{m} = \rho v A$, with the corresponding sign due to the mass inflow.

$$\frac{d}{dt} \iiint \frac{m}{V} dV - \dot{m}_{in} = 0 \tag{29}$$

The volume of the tank is going to be constant, so it is not affected by the differential, as a result it would be simplified in the first term. Grouping terms, the equation would be as follows:

$$\frac{dm}{dt} = \dot{m}_{in} \tag{30}$$

By multiplying the time differential term, both sides can be integrated to eliminate the differentials.

$$\int_{m_0}^{m_n} dm = \dot{m}_{in} \int_{t_0}^{t_n} dt \tag{31}$$

These limits of integration are given by what is explained in equation (26), being known in this case as the mass inflow. Solving the integrals finally is obtained:

$$m_n = m_0 + \dot{m}_{in} \cdot \Delta t \tag{32}$$

As this formula will also be implemented in an excel sheet, in order to solve the intervals that follow the initial one, it can be written it this way:

$$m_n = m_{n-1} + \dot{m}_{in} \cdot \Delta t \tag{33}$$

So, the initial step becomes the previous step, from which we will have calculated the value at the previous instant of time, and so on until the desired time.

As explained in the introduction to the chapter, the purging process will be carried out at a certain pressure, so the optimal situation would able to compare the pressure inside the tank at any time with the temperature inside.

Since nitrogen is been used and it behaves like an ideal gas, there is a way to relate mass to pressure, through density $\rho = p/(RT)$, so if the mass balance equation is used again (28), the following will be obtained:

$$\frac{d}{dt} \left( \frac{pV}{RT_n} \right) = \dot{m}_{in} \tag{34}$$

In order to solve this equation, it is first necessary to separate the terms that will be constant from the variables. The properties of nitrogen are constant, as are the mass inflow and the volume of the tank.

$$\left(\frac{R\dot{m}_{in}}{V}\right) = \frac{dp}{T_n} \cdot \frac{1}{dt} \tag{35}$$

$$\left(\frac{R\dot{m}_{in}}{V}\right) = \frac{1}{T_n}\frac{dp}{dt} - p_n\frac{d}{dt}\frac{1}{T_n} \tag{36}$$

If the second term on the right side of the equality is multiplied and divided by the temperature, it allows to transform it into something that can be solved. As can be seen in the following equation:

$$\left(\frac{R\dot{m}_{in}}{V}\right) = \frac{1}{T_n}\frac{dp}{dt} - \frac{p_n}{T_n{}^2}\frac{dT}{dt} \tag{37}$$

The term $dT/dt$ is given by the equation (24), so it would only have to be replaced in the equation (37). After clearing the term of the pressure, finally an expression is obtained that allows the pressure to be related to the temperature inside of the tank.

$$\frac{dp}{dt} = \left(\frac{R\dot{m}_{in}}{V} + \frac{p_n}{T_n{}^2}\frac{\dot{m}_{in}\,[RT_{in} + Cv(T_{in} - T_n)]}{m_n Cv}\right)T_n \tag{38}$$

If equations (33) and (38) are combined, an expression will be obtained, in which all the parameters are known or can be established.

$$\int_{p_0}^{p_n} dp = \left(\frac{R\dot{m}_{in}}{V} + \frac{p_n}{T_n{}^2}\frac{\dot{m}_{in}\,[RT_{in} + Cv(T_{in} - T_n)]}{(m_{n-1} + \dot{m}_{in}\cdot\Delta t)Cv}\right)T_n\int_{t_0}^{t_n} dt \tag{39}$$

Solving the integrals, the following is obtained. In equation (41) it is shown how the formula would look to implement it in excel. Although in this case it will not be necessary since the terms $dT/dt$ and $m_n$ can be implemented as cells of another column of the table.

$$p_n = p_0\left(\frac{R\dot{m}_{in}}{V} + \frac{p_n}{T_n{}^2}\frac{\dot{m}_{in}\,[RT_{in} + Cv(T_{in} - T_n)]}{(m_{n-1} + \dot{m}_{in}\cdot\Delta t)Cv}\right)T_n\cdot\Delta t \tag{40}$$

$$p_n = p_{n-1}\left(\frac{R\dot{m}_{in}}{V} + \frac{p_n}{T_n{}^2}\frac{\dot{m}_{in}\,[RT_{in} + Cv(T_{in} - T_n)]}{(m_{n-1} + \dot{m}_{in}\cdot\Delta t)Cv}\right)T_n\cdot\Delta t \tag{41}$$

In this way, using the equation (27), the equation (33) and the equation (41) at the same time, the conditions in the tank can be obtained for each instant of time as a function of the mass inflow.

### 4.2.1.2 Non-adiabatic case

In this section, the method to quantify how much the term of the heat outflow rate affects the temperature inside the control volume will be presented.

For this, the energy balance (20) and the conservation of mass equation (28) are used, both applied to a control volume, which will be the tank with its corresponding inflow. Applying the assumptions explained at the beginning of the chapter 4.2.1.1, and the heat rate being different from zero, both equations can be written as:

$$\frac{d}{dt} \iiint u\rho dV - \dot{m}_{in} h_{in} = \dot{Q} \tag{42}$$

$$\frac{d}{dt} \iiint \rho dV = \dot{m}_{in} \tag{43}$$

As it has been seen in the previous chapter, if this substitution $\rho = m/V$ is made, since the volume of the tank is always constant, it can be simplified, leaving only the mass in that term as a variable. Resulting from it:

$$\frac{d}{dt} (mu) = \dot{m}_{in} h_{in} + \dot{Q} \tag{44}$$

Modifying the partial derivative, equation (44) can be written as follows:

$$m\frac{du}{dt} + u\frac{dm}{dt} = \dot{m}_{in} h_{in} + \dot{Q} \tag{45}$$

If this equation is combined with the expression for the integration of the conservation of mass (26) and the equality obtained in equation (30), the following equation will be obtained, where different unknowns are still present.

$$(m_0 + \dot{m}_{in}t)\frac{du}{dt} + \dot{m}_{in}u = \dot{m}_{in} h_{in} + \dot{Q} \tag{46}$$

By dividing both terms by the mass inflow, the expression can be slightly simplified. Moreover, the heat would now be divided by the mass inflow, which is helpful when working with it, as will be seen later.

$$\left(\frac{m_0}{\dot{m}_{in}} + t\right)\frac{du}{dt} + u = h_{in} + \frac{\dot{Q}}{\dot{m}_{in}} \tag{47}$$

The first term is dimensionless, so to simplify this expression this fraction can be treated as a characteristic time $t^* = \dot{m}_0/\dot{m}_{in}$.

To solve the term of the heat rate, the appendix A present in the article *Estimation of final hydrogen temperature from refuelling parameters* [27], where the procedure that is followed is very similar to that explained below.

The specific heat inflow can be written as follows:

$$q = \frac{\dot{Q}}{\dot{m}_{in}} = \frac{a_f A_S}{\dot{m}_{in}} (T_{amb} - T) \qquad (48)$$

If the dimensionless heat transfer coefficient is used, which relates the system's capacity to transfer heat, with the total heat capacity change $\alpha = (A_S \alpha_f / C_v \dot{m}_{in})$, it is possible to leave the specific heat term solely depending on the properties of nitrogen.

$$q = \frac{\dot{Q}}{\dot{m}_{in}} = \alpha C_v (T_{amb} - T) \qquad (49)$$

Where the dimensionless heat transfer coefficient can be calculated as a numerical value, using this formula based on the conductive properties of the gas, obtained in the following reference [30], for a temperature around 294K:

$$\alpha = \frac{k}{\rho C_p} \qquad (50)$$

When substituting equation (49) in equation (47), an expression remains where the value of the heat rate can be calculated based on known or imposed parameters.

$$(t^* + t)\frac{du}{dt} + u = h_{in} + \alpha C_v (T_{amb} - T) \qquad (51)$$

With the assumption of ideal gas conditions, internal energy can be written as $u = C_v T$, and the enthalpy as $h = C_p T$, as it is the mass inflow enthalpy, the temperature is $T_\infty$, which is known. With these notations the energy balance equation can be written as follows:

$$(t^* + t)\frac{dT}{dt}C_v + C_v T = C_p T_{in} + \alpha C_v (T_{amb} - T) \qquad (52)$$

It is possible to simplify this equation by grouping terms and using the notation $\gamma = C_p / C_v$, as can be seen in the next step.

$$(t^* + t)\frac{dT}{dt} + T = \gamma T_{in} + \alpha (T_{amb} - T) \qquad (53)$$

In order to make the future integration easier, a good way is creating a dimensionless term for the temperatures called: $T^* = \frac{\gamma T_{in} + \alpha T_{amb}}{1 + \alpha}$. So, clearing the differential term and applying the dimensionless term for the temperatures it is obtained:

$$\frac{dT}{dt} = (1 + \alpha)\frac{T^* - T}{(t^* + t)} \qquad (54)$$

Clearing the differential term and applying the integrals with the limits commonly used, taking as initial moment $t_0 = 0$, and $T_0$ as the temperature inside the tank just before filling begins, the following expression is obtained as a result:

$$\frac{T^* - T}{T^* - T_0} = \left(\frac{1}{1 + \frac{t}{t^*}}\right)^{1+\alpha} \tag{55}$$

It cannot be forgotten that the term $t^*$ depends on the mass inside the tank, which is unknown, so the conservation of mass equation (43) must be used to solve this term. For this the equation is integrated as follows.

$$\int_{m_0}^{m} dm = \dot{m}_{in} \int_{t_0=0}^{t_n} dt \tag{56}$$

Resulting in:

$$m = m_0 + \dot{m}_{in} t \tag{57}$$

Continuing with the strategy of dimensioning all possible terms to simplify calculations, dividing both terms by the initial mass $m_0$, it is possible to get to obtain the mass in the tank as a function of the dimensionless time proposed after equation (47), for this the following procedure is used.

$$\frac{m}{m_0} = 1 + \frac{\dot{m}_{in}}{m_0} t = 1 + \frac{t}{m_0/\dot{m}_{in}} = 1 + \frac{t}{t^*} \tag{58}$$

By substituting this term in equation (55), it is possible to obtain an expression that gives us the temperature as a function of the mass inside the tank.

$$\frac{T^* - T}{T^* - T_0} = \left(\frac{m_0}{m}\right)^{1+\alpha} \tag{59}$$

To calculate the mass inside the tank, equation (57) can be used. In the same way, equation (41) allows knowing the pressure at which the tank is at each instant of time. To be able to implement the equation (59) in an excel sheet, it can be written in the following way:

$$T_n = \left(\frac{m_{n-1}}{m}\right)^{1+\alpha} T_{n-1} + \left(1 - \left(\frac{m_{n-1}}{m}\right)^{1+\alpha}\right) T^* \tag{60}$$

In this way, using the equation (41), the equation (57) and the equation (60) at the same time, the conditions in the tank can be obtained for each instant of time as a function of the mass inflow.

In the section 4.2.2.2 it is possible to see the difference in results that exists between the case 4.2.1.1. and the case 4.2.1.2, and therefore how the term of the heat rate affects the final nitrogen temperature depending on the pressure.

## 4.2.1.3 Application of the heat capacity of the walls

The previous calculations only consider the properties of the gas. The tank only appears as a constant volume, which is something that is quite far from the real conditions. In this section, a thermodynamic system that includes the nitrogen inside the tank and the heat capacity of the walls will be considered.

In order to carry out this study, an analogy of the general rule of mixtures will be used. It is an equation that is generally used to study the properties of nanocomposites or hybrid materials, since it allows us to count how the value of a certain characteristic of each material affects the final magnitude of the composite material.



Composite material showing aligned fibres within the matrix

The approximation used in the Rule of Mixtures
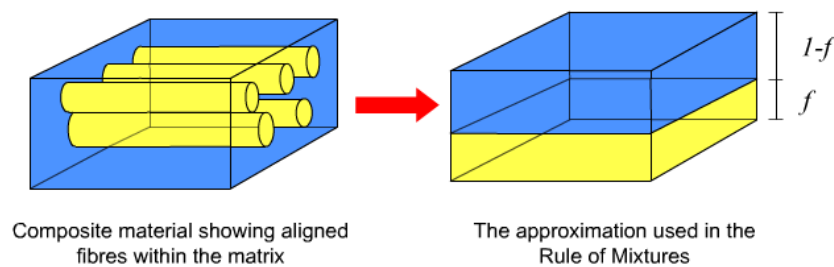
Figure 31 basic operation of the rule of mixtures [31]

The analogy that is intended to be used for this study is that instead of being two solids forming a composite material, it is a solid (carbon fibre composite) and a gas (nitrogen) forming a thermodynamic system, where its properties as a whole can be calculated using this procedure.

For this, certain simplifications must be made in terms of the structure and materials of the tank:

- Parts made of metal are not taken into account.
- The polymeric liner coating on the inside of the tank is not introduced into the calculations, since its mass is negligible compared to carbon fibre composite (Figure 32)
- All the thermal properties of carbon fibre composite are assumed to be isotropic.
- The walls of the tank are considered adiabatic.



Figure 32 type IV pressure tank structure [32]

In a two-phase system, the property of the system can be calculated based on the volume fraction that each phase occupies within the system [33]. This rule can be written as an equation as follows:
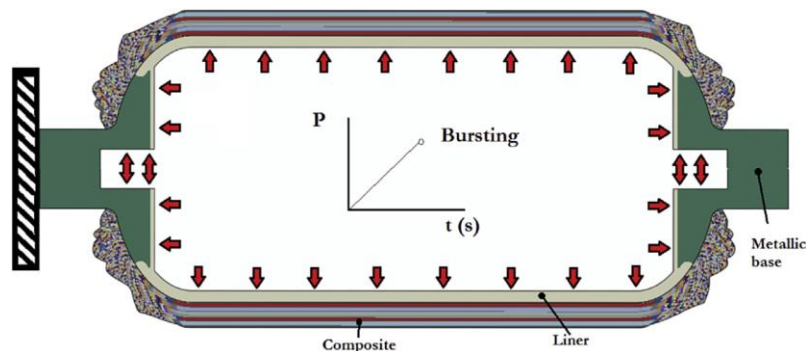
$$P = f_A P_A + f_B P_B = (1 - f_A) P_B \tag{61}$$

This equation is considered the upper bound (Reuss model). On the other hand, if the composition of each phase of the system is divided, for each of the properties, the lower bound is obtained.

$$\frac{1}{P} = \frac{f_A}{P_A} + \frac{f_B}{P_B} = \frac{f_A}{P_A} + \frac{(1 - f_A)}{P_B} \tag{62}$$

This lower bound is used when the property to be calculated largely depends on the fibre direction of the composite material or its porosity. In the case to be studied in this chapter, the heat capacity does not depend on the structure of the mixture of composites [27], so only the upper bound equation (61) will be used.

To find the temperature inside the tank, an energy balance of the thermodynamic system can be considered, between the initial- and the final moment. As seen previously, the kinetic energy is negligible compared to the internal energy, and when working with a gas, the potential energy will be practically zero.

Using the first law of thermodynamics [34] to calculate the internal energy in each state and in each phase that forms the system, the following expression is obtained.

$$m_0 C_v T_0 + m_w C_w T_{w0} + (m - m_0) C_p T_{in} = m C_v T + m_w C_w T_w \tag{63}$$

The third term on the left side of the equality represents the amount of mass that has entered the system, whose inlet pressure and temperature are constant.

To continue this process, it is necessary to assume that the thermal resistance of the tank wall is negligible. Below is a brief demonstration of why this is.

According to the article *Thermal properties of carbon fiber-epoxy composites with different fabric waves* [35] it can be assumed that the carbon fibre composite has a thermal conductivity of $24\ W/(mK)$. In addition, the dimensions of the tank wall are also known, that at an intermediate point, the thickness of this material is 0.05 m. So, with these data, it is possible to calculate the value of the thermal resistance of the wall using the following formula [36].

$$R = \frac{L}{k} = \frac{0.05\ m}{24\ W/(mK)} = 0.00208\ Km^2/W \tag{64}$$

This shows that the thermal resistance of the wall can be neglected, and therefore it can be assumed that the temperature of the nitrogen inside the tank is the same as the temperature of the wall of the tank. $T_w = T$ , $T_{w0} = T_0$. Transforming the equation (63) into the following.

$$m_0 C_v T_0 + m_w C_w T_0 + (m - m_0) C_p T_{in} = m C_v T + m_w C_w T \tag{65}$$

In accordance with what was previously explained regarding the general rule of mixtures, it is possible to create a parameter or property of the thermodynamic system. This relates the initial heat capacity of the system with the available heat capacity, as a function of the mass of nitrogen inside the tank. That property is going to be called $f_{MC}$, and it can be written as:

$$f_{MC} = \frac{m_0 C_v + m_w C_w}{m C_v + m_w C_w} \tag{66}$$

Taking the equation (65) as a starting point, and transforming it into the form of the upper bound equation (61) seen above by using the factor $f_{MC}$, an expression is obtained that provides the temperature inside the tank in function of known or established parameters.

$$T = f_{MC} T_0 + (1 - f_{MC}) \gamma T_{in} \tag{67}$$

Since a study will be carried out during the entire filling process, it is necessary to also know the intermediate conditions of the process, so that the mass in the tank will vary as a function of time. This variation is given by the equation of conservation of mass (33). Therefore, when implementing the temperature equation in the excel sheet, it should be done as follows.

$$T_n = \left( \frac{m_0 C_v + m_w C_w}{m_n C_v + m_w C_w} \right) T_0 + \left( 1 - \frac{m_0 C_v + m_w C_w}{m_n C_v + m_w C_w} \right) \gamma T_{in} \tag{68}$$

The properties of the tank wall are not yet known, for this it is possible to resort to previously carried out studies, which can provide an estimate of these properties. In the case of the carbon fibre composite mass, Figure 33 published in the reference [37] can be used. Where the geometry of the tank and the mass of hydrogen that can store at 700 bar are known, it is possible to establish an approximate mass of given material.

| FE model | H$_2$, kg | L/D | ID, mm | Thickness, mm | | | | CF composite weight, kg |
|----------|-----------|-----|--------|---------|------|-------|---------|-------------------------|
| | | | | Helical | Hoop | Doily | End-cap | |
| V36-DY-30 | 1.4 | 3.0 | 246 | 9.0 | 11.1 | 4.5 | No | 23.1 |
| V52-DY-25 | 2.0 | 2.5 | 300 | 11.0 | 13.3 | 5.0 | No | 33.3 |
| V73-DY-30 | 2.8 | 3.0 | 310 | 11.3 | 14.0 | 5.5 | No | 46.0 |
| V104-DY-16 | 4.0 | 1.6 | 378 | 15.5 | 20.0 | 6.0 | No | 68.0 |
| V145-ND-15 | 5.6 | 1.5 | 521 | 22.4 | 23.5 | – | No | 103.6 |
| V145-DY-15 | 5.6 | 1.5 | 521 | 17.8 | 23.5 | 6.5 | No | 93.1 |
| V145-ND-30a | 5.6 | 3.0 | 391 | 18.5 | 19.6 | – | No | 107.4 |
| V145-ND-30b | 5.6 | 3.0 | 391 | 18.5 | 17.6 | – | No | 102.0 |
| V145-DY-30 | 5.6 | 3.0 | 391 | 14.3 | 17.6 | 5.5 | No | 91.0 |
| V145-EC-30 | 5.6 | 3.0 | 391 | 14.3 | 17.6 | – | 5.0 | 92.6 |

Figure 33 Geometry and weight of the composite for different models [37]

To obtain a valid value of the heat capacity of the wall, the experimental results produced by the following study titled: *Thermal properties of autoclave and out-of-autoclave carbon fiber-epoxy composites with different fiber weave configurations* [35].

## 4.2.2 Results and discussion

The data and values used throughout this section will be presented. It also indicates in more detail how those properties of nitrogen have been obtained, that cannot be found directly in tables or records.

Table 5 Nitrogen properties

| Nitrogen properties | |
|---|---|
| Density (0,1MPa) | 1,2504 |
| K (W/(k·m)) | 0,02598 |
| Cp (J/kg·K) | 1040 |
| α | 2,00E-05 |
| γ | 1,4 |
| R (J/kg·K) | 297 |
| Cv (J/kg·K) | 743 |

To calculate the dimensionless heat transfer coefficient α, equation (50) has been used as follows.

$$\alpha = \frac{k}{\rho C_p} = \frac{0.55}{1.2504 \times 1040} \approx 4.2 \times 10^{-4}$$

It should be noted that during the filling process, the nitrogen density does not have to be kept strictly constant since the pressure and temperature increases. But using the conservation of mass equation, it can be verified that the increase in mass will always be constant and will be the reference that will be used.

Below are the values used for ambient temperature and properties of the mass inflow.

| Temperatures | | Mass inflow | |
|---|---|---|---|
| $T_{amb}$ (K) | 294 | Mass inflow (kg/s) | 0,01 |
| | | $T_{in}$ (K) | 294 |

These data can be modified depending on the conditions in which the experiment is carried out, and the program created in the excel sheet (Appendix B) will calculate the new results of temperature and pressure in the tank at each instant of time.

Finally, these are the data related to the type IV hydrogen tank that will be used for the experiment.

Table 6 Tank properties

| Tank properties | |
|---|---|
| Volume (m^3) | 0,0368 |
| $m_0$ (kg) | 0,0421 |
| $p_0$ (bar) | 1 |
| C wall (J/kg·K) | 1040 |
| Tank wall mass (kg) | 28 |
| $T_0$ (K) | 294 |

The data of the volume can be found in appendix A, while the data of the mass of material in the walls is present in the Figure 33. Finally, the data on the heat capacity of the wall has been obtained from the reference [38].

### 4.2.2.1 Adiabatic case

In the Table 7 first rows of the created excel table are shown.

Table 7 Adiabatic case excel configuration

| Time (s) | Pressure (Bar) | Tank Temperature (K) | Tank Mass (kg) | dT/dt | dP/dt |
|---|---|---|---|---|---|
| 0 | 1,00 | 294,000 | 0,042 | 27,885 | 0,033 |
| 0,1 | 1,03 | 296,789 | 0,043 | 26,592 | 0,033 |
| 0,2 | 1,07 | 299,448 | 0,044 | 25,388 | 0,033 |
| 0,3 | 1,10 | 301,987 | 0,045 | 24,263 | 0,033 |
| 0,4 | 1,13 | 304,413 | 0,046 | 23,211 | 0,033 |
| 0,5 | 1,17 | 306,734 | 0,047 | 22,227 | 0,033 |
| 0,6 | 1,20 | 308,957 | 0,048 | 21,303 | 0,033 |
| 0,7 | 1,23 | 311,087 | 0,049 | 20,436 | 0,033 |
| 0,8 | 1,27 | 313,131 | 0,050 | 19,621 | 0,033 |
| 0,9 | 1,30 | 315,093 | 0,051 | 18,854 | 0,033 |
| 1 | 1,33 | 316,978 | 0,052 | 18,131 | 0,033 |

In the first column the time interval appears, which must be set by the user. In the second column, equation (41) has been introduced to calculate the pressure inside the tank, the initial pressure inside the tank must also be set by the user. In the case of temperature, equation (27) has been introduced, although like the pressure, the initial temperature in the tank is a condition set by the user.

The last two columns have been added to observe how the increase in temperature varies as the tank fills, and in the case of the variation of pressure as a function of time, it serves as a control parameter that the conservation equation of the mass is being fulfilled. For this purpose, equation (24) and equation (38) have been used respectively.

Table 8 Pressure which reach critical safety temperature

| Time (s) | Pressure (bar) | Temperature (K) | Mass (kg) | dT/dt | dP/dt |
|---|---|---|---|---|---|
| 4,5 | 2,49 | 355,39 | 0,087 | 6,44 | 0,033 |
| 4,6 | 2,53 | 356,03 | 0,088 | 6,29 | 0,033 |
| 4,7 | 2,56 | 356,66 | 0,089 | 6,15 | 0,033 |
| 4,8 | 2,59 | 357,27 | 0,090 | 6,01 | 0,033 |
| 4,9 | 2,63 | 357,88 | 0,091 | 5,88 | 0,033 |
| 5 | 2,66 | 358,46 | 0,092 | 5,75 | 0,033 |
| 5,1 | 2,69 | 359,04 | 0,093 | 5,63 | 0,033 |
| 5,2 | 2,73 | 359,60 | 0,094 | 5,51 | 0,033 |
| 5,3 | 2,76 | 360,15 | 0,095 | 5,39 | 0,033 |

For a purging pressure of 2.63 bar, 85°C is reached, which is the maximum temperature that the tank manufacturer allows, due to safety reasons. This pressure is far from a reasonable purge pressure, and much farther from the 700 bar of hydrogen that the tank can store. It is true that the properties of nitrogen and hydrogen are different, but this does not justify this low pressure.

There are two reasons for this. The first is that the tank is being considered adiabatic, so the heat cannot leave it, the second is that the heat that the walls are capable of storing is not being taken into account. In the following chapters it will be shown how these two reasons affect the final result of the temperature.
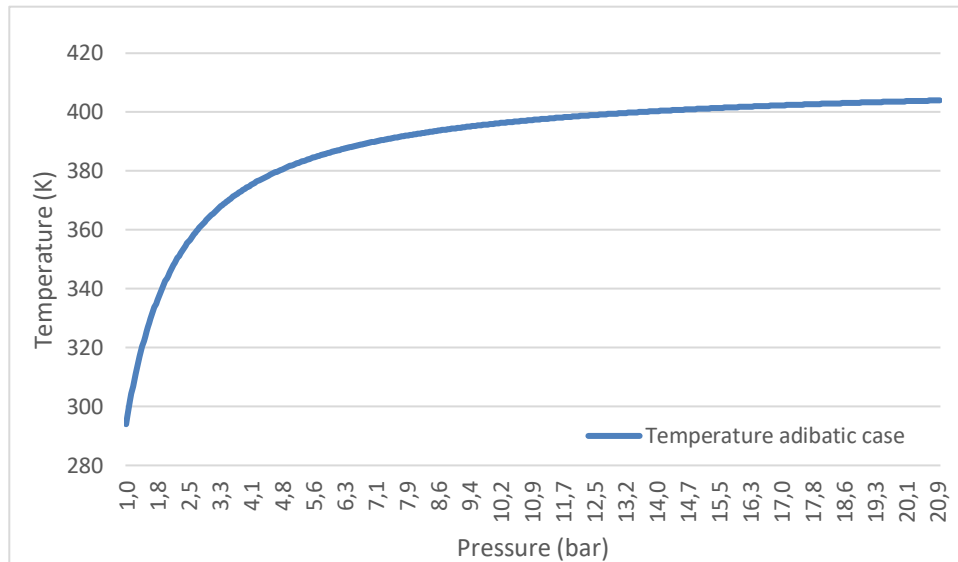


Figure 34 Temperature results as a function of pressure

At first, the temperature increases rapidly because the mass inside the tank is smaller, and the temperature difference between the mass inflow and the interior is not very high. As the mass inside the tank increases, it is more difficult to gain temperature. In addition, the mass inflow begins to have a cooling effect because its temperature is much lower than that of the interior, so the curve will flatten out.

This curve is for a mass flow of 0.01kg/s, but if the mass flow were too high (greater than 0.5kg/s) a very high temperature increase would occur in the first instant of time and then the mass flow would act as a coolant until the temperature stabilized at one point.
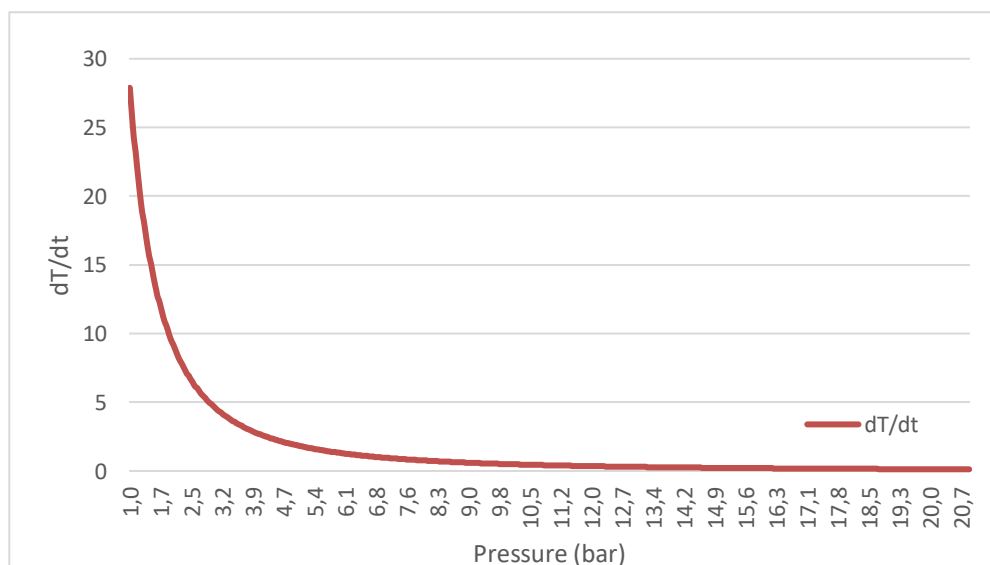


Figure 35 dT/dt as a function of pressure

Everything explained above can be seen in the Figure 35 as at first the temperature increase is very high, but the curve flattens when the pressure increases. Being the shape of the opposite curve to the Figure 34.
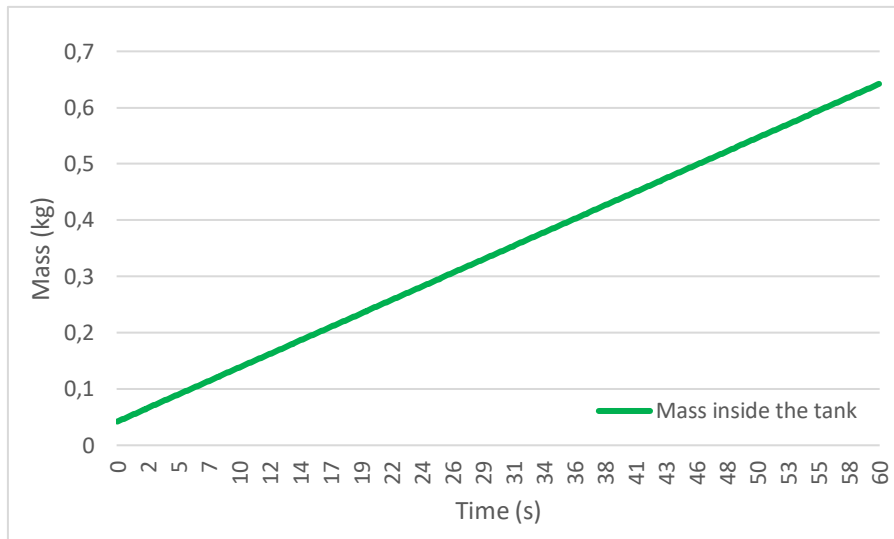


Figure 36 Mass inside the tank as a function of time

Finally, Figure 36 shows that the equation for the conservation of mass is being fulfilled, since the slope of the line always remains constant. This slope is only given by the mass inflow.

## 4.2.2.2 Non-adiabatic case

In this chapter the term of the heat rate will be considered. However, the control volume will continue to be the interior of the tank, so the properties of the walls do not intervene in the equation (60).

It will only be observed how the thermodynamic properties of the gas affect the temperature of the gas when it increases in pressure, and if indeed this term can be neglected without affecting the final result.

To calculate the value of this term, equation (49) will be used, where the term $\alpha$ has already been calculated in section 4.2.2, and will remain constant for any temperature since it only depends on the properties of nitrogen. As an example, it is shown how the $\dot{Q}$ value has been calculated for a temperature inside the tank of 320 K.

$$\dot{Q} = \dot{m}_{in}\alpha C_v \left(T_f - T\right) = 0.01 \times 2 \times 10^{-5} \times 743 \times (294 - 320) = -0.003864 \, W$$

As seen above the heat rate is very low, this is because the heat transfer coefficient is in the order of $10^{-5}$ and the mass inflow is not too high. It has a negative sign because the heat is leaving the thermodynamic system.

The following shows how the heat rate evolves as a function of the pressure inside the tank.
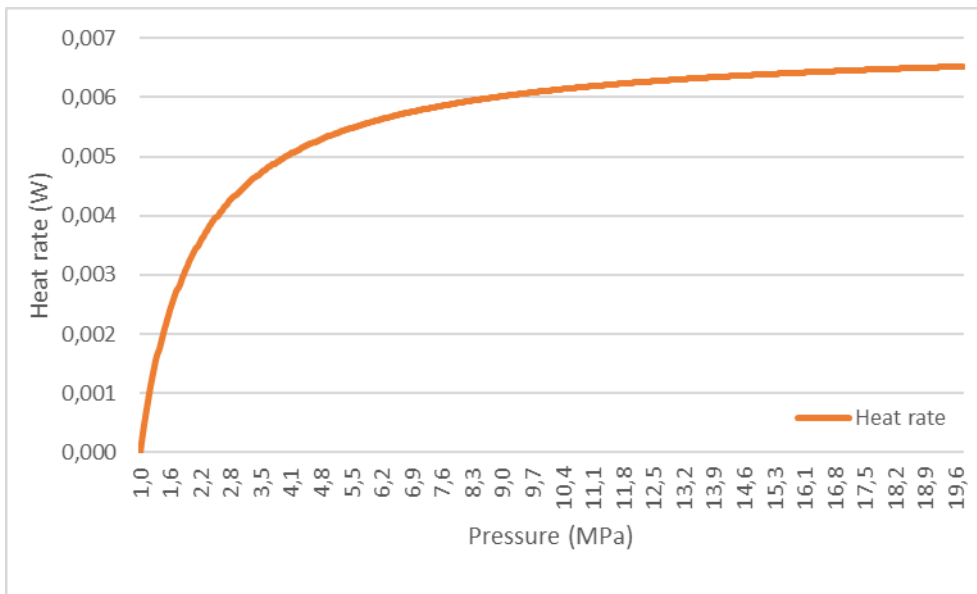
Figure 37 Heat rate as a function of pressure

It is logical to think that this graph is going to have a very similar shape to the temperature, because the heat rate basically depends on the temperature difference between the gas inside the tank and the temperature of the external fluid. Therefore, when the temperature inside stabilizes, so does the heat flow.

Following the same procedure as in the previous section, the equations (41),(57) and (60) have been entered in an excel sheet, creating 0.1 second intervals to establish the time. In the Figure 38 Non-adiabatic case temperature as a function of pressure it is possible to observe how the temperature evolves as a function of time.
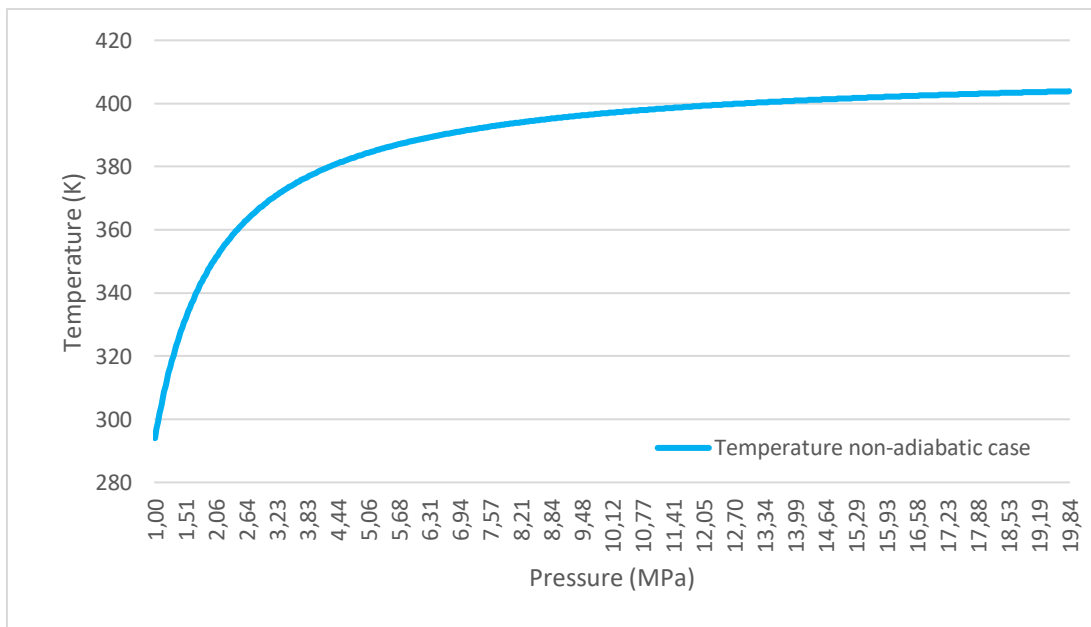


Figure 38 Non-adiabatic case temperature as a function of pressure

As expected, it has a shape similar to that of the adiabatic case. In Figure 39 the temperature of the adiabatic case is compared with that of the non-adiabatic.
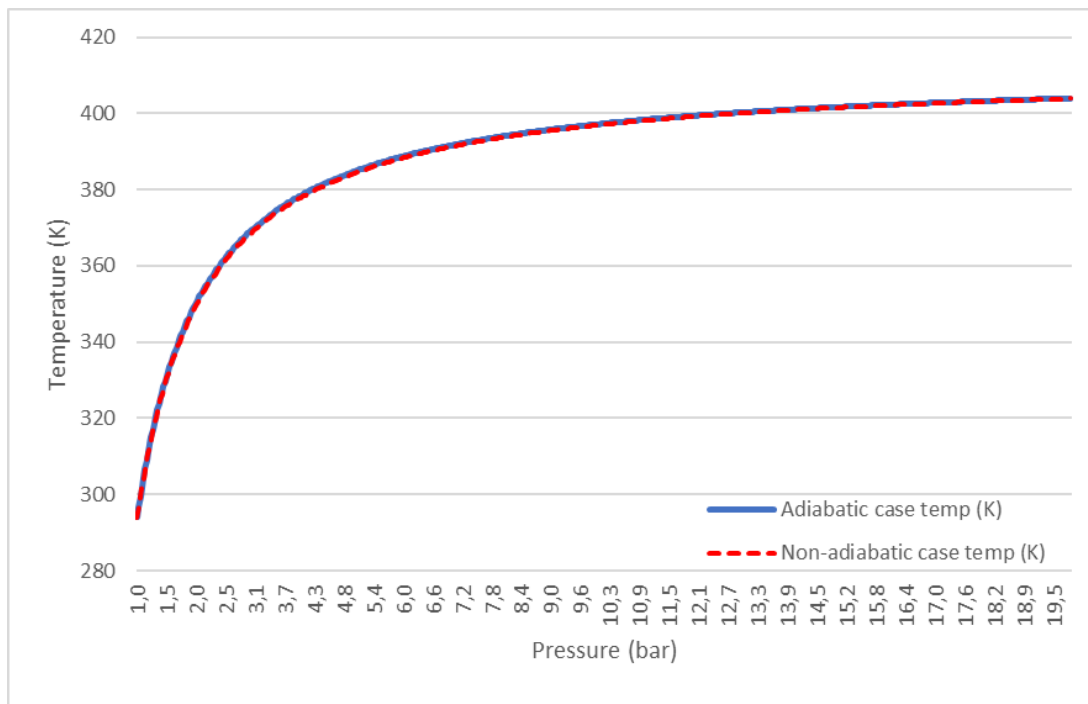


Figure 39 Adiabatic and non-adiabatic case temperatures comparison

At a first glance it is hardly possible to see any difference between the two cases, which confirms that it is possible to eliminate the term of the heat rate since it is practically negligible and does not affect the final temperature.

Table 9 Adiabatic and non-adiabatic temperature comparation

| Adiabatic and non-adiabatic case temperatures comparation | | | |
|---|---|---|---|
| Time (s) | Pressure (bar) | Adiabatic case temp (K) | Non-adiabatic case temp (K) |
| 0 | 1,00 | 294 | 294 |
| 0,1 | 1,02 | 296,78 | 296,72 |
| 0,2 | 1,05 | 299,44 | 299,32 |
| 0,3 | 1,07 | 301,98 | 301,81 |
| 0,4 | 1,10 | 304,41 | 304,19 |
| 0,5 | 1,12 | 306,73 | 306,47 |
| 0,6 | 1,15 | 308,95 | 308,65 |
| 0,7 | 1,17 | 311,08 | 310,75 |

For more details see the excel document in appendix B. Also, the Table 9 shows in more detail how the difference is between the two cases, and it can be seen that it barely reaches 4 tenths of a degree, which not significant in this study.

### 4.2.2.3 Application of the heat capacity of the walls

In this section, the temperature closest to reality will be calculated according to the method explained above. This will show at what pressure the purging process can be carried out without exceeding the maximum recommended temperature inside the tank.

Firstly, it will be explained how the data regarding the tank wall have been obtained, based on the references [35] and [37].

To calculate the specific heat of the material, the data shown in Table 10 has been used. In this study a type 4 CFRP tank is being used.

Table 10 Relevant thermal properties of the tank material [38]

| Materials | Temperature(ºC) | Density (kg/m$^3$) | Thermal capacity (J/(kgK)) | Thermal conductivity (W/(mK)) |
|---|---|---|---|---|
| Type 4 tank CFRP layer | 23 | 1442 | 942 | 0.53 |
| | 40 | 1439 | 1010 | 0.54 |
| | 60 | 1434 | 1069 | 0.56 |
| | 80 | 1430 | 1129 | 0.56 |
| | 100 | 1434 | 1221 | 0.58 |

The temperature inside the tank will always stay between 20ºC and 85ºC in the worst case, so being conservative a thermal capacity value of 1000 J/(kg·K) has been selected.

In the case of the carbon fibre composite mass, it is known that the tank can store 2kg of H$_2$. Using the drawings in the appendix A an L/D ratio of 2.84 is obtained. Observing Figure 33, the tank used for this study is in an intermediate case between the first and the second, so making an approximation using a linear regression concludes that a 28kg mass may be adequate.

Once the data from the tank wall have been obtained, the equations can be formulated. The temperatures obtained in section 4.2.2.2 have been used to have them as a reference.

To do this, it has started with Table 9 adding also two new columns to calculate the $f_{MC}$ factor and the final temperature inside the tank taking into account the heat that the walls can store.

Table 11 Tank wall capacity case

| Time (s) | Mass(kg) | Temp tank (K) | dT/dt | Pressure (bar) | $f_{MC}$ | Temp tank (K) (wall capacity) |
|---|---|---|---|---|---|---|
| 0 | 0,042 | 294 | 2,725 | 1,00 | 1 | 294 |
| 0,1 | 0,043 | 296,72 | 2,602 | 1,02 | 0,99996 | 294,003 |
| 0,2 | 0,044 | 299,32 | 2,486 | 1,05 | 0,99993 | 294,007 |
| 0,3 | 0,045 | 301,81 | 2,379 | 1,07 | 0,99990 | 294,011 |
| 0,4 | 0,046 | 304,19 | 2,278 | 1,10 | 0,99987 | 294,016 |
| 0,5 | 0,047 | 306,47 | 2,183 | 1,12 | 0,99984 | 294,020 |
| 0,6 | 0,048 | 308,65 | 2,094 | 1,15 | 0,99981 | 294,025 |
| 0,7 | 0,049 | 310,75 | 2,011 | 1,17 | 0,99978 | 294,030 |

To calculate the factor $f_{MC}$ the equation (66) has been used, where it can be seen that as the mass within the tank increases this factor decreases. This indicates that as the nitrogen mass increases, the ability to store heat in the walls decreases. Figure 40.
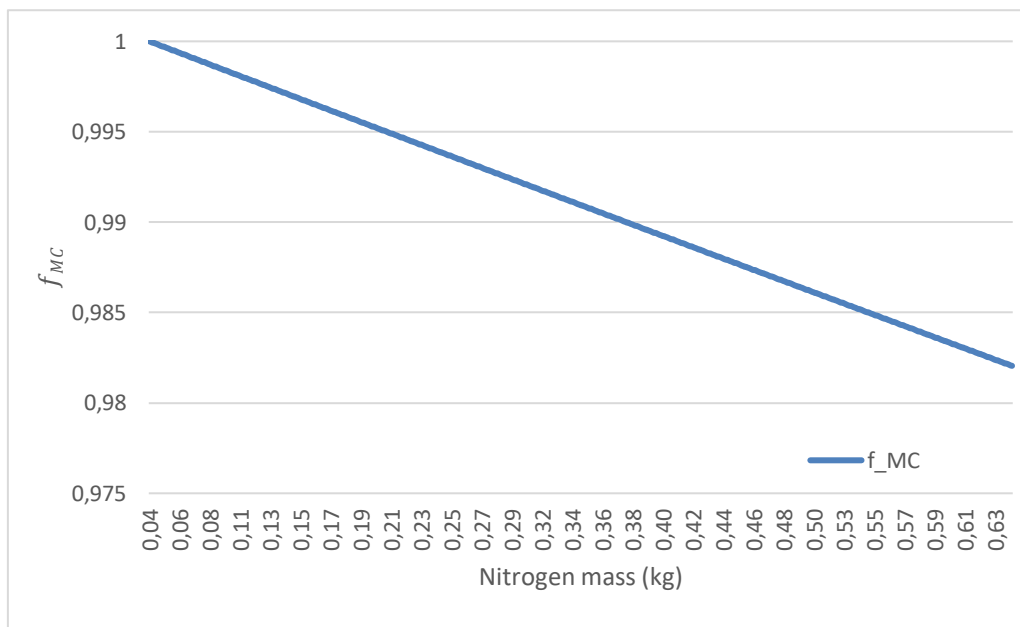


Figure 40 $f_{MC}$ as a function of nitrogen mass inside the tank

This factor decreases slowly because the mass of the gas compared to the mass of the tank wall is very small. The higher the density of the gas used, the greater the slope.

Finally, to calculate the temperature, equation (68) has been used, where the only variable is the factor $f_{MC}$. In this case it is not an integral equation which can be derivated to obtain each value, but it is possible to calculate the temperature as a function of the mass inside the tank, which in turn is dependent on the pressure.
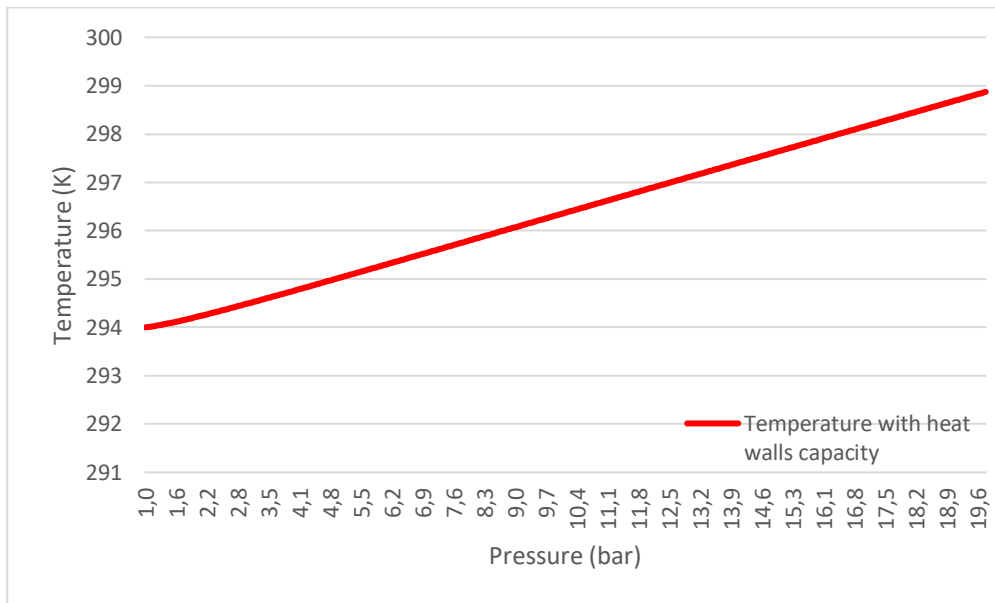
Figure 41 Temperature with heat walls capacity as a function of the pressure

In Figure 41, it is clearly seen how the temperature increases much more slowly now. In fact, with a pressure increase of 20 bars the temperature only increases by 5 K. These results may make sense, since the tank is built to be filled with hydrogen at 700 bar, so although it is true as the properties of nitrogen and hydrogen differ quite a bit, it should not be a problem in terms of temperatures, to carry out the purge process at pressures of around 10 bar.

As a curiosity, the Figure 42 shows the shape of the curve in general form for a pressure of 240 bar, since at a pressure of 20 bar the real trend cannot be seen.
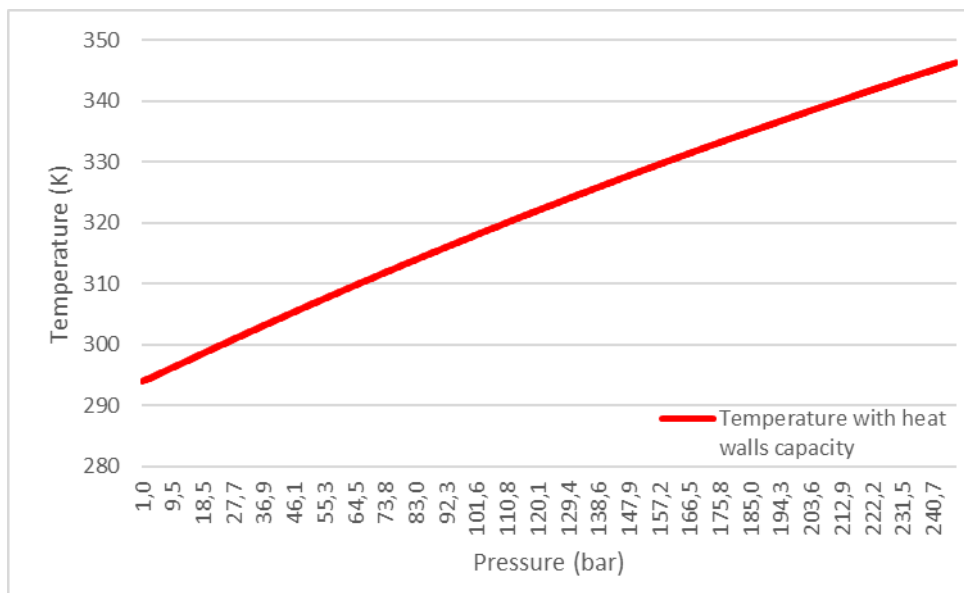


Figure 42 Temperature with heat walls capacity as a function of pressure

Lastly, a comparison is shown between the temperatures obtained in the section 4.2.2.2 and those obtained in this section 4.2.2.3. Here one can see the importance of including the tank walls in the thermodynamic system, but in a very simplified way, as has been done in this study.
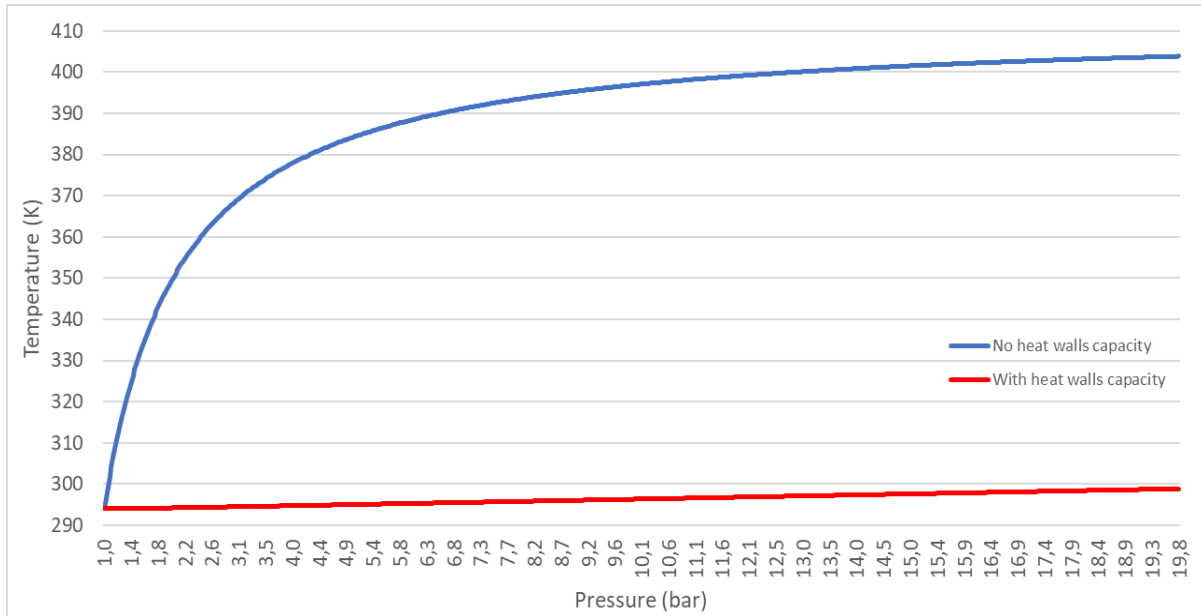


Figure 43 Comparison between temperatures in case 4.2.2.2 and case 4.2.2.3

In this method the heat that leaves the tank wall through conduction and convection is neglected. Although, since the difference between the wall temperature and the ambient temperature does not exceed 5 K, it can be considered practically zero. However, if the temperature increases more, using the one-way transient conduction method would be a viable way of dealing with the increase.

The excel program present in the appendix B is prepared to be able to change the initial and environmental conditions at all times and obtain new results.

# 5 Hydrogen filling process

After the purge process, the tank is filled with hydrogen to carry out future experiments. In this chapter the pressure and temperature conditions will be studied during this filling process. These conditions inside the tank are limited by the design conditions that are the following (Appendix A):

- The temperature inside the tank should never be higher than 358K (85°C).
- The maximum filling pressure is 875 bar.
- The maximum service pressure is 700 bar.
- The maximum pressure that can be in the system is 720 bar due to safety relief valve.

To calculate the temperature during the filling process, it is based on the data and results in the study entitled: *"Measured effects of filling time and initial mass on the temperature distribution within a hydrogen cylinder during refuelling"* [39] written by C.J.B. Dicken, and W. Mérida.

In this case it has not been possible to apply the method in section 4.2.1.3. This is because in this method it is considered that the tank walls are adiabatic, which when working with high pressures would make a big difference between the actual temperature in the inside the tank, and the one obtained mathematically.

This experiment [39] has been selected because a large number of thermocouples distributed uniformly throughout the tank have been used to carry out the measurements. This provides very accurate data despite the simplifications and hypotheses that must be performed in order to use those data in this study.

In the case of the cooling time when hydrogen does not go into the tank, an energy balance has been proposed for the tank wall, calculating the heat that passes through the wall at each moment by using the global transmission coefficient.

It must be taken into account that during the first filling, the initial pressure in the tank will be very low, therefore it will be seen how this affects the total time of the operation.

## 5.1 Method

Two different procedures have been used in this chapter. First there is the filling stage, when the hydrogen enters the tank and secondly there is the cooling stage, which is when there is no hydrogen entering the tank.

### 5.1.1 Filling stage

For this case, the same method could have been used as that used in chapter 4.2.1.3. However, when working with much higher pressures, it has been decided to use a more accurate method, obtained by taking real temperature data. This data have been taken from the reference [39], and below are the simplifications and considerations that had to be made to apply it to this study.

- It is assumed that the heat flow loss by a type 3 tank is almost identical to that of type 4.
- The diameter of the type 3 cylinder is 23% larger than the type 4 cylinder, so it is possible that the temperature in the type 4 cylinder is slightly higher. This effect will be neglected.
- The maximum filling pressure of the tank used in the article is 350 bar, while in this study it will be up to 700 bar.
- In the article, a constant mass inflow is not used. It decreases as the pressure in the tank increases. In this study, a constant average mass inflow has been calculated with the data provided in the article.
- Hydrogen is assumed to behave as an ideal gas.

When selecting the necessary data from the article, it has been taken into account that the tank in this project will be used to carry out future experiments related to hydrogen safety. For this reason, the filling time of the tank does not have to be as fast as possible since it is not in a transport application. It has been chosen to use the slowest filling time offered by the referenced article, which is 370 seconds and calculate the average mass inflow based on these data.
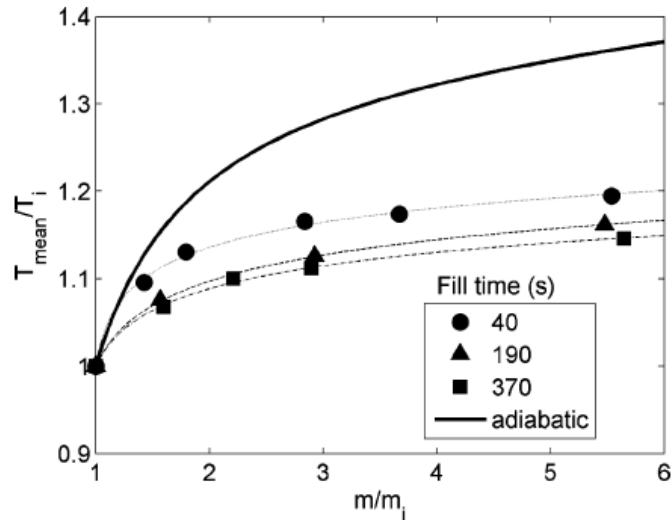


Figure 44 Normalized temperature vs. the normalized mass increase for three fill rates [39]

The total mass of hydrogen that the tank can have is 2.14 kg. So, using the data shown in Figure 44 for a filling time of 370 seconds, it can be deduced that the initial mass of the tank is one sixth of the total, that is, 0.35 kg.

$$\dot{m} = \frac{m - m_0}{t} \approx 0.005 kg/s \tag{69}$$

Once the mass flow is known, the temperature can be calculated, based on the mass of hydrogen inside the tank by using this expression.

$$\frac{T_{mean}}{T} = \left( A + B \left( \frac{m}{m_0} \right)^{1/2} \right)^c \tag{70}$$

In order to implement the equation inside the excel sheet, it can be written as follows:

$$T_n = T_0 * \left( A + B \left( \frac{m_n}{m_0} \right)^{1/2} \right)^c \tag{71}$$

This equation has been generated from experimental data, adjusting to the temperatures obtained for different masses inside the tank. Parameters A, B and C vary depending on the speed with which the tank fills, as can be seen in Figure 45.

| Fill time (s) | A | B | C |
|---|---|---|---|
| 40 | −35.17000 | 36.16000 | 0.04595 |
| 190 | −9.50400 | 10.50000 | 0.05526 |
| 370 | −10.51000 | 11.50000 | 0.04841 |

Figure 45 Curve fitting coefficient for the equation (71) [39]

Once the mass inflow is known, the mass inside the tank can be determined at each instant of time using equation (57). This will, in turn, be introduced into equation (71), where the temperature will be obtained.

As the pressure is a limiting factor, it is always necessary to be able to know the pressure inside the tank. For this, the ideal gas equation can be used, obtaining the following expression:

$$p_n = \frac{m_n \cdot R \cdot T_n}{V} \tag{72}$$

With these equations it is possible to know the pressure and temperature inside the tank during the filling stage, based on time and the mass inflow.

## 5.1.2 Cooling stage

Since the initial pressure of the tank in the first filling is going to be very low (1 bar), it is not possible to carry out the filling in a single stage due to pressure and temperature limitations. Therefore, it is necessary to introduce cooling stages, where the entry of gas into the tank is interrupted and the hydrogen already present inside, can lose temperature and as a consequence also reduce its pressure.

Due to the complexity of this topic, certain simplifications have been made regarding the structure and geometry of the tank, which are:

- A horizontal cylinder 0.9 meters long has been considered.
- The plastic layer has been neglected due to its small thickness compared to the carbon fibre composite layer.
- The heat lost through the boss of the tank has not been taken into account, since it is made of another material (steel) and the surface they occupy with respect to the carbon fibre composite, is small.

In order to obtain an expression that provides the hydrogen temperature at each instant of time, two concepts have been used. On one hand, an energy balance has been proposed for the hydrogen inside the tank. However, this time there is not mass inflow going into the control volume. [28].

$$\iiint \frac{d}{dt}(C_v T)\rho dV = -\dot{Q} \tag{73}$$

For the reasons explained in previous chapters, only the variation of internal energy is taken into account, in addition the heat cannot be neglected in this case, which is going to be considered with a negative sign since it leaves the system.

On the other hand, the overall heat transfer coefficient method has been applied to calculate the rate of heat leaving the tank as a function of the gas temperature and the outside temperature.

$$\dot{Q} = UA(T_{inside} - T_{amb}) \tag{74}$$

Combining the equation (73) and the equation (74) the following new expression is obtained.

$$\iiint \frac{d}{dt}(C_v T)\rho dV = -UA(T_{inside} - T_{amb}) \tag{75}$$

The volume of the tank will remain constant all the time and applying that $\rho = m/V$, the equation is simplified in this way.

$$\frac{d}{dt}C_v T m = -UA(T_{inside} - T_{amb}) \tag{76}$$

During the cooling stage the mass in the tank will remain constant since there is no mass inflow, the factor $C_v$ is also constant since it is an inherent property of the hydrogen, so the equation can be written like this.

$$\frac{dT}{dt} = \frac{1}{mC_v}(-UA(T_{inside} - T_{amb})) \tag{77}$$

Moving the temporal term to the other side of equality we can propose the following integral.

$$\int_{T_0}^{T_n} dT = \frac{-1}{mC_v}(UA(T_{inside} - T_{amb}))\int_{t_0}^{t_n} dt \tag{78}$$

Solving the integral gives the form of the final equation.

$$T_n = T_{n-1} - \frac{1}{mC_v}\left(UA(T_{n-1} - T_{amb})\right) \cdot \Delta t \tag{79}$$

Regarding the overall coefficient of heat transmission (UA), to calculate it the analogy of thermal resistances has been used (Figure 46), where it can be seen that there are three different types of heat transmission.

- Convection from hydrogen at a certain pressure to the inner wall of the tank.
- Conduction along the thickness of the wall.
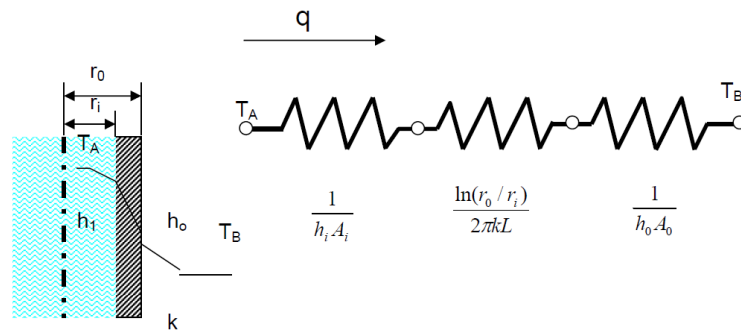- Natural convection from the outer wall to the outside.



Figure 46 Thermal resistances throughout the tank [40]

This overall coefficient is the inverse of the sum of the thermal resistances present in the system, so it can now be calculated as follows. [40]

$$UA = \frac{1}{R} = \frac{1}{\dfrac{1}{A_i h_i} + \dfrac{\ln{(r_0/r_i)}}{2\pi kL} + \dfrac{1}{A_o h_o}} \tag{80}$$

All the geometric data of the tank have been obtained from Appendix A, making the simplification to a cylinder. Regarding to the convection coefficients, for the interior the data provided by the references [41] and [42] have been used, from which it can be extracted that an adequate average coefficient for hydrogen under pressure is $250\ W/(m^2\ K)$.

The conduction coefficient of the tank material has been obtained from the thermal properties present in Table 7. Since the temperature varies, an average coefficient of 0.55 $W/(m\ K)$ has been chosen.

In the case of the external convection coefficient, it can be calculated analytically since the properties of air at 21ºC can be easily found. Specifically, the properties present in the Figure 47.

| Temp. $T$, °C | Density $\rho$, kg/m$^3$ | Specific Heat $c_p$ J/kg·K | Thermal Conductivity $k$, W/m·K | Thermal Diffusivity $\alpha$, m$^2$/s | Dynamic Viscosity $\mu$, kg/m·s | Kinematic Viscosity $\nu$, m$^2$/s |
|---|---|---|---|---|---|---|
| −150 | 2.866 | 983 | 0.01171 | $4.158 \times 10^{-6}$ | $8.636 \times 10^{-6}$ | $3.013 \times 10^{-6}$ |
| −100 | 2.038 | 966 | 0.01582 | $8.036 \times 10^{-6}$ | $1.189 \times 10^{-6}$ | $5.837 \times 10^{-6}$ |
| −50 | 1.582 | 999 | 0.01979 | $1.252 \times 10^{-5}$ | $1.474 \times 10^{-5}$ | $9.319 \times 10^{-6}$ |
| −40 | 1.514 | 1002 | 0.02057 | $1.356 \times 10^{-5}$ | $1.527 \times 10^{-5}$ | $1.008 \times 10^{-5}$ |
| −30 | 1.451 | 1004 | 0.02134 | $1.465 \times 10^{-5}$ | $1.579 \times 10^{-5}$ | $1.087 \times 10^{-5}$ |
| −20 | 1.394 | 1005 | 0.02211 | $1.578 \times 10^{-5}$ | $1.630 \times 10^{-5}$ | $1.169 \times 10^{-5}$ |
| −10 | 1.341 | 1006 | 0.02288 | $1.696 \times 10^{-5}$ | $1.680 \times 10^{-5}$ | $1.252 \times 10^{-5}$ |
| 0 | 1.292 | 1006 | 0.02364 | $1.818 \times 10^{-5}$ | $1.729 \times 10^{-5}$ | $1.338 \times 10^{-5}$ |
| 5 | 1.269 | 1006 | 0.02401 | $1.880 \times 10^{-5}$ | $1.754 \times 10^{-5}$ | $1.382 \times 10^{-5}$ |
| 10 | 1.246 | 1006 | 0.02439 | $1.944 \times 10^{-5}$ | $1.778 \times 10^{-5}$ | $1.426 \times 10^{-5}$ |
| 15 | 1.225 | 1007 | 0.02476 | $2.009 \times 10^{-5}$ | $1.802 \times 10^{-5}$ | $1.470 \times 10^{-5}$ |
| 20 | 1.204 | 1007 | 0.02514 | $2.074 \times 10^{-5}$ | $1.825 \times 10^{-5}$ | $1.516 \times 10^{-5}$ |
| 25 | 1.184 | 1007 | 0.02551 | $2.141 \times 10^{-5}$ | $1.849 \times 10^{-5}$ | $1.562 \times 10^{-5}$ |

Figure 47 Properties of air at 1 atm pressure [43]

To calculate the convection coefficient, we use the expression that relates it to the Nusselt number ($Nu$), which in the case of a cylinder is [44]:

$$h_o = \frac{Nu \cdot k}{D} \tag{81}$$

In the case of long horizontal cylinders, the Nusselt number can be calculated using the Rayleigh number, which in turn, is based on the geometric properties of the cylinder and the thermodynamic properties of the surrounding air.

$$Nu = C \cdot Ra^n \tag{82}$$

$$Ra = \frac{g\beta D_o{}^3(T_s - T_\infty)}{\alpha\nu} \tag{83}$$

The thermal expansion coefficient of air ($\beta$), can be obtained from the reference [45], for an average temperature of 328 K.

The factors "C" and "n" are given by the following table as a function of the Rayleigh number value.

Table 12 Value of "C" and "n" as a function of Rayleigh number [44]

| Ra | C | n |
|---|---|---|
| $10^{-10}$-$10^{-2}$ | 0,675 | 0,058 |
| $10^{-2}$-$10^2$ | 1,02 | 0,148 |
| $10^2$-$10^4$ | 0,850 | 0,188 |
| $10^4$-$10^7$ | 0,480 | 0,250 |
| $10^7$-$10^{12}$ | 0,125 | 0,333 |

The value obtained for the external convection coefficient after solving the equation (81) is $5.44\ W/(m^2\ K)$, which is within the expected values.

Once all the necessary data has been collected or calculated, the final equation of the cooling stage to calculate the temperature at each instant of time, would be as follows.

$$T_n = T_{n-1} - \frac{1}{mC_v}\left(\frac{(T_{n-1} - T_{amb})}{\frac{1}{A_i h_i} + \frac{\ln(r_0/r_i)}{2\pi kL} + \frac{1}{A_o h_o}}\right) \cdot \Delta t \tag{84}$$

## 5.2 Results and discussion

To solve the equations, an excel sheet has been used, in which one-second intervals have been proposed for both the filling and cooling stages. Below are all the data used to solve the equations.

| Hydrogen propierties | |
|---|---|
| Density (1bar) | 0,0899 |
| K (W/(k·m)) | 0,1815 |
| Cp (J/kg·K) | 14319,3 |
| α | 1,40E-04 |
| γ | 1,405 |
| R (J/kg*K) | 4124,18 |
| Cv (J/kg·K) | 10191,9 |

| Heat transfer coeficients | |
|---|---|
| hi (W/(m^2·K) | 250 |
| ho (W/(m^2·K) | 5,44 |
| UA | 3,3576 |

| Temperatures and factors | |
|---|---|
| To (K) | 294 |
| T amb (K) | 294 |
| A | -10,51 |
| B | 11,50 |
| C | 0,0484 |

| Mass inflow | |
|---|---|
| Mass flow (kg/s) | 0,005 |
| Tin (K) | 294 |

| Tank propieties | |
|---|---|
| Volume (m^3) | 0,0368 |
| Mo (kg) | 0,003035 |
| Po (Bar) | 1 |
| C wall (J/kg·K) | 1040 |
| Tank wall mass (kg) | 28 |
| k wall(W/(K·m)) | 0,55 |
| R outside (m) | 0,1604 |
| R inside (m) | 0,1104 |
| L total (m) | 0,9 |
| A outside (m^2) | 1,0687 |
| A inside (m^2) | 0,7009 |

Figure 48 Data used to make the excel sheet

The excel sheet has been made as seen in Figure 49. It begins with the filling stage, where the equations (71) and (72) are applied to obtain the temperature and pressure, respectively. Once either of the two limit conditions is reached ($P_{lim}$=720 bar or $T_{lim}$=358K), the cooling stage begins.

| First filling stage (T lim=358K) | | | | First cooling stage | | | Second filling stage (P lim=720 bar) | | | | |
|---|---|---|---|---|---|---|---|---|---|---|---|
| Time (s) | m tank (kg) | m/m0 | Temp tank (K) | Pressure (bar) | Time (s) | Temp tank (K) | Pressure (bar) | Time (s) | m tank (kg) | m/m0 | Temp tank (K) | Pressure (bar) |
| 0 | 0,00304 | 1,000 | 293,857 | 1,000 | 21 | 357,8918 | 43,332 | 2003 | 0,10804 | 1 | 294,1502 | 35,614 |
| 1 | 0,00804 | 2,647 | 325,529 | 2,931 | 22 | 357,6970 | 43,308 | 2004 | 0,11304 | 1,04628 | 297,3807 | 37,672 |
| 2 | 0,01304 | 4,295 | 333,264 | 4,868 | 23 | 357,5027 | 43,285 | 2005 | 0,11804 | 1,09256 | 300,0819 | 39,695 |
| 3 | 0,01804 | 5,942 | 337,715 | 6,826 | 24 | 357,3091 | 43,261 | 2006 | 0,12304 | 1,13884 | 302,3314 | 41,687 |
| 4 | 0,02304 | 7,590 | 340,822 | 8,798 | 25 | 357,1160 | 43,238 | 2007 | 0,12804 | 1,18513 | 304,2562 | 43,657 |
| 5 | 0,02804 | 9,237 | 343,200 | 10,783 | 26 | 356,9236 | 43,215 | 2008 | 0,13304 | 1,23141 | 305,9366 | 45,613 |
| 6 | 0,03304 | 10,885 | 345,122 | 12,777 | 27 | 356,7317 | 43,191 | 2009 | 0,13804 | 1,27769 | 307,4261 | 47,558 |
| 7 | 0,03804 | 12,532 | 346,733 | 14,780 | 28 | 356,5404 | 43,168 | 2010 | 0,14304 | 1,32397 | 308,7626 | 49,494 |
| 8 | 0,04304 | 14,179 | 348,118 | 16,790 | 29 | 356,3497 | 43,145 | 2011 | 0,14804 | 1,37025 | 309,9737 | 51,426 |
| 9 | 0,04804 | 15,827 | 349,333 | 18,806 | 30 | 356,1596 | 43,122 | 2012 | 0,15304 | 1,41653 | 311,0802 | 53,352 |
| 10 | 0,05304 | 17,474 | 350,414 | 20,827 | 31 | 355,9700 | 43,099 | 2013 | 0,15804 | 1,46281 | 312,0981 | 55,276 |
| 11 | 0,05804 | 19,122 | 351,387 | 22,854 | 32 | 355,7811 | 43,076 | 2014 | 0,16304 | 1,50909 | 313,0401 | 57,197 |
| 12 | 0,06304 | 20,769 | 352,272 | 24,886 | 33 | 355,5927 | 43,053 | 2015 | 0,16804 | 1,55538 | 313,9163 | 59,116 |
| 13 | 0,06804 | 22,417 | 353,083 | 26,922 | 34 | 355,4048 | 43,031 | 2016 | 0,17304 | 1,60166 | 314,7349 | 61,034 |
| 14 | 0,07304 | 24,064 | 353,832 | 28,961 | 35 | 355,2176 | 43,008 | 2017 | 0,17804 | 1,64794 | 315,5028 | 62,950 |
| 15 | 0,07804 | 25,711 | 354,527 | 31,005 | 36 | 355,0309 | 42,985 | 2018 | 0,18304 | 1,69422 | 316,2256 | 64,867 |
| 16 | 0,08304 | 27,359 | 355,176 | 33,052 | 37 | 354,8448 | 42,963 | 2019 | 0,18804 | 1,74050 | 316,9082 | 66,782 |
| 17 | 0,08804 | 29,006 | 355,783 | 35,102 | 38 | 354,6593 | 42,940 | 2020 | 0,19304 | 1,78678 | 317,5545 | 68,698 |
| 18 | 0,09304 | 30,654 | 356,355 | 37,155 | 39 | 354,4743 | 42,918 | 2021 | 0,19804 | 1,83306 | 318,1682 | 70,614 |

Figure 49 Excel calculations for hydrogen filling

In the cooling stage the mass remains constant, in terms of temperature. Equation (84) is applied to see its evolution, while for pressure the equation (72) continues to be used.

For the initial pressure of 1 bar, three filling and three cooling stages have been proposed, the last of which is a stabilization stage until 300 K is reached. Because filling the tank at 100% would require many more stages, it has been chosen to do a study until the tank reaches 2kg of hydrogen inside, which represents 94.34% of its total capacity.
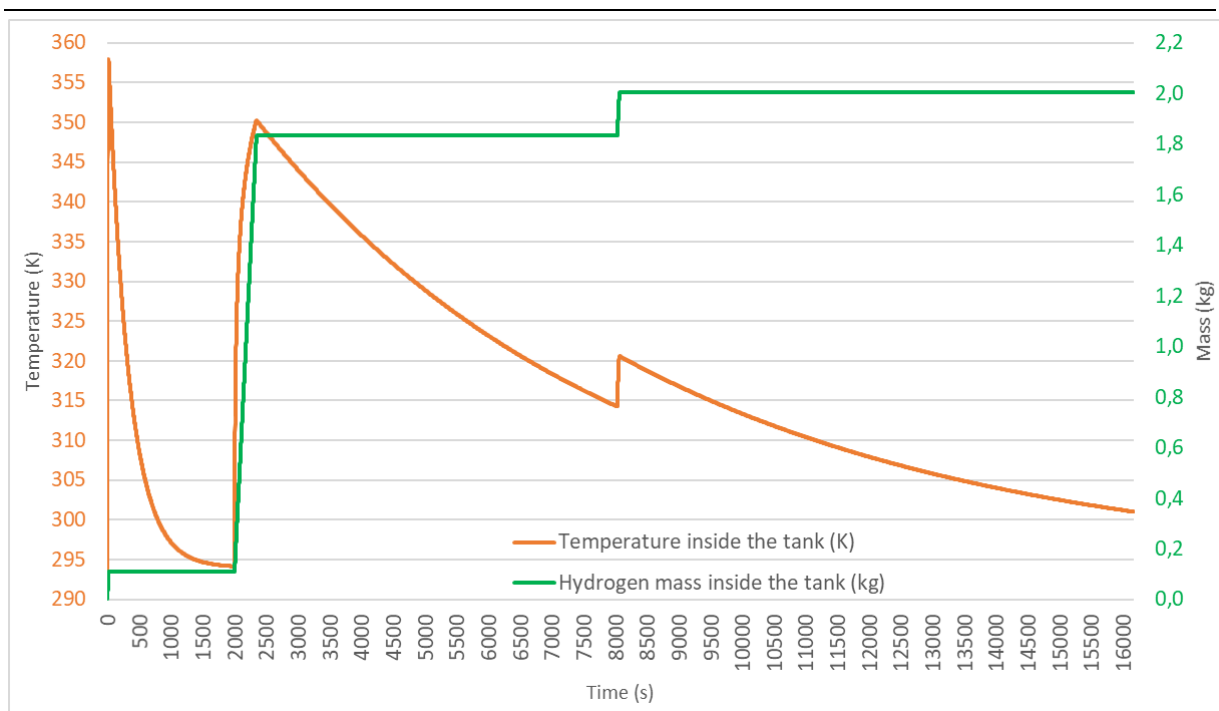
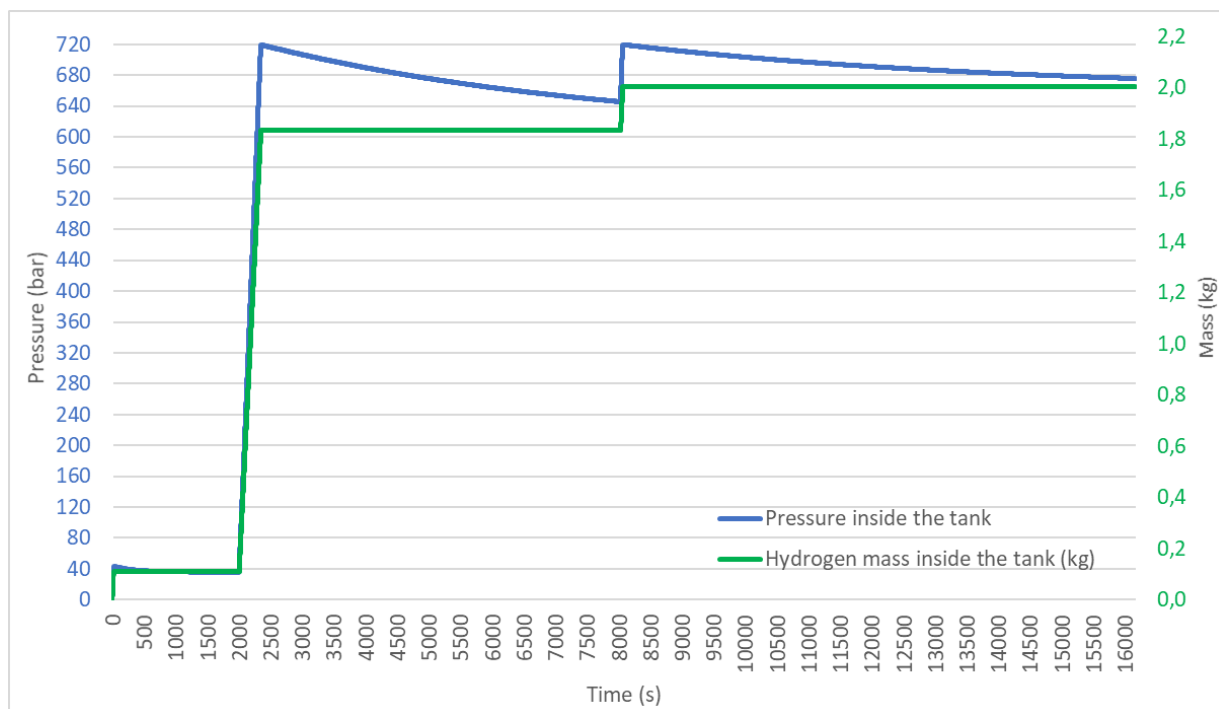Figure 50 Temperature and mass inside the tank as a function of time



Figure 51 Pressure and mass inside the tank as a function of time

When filling the tank, various strategies can be followed, in this case it has been chosen to perform the fewest number of stages possible and cool as much as possible during the first stage of cooling. As seen in Figure 50, the lower the mass in the tank the faster its temperature drops.

In order not to distort the graph too much, 300K has been set as the final cooling temperature.

Figure 51 displays how the maximum pressure limitation of the system influences time. Without this limitation, during the second stage, the tank could be filled up to 850 bar. When the temperature drops and stabilizes, the pressure reaches 700 bar, making it possible to fill the tank 100% in just two stages. However, in this case this is not possible, so to fill the tank it would be necessary to carry out several stages with long cooling times.

Table 13 Time to fill a certain percentage of the tank for different initial pressures

| Initial pressure ($P_0$) | Filling percentage | |
|---|---|---|
| | 94.4% | 98.5% |
| 1 bar | 4h 30min | 5h 6min |
| 5 bar | 4h 20min | 4h 55min |
| 10 bar | 4h 18 min | 4h 53min |
| 15 bar | 4h 16 min | 4h 51min |

In Table 13 is a summary of how the initial pressure affects filling times, and the increase in time that leads to an increase in filling of approximately 4%.

All the results and calculations obtained are referred to appendix E.

# 6 **MATLAB simulation**

A numerical simulation using MATLAB has been created to find overpressure in an enclosure with a single vent. The model has been created by Are Mjaavatten and Andre Vagner Gaathaug. In this bachelor thesis the model is used to evaluate safe vent size configuration, by calculating the theoretical overpressure that arises in the enclosure. Finding a max overpressure threshold allows for the determination of vent size and TPRD nozzle diameter to prevent structural damage to residential garages.
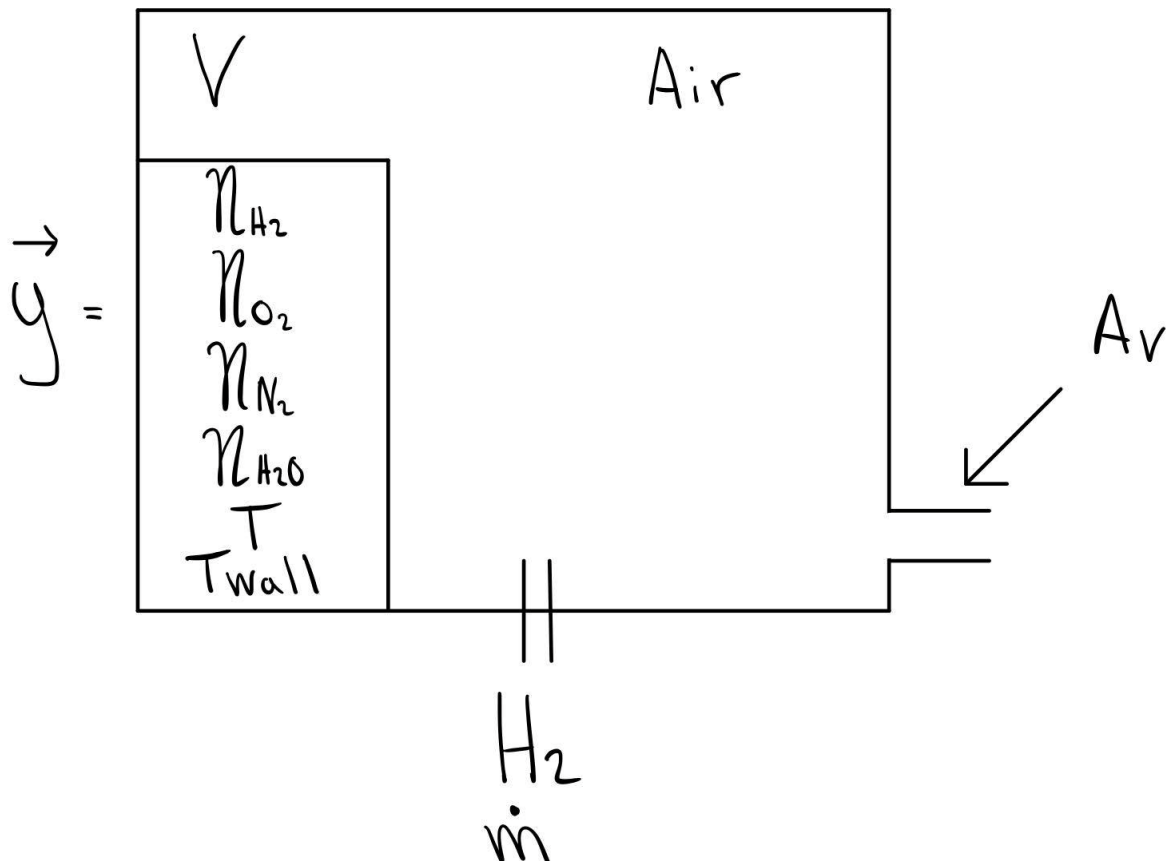


Figure 52 Model illustration

The goal is to determine the total mole rate in and the change in pressure and temperature over time given that the volume is constant. Shown above is a sketch displaying the variables to account for in the calculation. With the given variables will volume V and Vent area $A_V$ be constant. The change in quantity of moles can be expressed using the following derivations:

$$\frac{d\vec{y}}{dt} = \begin{array}{c} \frac{dn_{H_2}}{dt} \\ \frac{dn_{O_2}}{dt} \\ \frac{dn_{N_2}}{dt} \\ \frac{dn_{H_2O}}{dt} \\ \frac{dn_T}{dt} \\ \frac{dn_{Twall}}{dt} \end{array} \tag{85}$$

Applying this derivation to the system, mole quantity change can be expressed as following.

$$\frac{dn_{H_2}}{dt} = \dot{n}_{H_2in} - \dot{n}_{H_2out} + (\dot{n}_{H_2,RX}) \tag{86}$$

$$\frac{dn_{O_2}}{dt} = \dot{n}_{O_2in} - \dot{n}_{O_2out} + (\dot{n}_{O_2,RX}) \tag{87}$$

$$\frac{dn_{N_2}}{dt} = \dot{n}_{N_2in} - \dot{n}_{N_2out} + (\dot{n}_{N_2,RX}) \tag{88}$$

$$\frac{dn_{H_2O}}{dt} = \dot{n}_{H_2Oin} - \dot{n}_{H_2Oout} + (\dot{n}_{H_2O,RX}) \tag{89}$$

During unignited release, only hydrogen moles quantity will increase due to no chemical reaction between air and hydrogen. Therefore, molar flow in, if unignited is:

$$\dot{n}_{O_2in} = \dot{n}_{N_2in} = \dot{n}_{H_2Oin} = 0 \tag{90}$$

The stoichiometric reaction with hydrogen and oxygen produces water as a result. The balanced chemical reaction for the combustion can be written as:

$$2H_2 + O_2 \rightarrow 2H_2O \tag{91}$$

This is based on the law of conservation of mass which states that atoms are neither created, nor destroyed, during any chemical reaction. The stoichiometric ratio of the combustion can then be written as [22]:

$$H_2 + \frac{1}{2}O_2 \rightarrow H_2O \tag{92}$$

Given the stoichiometric ratio, when hydrogen release is ignited the molar flow rate is calculated as follows:

$$\dot{n}_{H_2O,rx} = \dot{n}_{in} \tag{93}$$

$$\dot{n}_{O_2,rx} = -\frac{1}{2}\dot{n}_{in} \tag{94}$$

$$\dot{n}_{H_2,rx} = -\dot{n}_{in} \tag{95}$$

$$\dot{n}_{H_2 in} = \dot{n}_{in} \tag{96}$$

$$\dot{n}_{in} \rightarrow P(t) \tag{97}$$

To calculate the molar flow out, the discharge velocity in the vent must first be calculated using Bernoulli's equation. Bernoulli's equation, based on the derivation of Euler's equation along fluid flow streamline [22]:
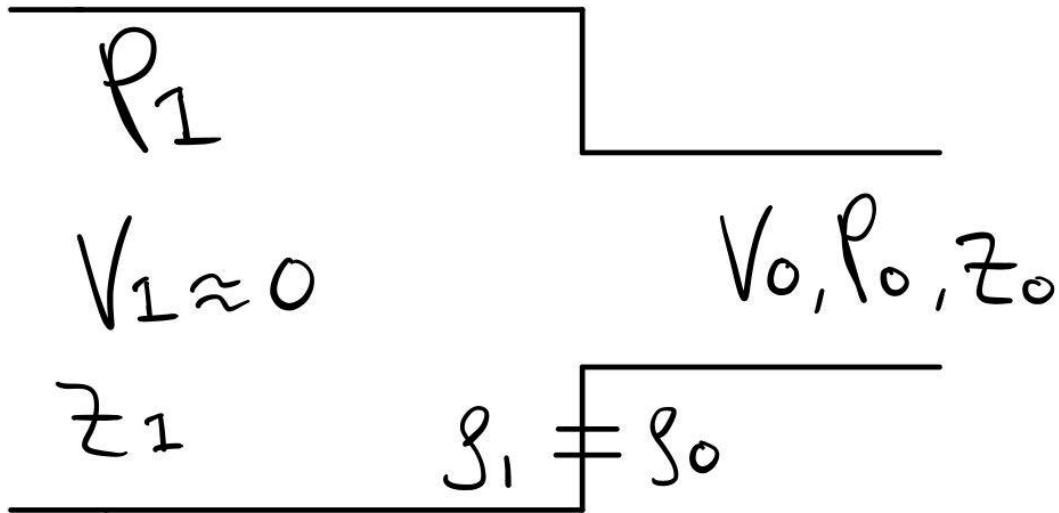


Figure 53 Illustration Bernoulli

$$\frac{V_1^2}{2} + g*Z_1 + \frac{P_1}{\rho_1} = \frac{V_0^2}{2} + g*Z_0 + \frac{P_0}{\rho_0} \tag{98}$$

The velocity inside the enclosure is assumed to be zero. Along with the density and height it is also assumed to remain the same. The equation can then be simplified, and the velocity can be calculated:

$$\frac{P_1 - P_0}{\rho} = \frac{V_0^2}{2} \rightarrow V_0 = \sqrt{\frac{2(P_1 - P_0)}{\rho}} \tag{99}$$

The mass flow is given by:

$$\dot{m} = \rho * C * A * V_0 \tag{100}$$

Knowing that mass flow can also be written as $\dot{m} = n * M_W$, a combination of the equations (99) and (100) allow for calculations of total mole out of the enclosure.

$$\dot{n}_{tot,out} * M_{W,tot} = C * A \sqrt{\frac{2(P_1 - P_0) * n_{tot} * M_{W,tot}}{V}} \tag{101}$$

To calculate molar rate out, the following equation is given:

$$\dot{n}_{tot,out} = C * A \sqrt{\frac{2(P_1 - P_0) * n_{tot}}{V * M_{W,tot}}} \tag{102}$$

The molar ratio of a given molecule is $X_i = \frac{n_i}{n_{tot}}$. Molar flow out, given a specific molecule can then be written as:

$$\dot{n}_{i,out} = X_i * \dot{n}_{tot,out} \tag{103}$$

Starting from the general equation of the energy balance applied to a control volume, the following is assumed [22]:

- The mass of the hydrogen is negligible; thus, the potential energy is zero.
$$g * z = 0$$
- The velocity inside the enclosure is assumed to be zero, therefore kinetic energy is taken out of the equation.
- There is no shaft work on the air inside the enclosure making the total work zero.
- The volume of the enclosure remains constant

The final energy balance is presented below:

$$\frac{dU}{dt} = (H_{in}) - (H_{out}) + \dot{Q}_{rx} - \dot{Q}_{loss} \tag{104}$$

At constant volume the internal energy is $U = n * \hat{U}$. The total internal energy reference inside the enclosure can then be calculated dependent on the reference temperature given; $T_{ref} = 298.15\ K$. Due to temperature not being constant, the change in internal energy in the enclosure can be calculated using the following:

$$\hat{U} = \hat{U}_{ref} + \int_{T_{ref}}^{T} C_v \, dT \tag{105}$$

$$U = n * \left( U_{ref} + \int_{T_{ref}}^{T} C_v \, dT \right) = n * (U_{ref} + C_v(T - T_{ref})) \tag{106}$$

$$U = \sum U_i = \sum n_i * (U_{ref} + C_{v_i}(T - T_{ref})) \tag{107}$$

$$U = \sum n_i * U_{ref} + \sum n_i * C_{v_i}(T - T_{ref})) \tag{108}$$

The internal energy is derivated using the product rule, calculating the change in internal energy over time. Since $U_{ref}$ is constant, $\sum n_i * U_{ref}$ is nulled out. Using the product rule $\frac{dU}{dt}$ is shown below:

$$U = \sum C_{v_i} * (T - T_{ref}) * \sum \frac{dn_i}{dt}$$
$$+ \sum n_i * (T - T_{ref}) * \frac{dC_{v_i}}{dt} + \sum n_i * C_{v_i} * \frac{d}{dt}(T - T_{ref}) \tag{109}$$

$\sum n_i * (T - T_{ref}) * \frac{dC_{v_i}}{dt}$ is nulled out do to $C_V$ will remain constant. Given the change in internal energy in the enclosure, calculations to figure out the change in temperature can proceed. The temperature inside the enclosure is calculated as following:

$$\frac{dT}{dt} = \frac{1}{\sum n_i * C_{v_i}} \left( (H_{in}) - (H_{out}) + \dot{Q}_{rx} - \dot{Q}_{loss} - (T - T_{ref}) \sum C_{v_i} * \frac{dn_i}{dt} \right) \tag{110}$$

The enthalpy H is the sum of the internal energy and the product of volume and pressure. Enthalpy only changes due to temperature variation. The enthalpy rate in can so be calculated by the following equation.

$$\dot{H}_{in} = \sum_i \dot{n_{in}} * \hat{H}_{in} \tag{111}$$

Where $\hat{H}$ is:

$$\hat{H}_{in} = H_{ref} + \int_{T_{ref}}^{T_{in}} C_{p_i} \, dT \tag{112}$$

Enthalpy rate out is calculated in the same procedure but uses the temperature in the enclosure and not the temperature at the tank nozzle. It also uses the mole rate out of the enclosure. $\dot{Q}_{rx}$ is the heat from the reaction, therefore the heat rate can be calculated as shown below, where HHV is the higher heating value.

$$\dot{Q}_{rx} = \frac{dn_{H2O}}{dt} * HHV \tag{113}$$

The heat loss can be assumed as the heat transfer due to a convection process from the walls of the enclosure to the outside atmosphere. That means that the following assumptions are being made:

- The temperature of the walls is the same as the temperature of the gas inside.
- Conduction is neglected, therefore temperature is assumed to be constant through the wall.

So, the heat loss finally can be written as [22]:

$$\dot{Q}_{loss} = h * A_{wall} * (T - T_{wall}) \tag{114}$$

# 6.1 Results

## 6.1.1 Overpressure

The pressures generated in the unignited releases is overall much lower than its ignited counterpart. However, the unignited release also poses a risk in terms of structural damage. In this sub-chapter the unignited release from the MATLAB model is presented in terms of a relationship between the TPRD diameter, vent size and overpressure. Below are the results displaying the relations for unignited and ignited release;
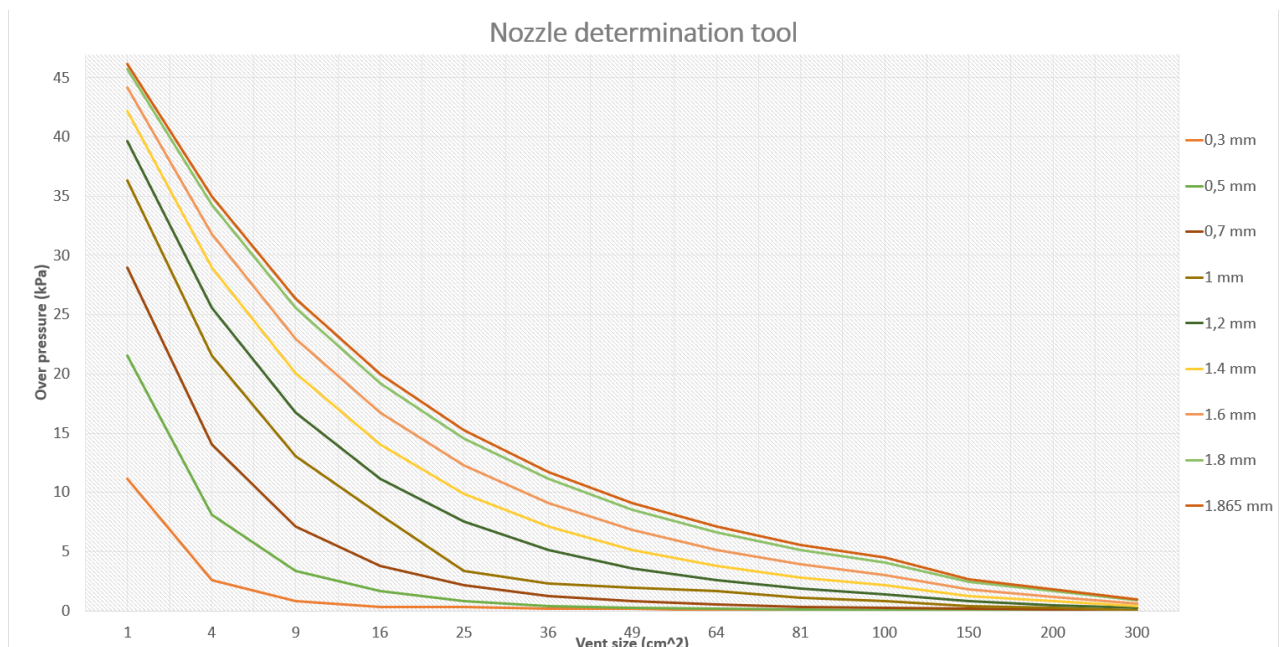


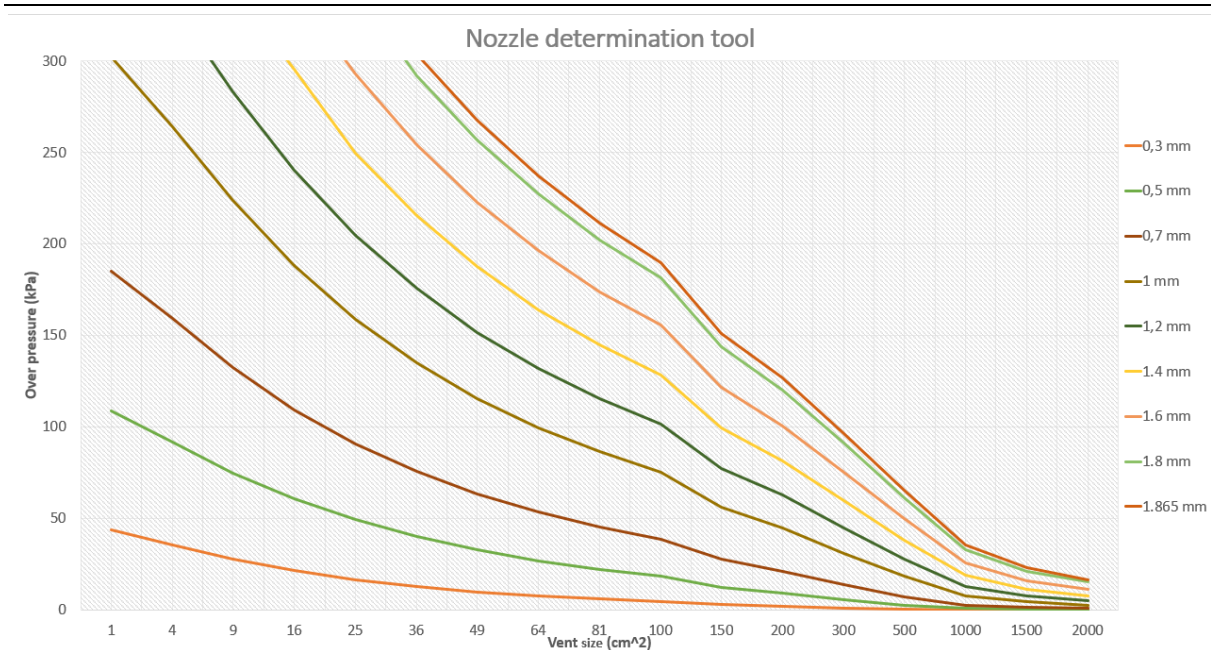Figure 54 Unignited MATLAB results (Appendix D)

Figure 55 Ignited MATLAB results (Appendix D)

All MATLAB results are given in Appendix D. MATLAB code is in Appendix L.

# 7 Structural analysis

In the upcoming years the use of hydrogen powered automobiles will become more widespread, and they will likely be housed in residential garages. The need for knowledge regarding safe hydrogen application is essential with emerging technologies. Hydrogen being extremely explosive, leads to many concerns and therefore safety analysis must be carried out thoroughly before action can be taken. Understanding and learning how to cope with such hazards will generate steps, that allow for safer application as well as knowledge regarding safer design.

This chapter will focus on the structural analysis of traditional detached garages when hydrogen gas is released. The structural analysis performed with Solidworks, will define the pressure threshold for 2 types of garages; a leca garage and a wood garage. The garages will be designed to replicate approximately real-life scenarios. The two types of garages will have the same dimensions of 2.6 x 2.6 x 4.5 m, representing a typical small garage. [46]

The article "*Pressure effects of an ignited release from onboard storage in a garage with a single vent*" written by Brennan, Hussein, Makarov, Shentsov, and Molkov, present a numerical study of hydrogen release inside a garage of 30.42 $m^3$ with a single vent. The release of hydrogen at 70 MPa through TPRD of 3.34mm diameter and vent size of 0.1925 $m^2$. The pressure reaches over 55 kPa in under 1 s, exceeding the threshold set for potential structural damage. The threshold is set to maximum of 20 kPa, as greater pressure will most likely lead to great structural damage. [8]

The article "*Explosion of gas layers in a room size chamber*" by Buckland explain the threshold limits of a room size chamber of 27 $m^3$ with different materials. Buckland concludes a threshold limit of 21 kPa with cinder block walls up to 300mm will be capable of between 14-21 kPa unreinforced. For wooden chambers, it was documented that 19mm thick chipboard shattered at 7 kPa, but nails that hold in place the wooden boards lose function at only 3 kPa. [47]

# 7.1 Leca garage

In this subchapter the material, method and simulation of a Leca garage will be presented and discussed.

Leca is a versatile material used in a wide variety of buildings and constructions. Along with garage structures, it is used as foundation for many buildings and as a fillings mass (Leca spheres). It is a close resemblance to cinderblocks in terms of both looks, strength and density. It is a strong and cheap building material with many uses.

## 7.1.1 Garage properties

### 7.1.1.1 Material

Leca, or light expanded clay aggregate, is a commonly used material all over the world. It has slight variations in terms of the way it is produced but has generally the same properties. They are made by extracting natural clay from clay pits. Furthermore, the clay is heated in kilns at high temperatures, up to 1150˚C [48]. The heat expands the clay and gives it a hard ceramic outer shell and porous interior. It is a strong material compared to density, it has low thermal conductivity and is a good sound insulator, to name a few properties [48]. The company that makes leca in Norway, Leca International, uses the expanded clay to make blocks, commonly referred to as leca blocks. These are widely used in construction and a good material for making garages.

The leca blocks are made in different sizes and with different properties. The blocks themselves are made by moulding leca spheres, cement and water. In this report a leca block with measurements of 498x149x247 mm has been chosen for further study.
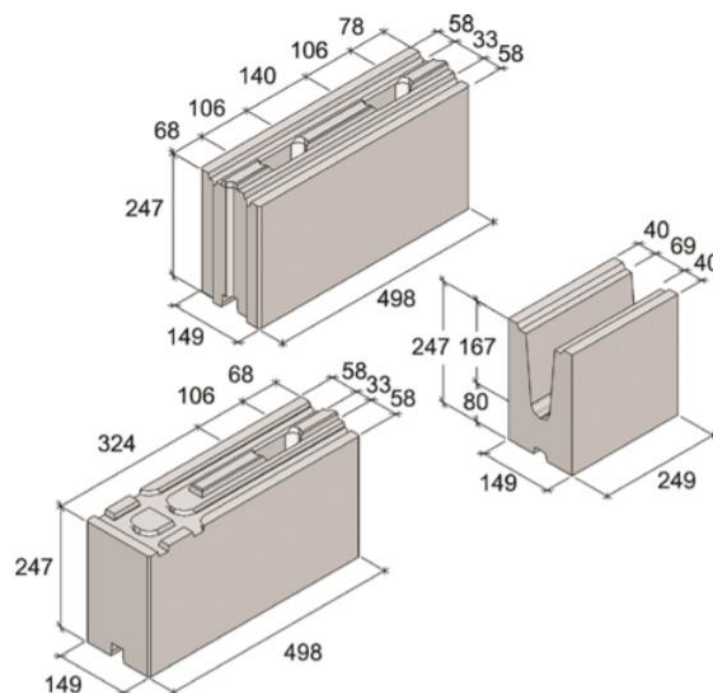


Figure 56 Leca Basicblock LSX Dimensions (Appendix C)

The most important mechanical property of leca blocks in construction are the compressive strength. For the block used to make this garage, Leca Basicblock LSX, the compressive strength is 2.6 MPa.

Further, the leca block has a tensile strength of only 0.5 MPa and an E-modulus of 3200 MPa [49]. The properties introduced here are also applicable to a wall made of leca blocks without reinforcement. When building the garage, a mortar is used to bind the blocks together. The mortar used is "weber M5 Murmørtel" as recommended by the manufacturer. The mortar has a characteristic compressive strength of 5 MPa. [50]

Table 14 Mechanical properties of leca [50]

| Compressive strength: | 2.6 MPa |
|---|---|
| Tensile strength: | 0.5 MPa |
| Shear modulus: | 318.9 MPa |
| E-modulus: | 3200 MPa |
| Density: | 630 Kg/m$^3$ |

In Norwegian leca garages the walls are usually reinforced with 18 mm steel rods lying horizontally inside the mortar between the blocks. This is beneficial to the wall structure if a horizontal load is applied. The steel reinforcement has a yield strength of 850 MPa, tensile strength of 580 MPa and an E-modulus of 1.92e5 MPa. All mechanical properties of leca masonry are calculated as a solid block without the interior holes [49].

### 7.1.1.2 Structure

A garage made of leca blocks is most commonly built on a foundation of either concrete or special leca blocks made specifically for foundation purposes. On the foundation one simply stacks the blocks on top of each other using mortar between the blocks to bind them together. Steel reinforcements should be used every other horizontal joint.

When building a garage with leca masonry it is important to follow the guidelines made by Leca Norway to make sure the construction follows the given standards.

## 7.1.2 Solidworks Simulation

In order to simulate a garage made of leca blocks a few simplifications had to be made to the model. The walls of the garage have been modelled so that there are no joints between the blocks. Due to the fact that the mortar used in the construction of leca structures is stronger than the block itself, one can assume that the global mechanical properties of the structure is the same for simulation purposes [50].

The wall is made by sketching a square section of the wall with measurements of 149x2600 mm and extruding it 4500 mm length wise. The parts of the roof, floor and walls in the model are made with extruded squares on each side with length of 4500 mm, height of 149 mm and depth of 600 mm. These are merged with the rest of the wall.
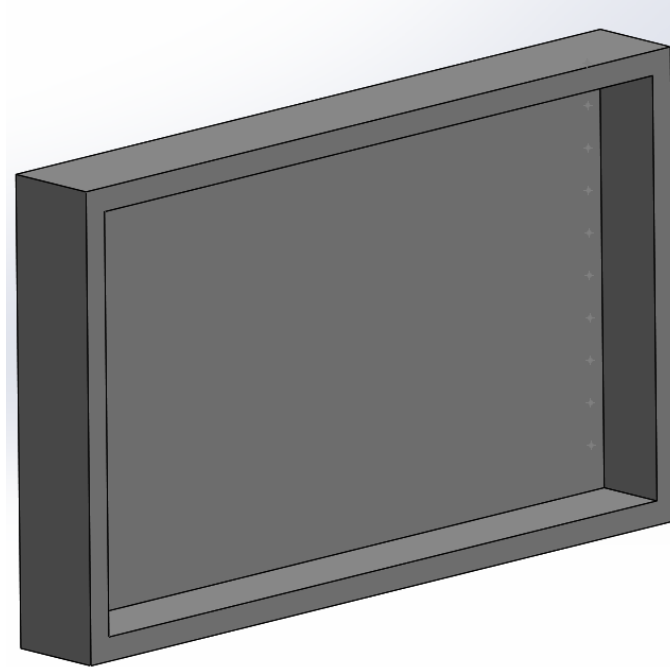


Figure 57 Model of leca wall from Solidworks

The reinforcements are two extruded steel rods with a diameter of 18 mm. Holes for the reinforcements are cut into the wall using extrude cut feature, with a diameter of 18 mm. There are 10 holes in total, equally spaced downwards with 245 mm between them and 35 mm between the holes.
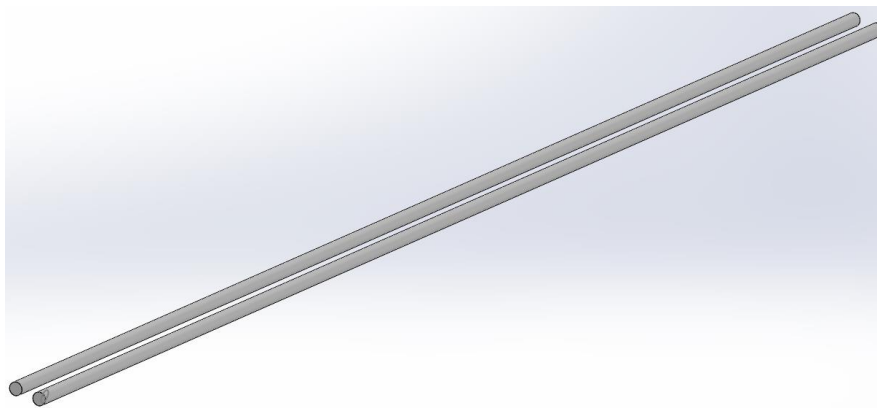


Figure 58 Steel reinforcement used in simulations

For the simulation itself an assembly were made with the modelled leca wall and reinforcements. The steel rods are mated with the inside holes of the wall. There are 10 steel reinforcements in total, one for each hole.

### 7.1.2.1 Boundaries

The simulation has been restricted to be just one of the longest walls, in addition to parts of the roof, floor and walls. This is done mainly due to a lack of computer power to simulate the entire structure. A restriction like this does limit the analysis but gives a good estimation of how the structure will respond to the given pressure. The parts of the walls, roof and floor in the simulation is mainly there to limit the strain on the edges of the wall.

For the leca garage the bonding between the reinforcements and mortar in the joints are an important part. When constructing with leca blocks, the steel rods are to be fully engulfed in mortar to make sure that the reinforcements are joined with the blocks [51]. In order to simulate this the global bonding connection in Solidworks has been applied. This connection "bonds" every part of the assembly together and creates common nodes for the faces that are connected.

In order to simulate the pressure on the wall, roof and floor the fixtures are put on the sides of the structure as shown below. These fixtures will resemble the walls currently not in the model and the rest of the roof and floor. There is also a fixture on the bottom, to simulate the concrete floor of the garage.
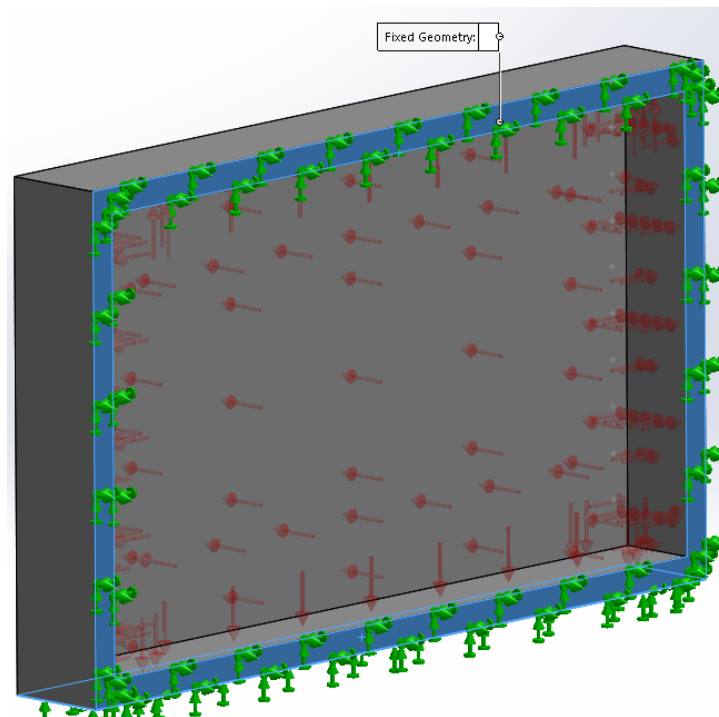


Figure 59 Fixtures

In this simulation the walls are assumed completely fixed with no movement. This is done to simplify the simulation and due to the lack of knowledge about the global movement of the structure. In reality the walls and roof are able to move to a certain extent.

The pressure in the garage comes from a release of hydrogen assumed to originate from the centre of the garage. This pressure is applied equally to all surfaces inside the garage at the same time. In this analysis the pressure used is the highest pressure achieved in a MATLAB simulation of the release.

Due to the reinforcement inside of the walls in the garage, the mesh used in the simulation had to be a finer mesh. When using a global bonding contact an incompatible or compatible mesh are selected based on the geometry of the assembly. The incompatible mesh has unequal elements and no node-to-node contact between the different faces. This leads to less accurate results. A finer mesh was possible to use in this simulation due to the smaller scale of the garage.
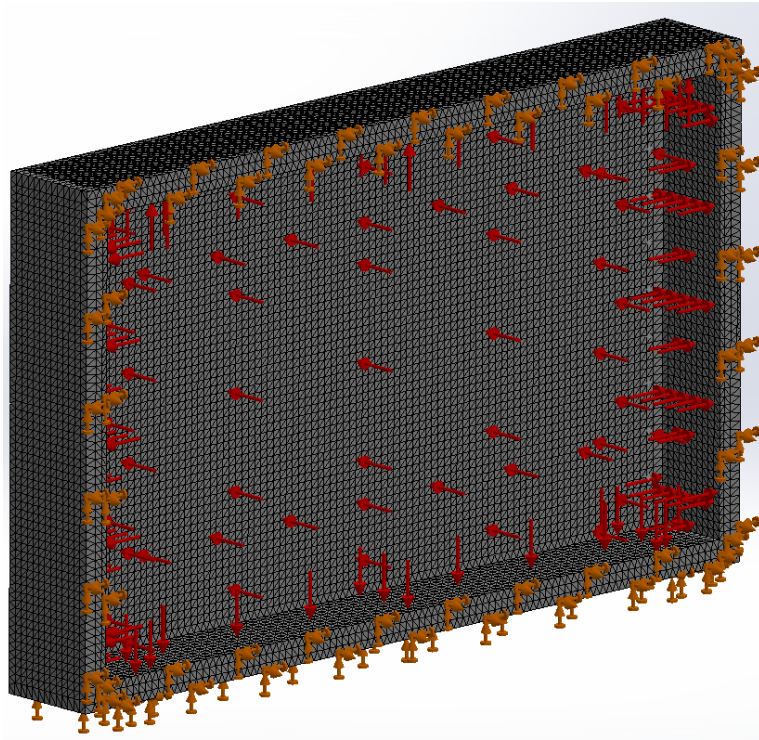


Figure 60 Meshing of the model

### 7.1.2.2 Results

Using the simulation above the maximum pressure the garage can withstand is 0.006 MPa. At this pressure the 150 mm leca blocks will begin to fracture. To find this threshold the first- and third principal stress from the simulation has been compared to the tensile- and compressive strength for the material. Leca has very low tensile strength, 0.5 MPa, so the force needed to cause damage to the structure is fairly low. Under is an iso clip from Solidworks showing where in the structure the strain is 0.5 MPa. This is where the damage to the wall will appear first.
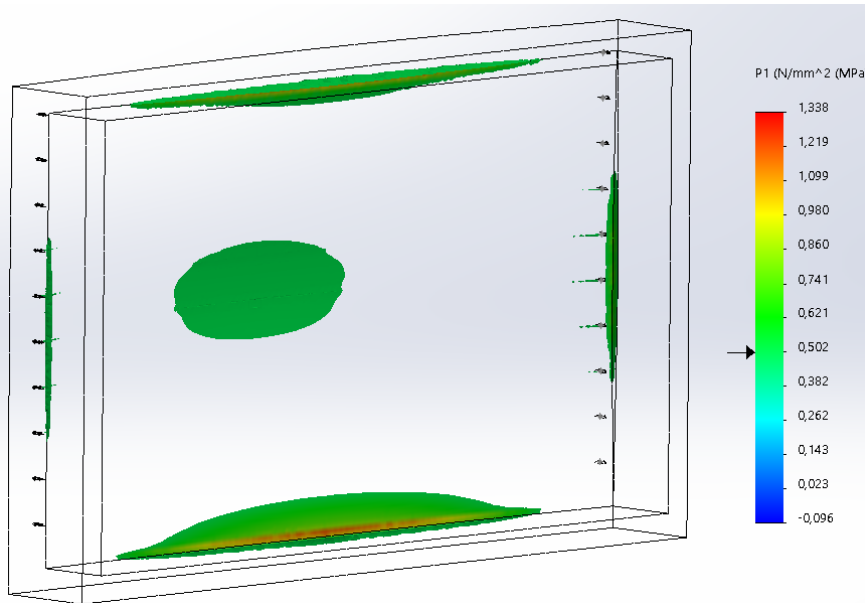


Figure 61 Iso clip from the structural analysis

On the edges between the walls, roof and floor there exists concentrated strains. During the simulation work several simulation tests has been done in order to see if these strains are a product of short sidewalls. It seems that if the length of the sidewalls increases, the concentrated strains decrease. As a result, the strains that arise in these areas are neglected. A more in-depth analysis of the complete garage structure must be done in order to address this.

Buckland et al. did experiments on natural gas to determine the pressures generated by an explosion in a room-sized structure of 27 m$^2$ [47]. Different materials were used to construct the enclosure used. Cinderblocks was a material used that is a good comparison to leca blocks. In this study 300 mm cinderblocks were used to build the enclosure. With a natural gas explosion an overpressure of 14-21 kPa caused structural damage to the cinderblocks. For comparison purposes a simulation of 300 mm leca blocks has been done. This simulation confirms Buckland et al. findings with tensile strains of 0.5 MPa at 14 kPa in the centre.

Solidworks model and simulation is in Appendix M.

# 7.2 Wood garage

Wood is the most traditional material both used for small and large constructions. Wood is a versatile material providing opportunities for strong constructions while preserving environmental properties, as well as low energy demand during production. Structural analysis will be carried out to try to find a reasonable threshold for a typical small wooden garage. [52]

## 7.2.1 Garage properties

### 7.2.1.1 Material

In Norway it is first and foremost Spruce (Picea abies) and pine (Pinus Sylvestris) that is mainly used for wood constructions. Spruce is mostly used for structural frames while pine is great for exterior boards. Though they have different mechanical properties, pine and spruce is seen as equal when used for construction purposes. [52]

Wood is made up of a fibre structure. Fibres parallel lengthwise with a total length of 2-6mm and diameter of 0.02-0.05 making up the majority of the wood mass. Some fibres lay perpendicular. That being said, the wood properties differ a lot lengthwise and perpendicular, and the properties are not the same on all wood. Cellulose and lignin are the major composition of the wood structure, lignin acting as an epoxy and cellulose as a reinforcement all essential for structural strength. [53]

Norwegian construction wood is strength graded according to NS-EN 338. The most common grades being C14, C18, C24, and C30 where the number represents the flexural strength of the material in $N/mm^2$. C24 is the most common out of the selection and in this case will be used as the strength grade constructing the garage. Factors like moisture content and temperature affect structural strength. According to NS-EN 14081, such strength grade material is marked with CE-badge and verifies that the material will provide adequate flexural strength up to 20% moisture content. [53]

Table 15 Mechanical properties of C24 with a safety factor of 1.25 according to NS-EN 338 [52]

| | |
|---|---|
| Bending strength: | 24 MPa |
| Tensile strength: | 14 MPa |
| Compressive strength parallel to fibres: | 21 MPa |
| Compressive strength perpendicular to fibres: | 5.3 MPa |
| Shear modulus: | 4 MPa |
| E-modulus: | 11000 MPa |
| Density: | 420 Kg/m$^3$ |

## 7.2.1.2 Structure

The standard construction system for walls in Norway, is based on support systems with typical 48 x 98 beams upright with a distance of 60cm apart. The beams are supported with horizontal beams both at the top and bottom of the upright beams. This garage will be constructed with a quite simple design where the outer boards will be the only layer of the walls. [53]

For simplification of the structural analysis, the outer boards will be on the inside of the beam support system. This will in theory likely not affect the results of the structural analysis, as the outer boards are assumed to be fully fixed to the beams. Garages will often have a 10mm chipboard, or plywood on the inside of the support beams, which will increase the rigidity of the walls. This analysis focus mainly on "weaker" garages as this will result in a more conservative threshold, which will be adequate for most garages.

Table 16 Hardware used in the assembly of garage

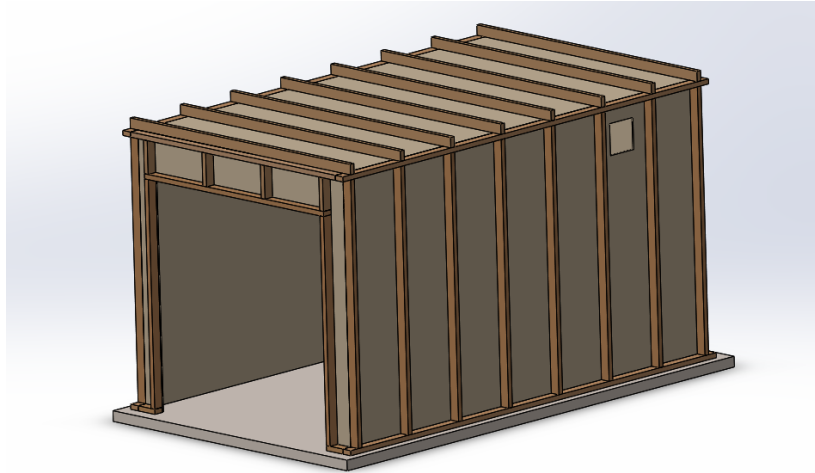| Description: | Quantity: | Material: |
|---|---|---|
| 48x98x4526mm | 4 | Spruce |
| 48x98x2626mm | 3 | Spruce |
| 48x98x2200mm | 1 | Spruce |
| 48x98x213mm | 2 | Spruce |
| 48x98x2152mm | 2 | Spruce |
| 48x98x2530mm | 21 | Spruce |
| 48x98x317mm | 4 | Spruce |
| 43.78 $m^2$ – 19mm thickness | 1 | Pine |
| Garage bedding | 1 | Concrete |

## 7.2.2 Solidworks simulation



Figure 62 Solidworks assembly

The design procedure for Solidworks analysis, is generally quite similar for each of the hardware. The main difference is dimension and the geometric orientation. Each beam is sketched and extruded to desired length. The inner wooden boards was constructed as a solid part and extrude cut function was used to create shell of the garage at 19mm thickness, and to satisfy the desired inner dimensions of 2.6 x 2.6 x 4.5m. Extrude cut function was also used to create garage gate opening of 2.2 x 2.2m. Then using mating feature, all hardware was fit together with the necessary relations.

Solidworks simulation uses the Finite Element Method which applies loads to the assembly and identify the structural behaviour of the hardware. FEM model gives a piece-wise estimation of the assembly solving equation by discretization of the domain with predefined mesh of the shapes. In this case pressure load will be applied to the garage assembly to define threshold of which the structure becomes damaged. In this simulation, a static analysis will be used where pressure is uniformly distributed on the inside of the garage.

### 7.2.2.1 Boundaries

When running any kind of simulation certain boundaries must be set to get the most accurate results possible. Boundary conditions is set to connect the simulation to its surroundings. If not, the simulation will not be defined or succeed. Firstly, the material is defined for all hardware in the simulation. The garage bedding is assumed to not be affected by the overpressure; it is therefore excluded from the analysis. The assembly material is defined with the properties given by NS-EN 338. [53]

As mentioned previously, the garage is detached, therefore the bottom of the bedding will be fixed. This allows for deformation in the walls as well as roof. Since the bedding is fixed, an assumption is made that the beams in contact with the bedding will not detach and is therefore fixed to the bedding. This assumption allows for strictly focus on the structural integrity and the material capacities when overpressure is applied.
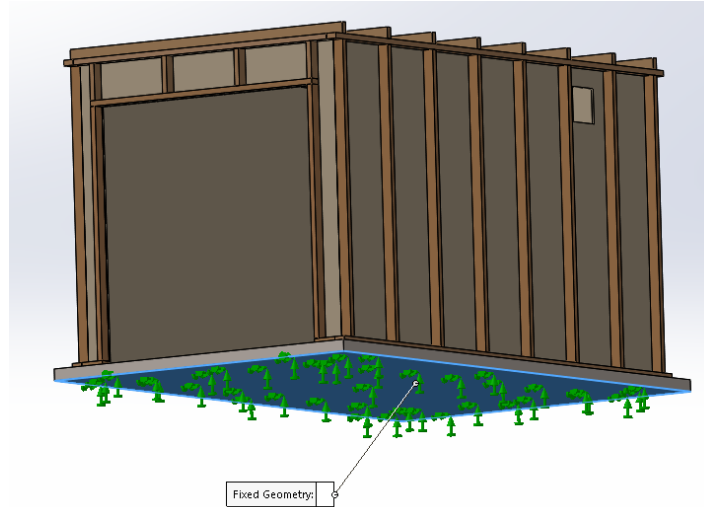
Figure 63 Fixture

The accuracy of the simulation is dependent on the element size regarding distribution of variables in the assembly. The domain, in other words the volume surrounding the assembly is cut up into small elements called mesh. The finer the mesh the more nodal points the domain will have. Increasing the amount of nodal points increase the total amount of calculations thus more accurate results. That being said, finer mesh will increase the total computation time as well as demand more computer power. [54]

In this simulation, Standard high-quality 4-point solid mesh was used. With this mesh the element size is 123.481mm and the assembly has a total of 34834 elements.
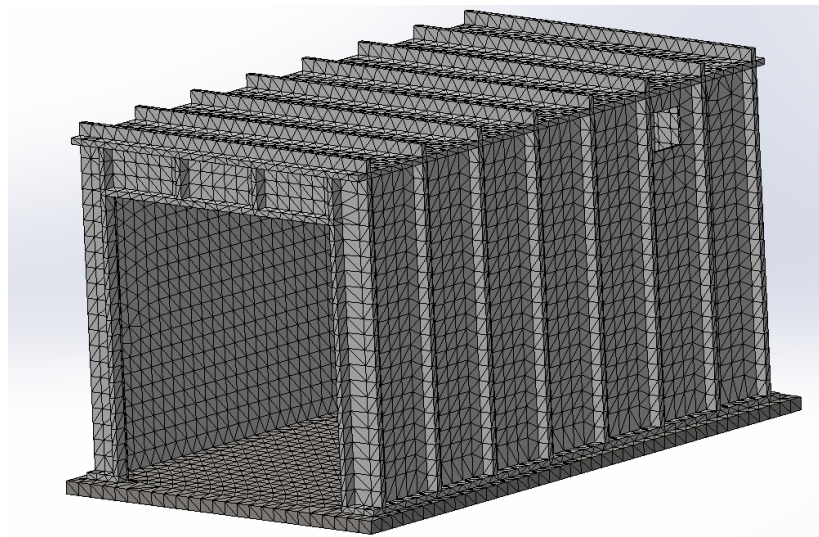


Figure 64 Mesh

At last, the structural load is applied, since the goal of the simulation is to find the pressure threshold for the garage. Pressure measured in MPa is loaded on the inside of the garage gradually increasing until material failure.
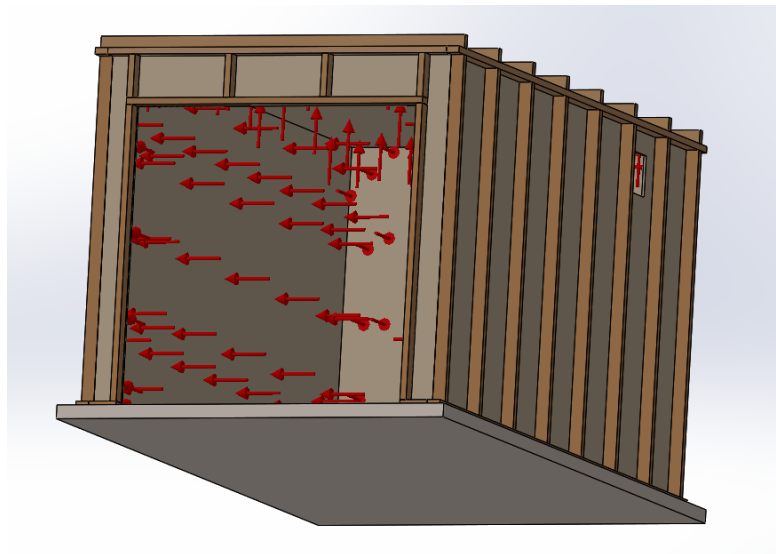
Figure 65 Pressure

## 7.2.2.2 Results

With the information given above, the total pressure acceptable for the garage constructed is 0.0078 MPa. For verification of this given threshold, the mechanical properties of the material are compared to the First and Third stress principle. The first principle defines the maximum tensile stress the material has capacity to reach, and the third principle defines the total compressive strength along the wood fibres. At 0.0078 MPa overpressure the tensile stress reaches 14 MPa, the max capacity of the material.
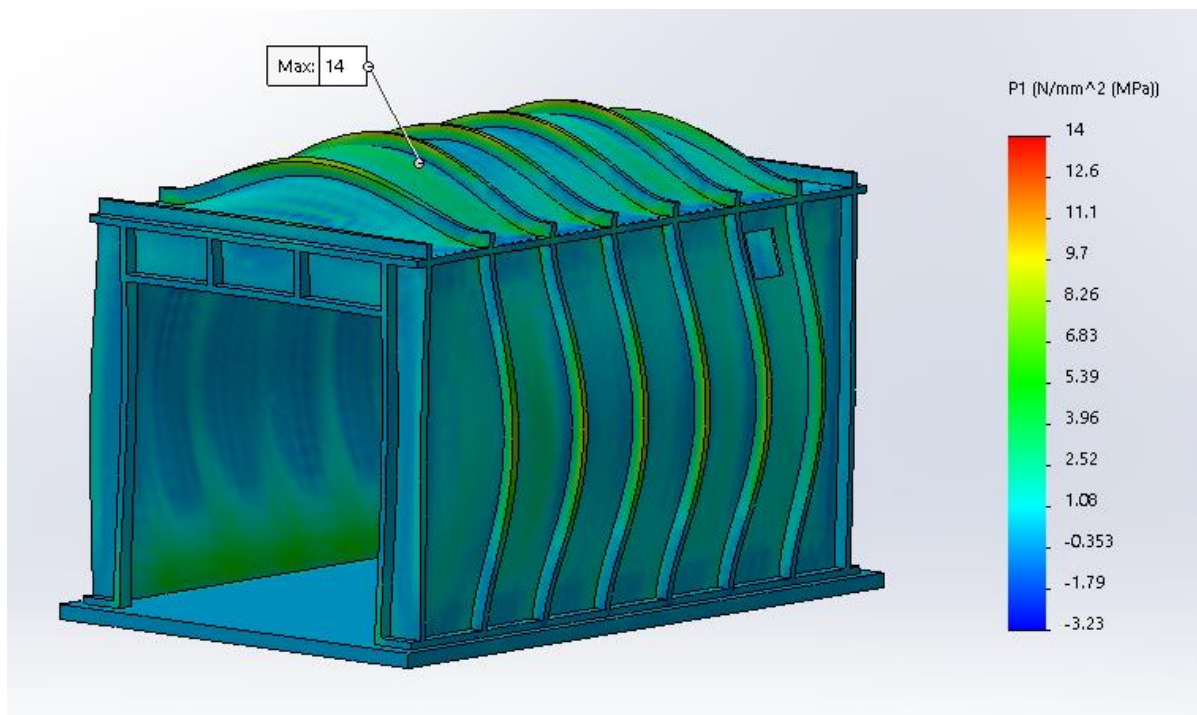


Figure 66 First principle stress

The third principle stress reaches a total of 16.3 MPa, 77.6% of the total capacity.
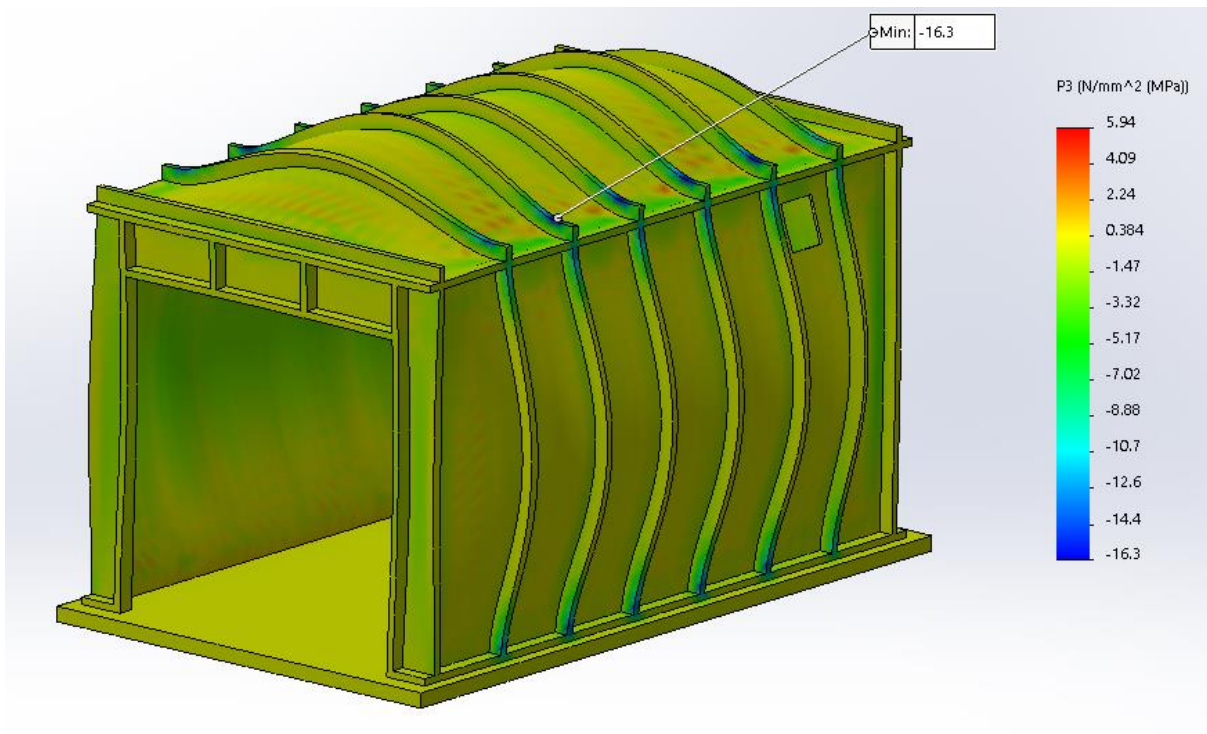


Figure 67 Third principle stress

Solidworks model and simulation is in Appendix N

# 8 Diameter and vent configuration

In an enclosure made for storing hydrogen vehicles the configuration of the vent and the diameter of the TPRD, are crucial parts of the safety during an unscheduled release. The enclosure needs sufficient venting in order to decrease the pressure build-up from the release. Furthermore, if an ignition source is present, the vent will decrease the overall pressure generated by the ignition of the hydrogen-air cloud. Therefore, adequate vent is an important part of the safety measures needed when making a garage to house a hydrogen-driven car.

The diameter of the TPRD needs to be sufficiently small to limit the mass flow out of the hydrogen vessel. Adequate TPRD is essential to limit max overpressure that may occur during hydrogen tank blowdown.

Brennan et. Al present acceptable PRD diameter which ensures acceptable unignited overpressure in a garage with a range of different volumes. The threshold limit in this study is a value of 20 kPa. Calculations of safe PRD diameter is based on storage tanks with capacities of 1, 5 and 13kg hydrogen and pressures at 350 and 700 bar. Decreasing PRD diameter will increase blow-down time thus result in lower overpressure. Sufficient vent size can then be found for safe blow-down of PRD's. [55]

Nomograms present the relationship between the volume, PRD diameter and ACH. ACH, being the air change per hour describing the volumetric air flow. The study uses ACH values of 0.03, 0.18, 0.3, 0.54, and 1. ACH values of 0.03 being extremely conservative, 0.18 will in this study be more representative. Using Bernoulli's equation, the volumetric rate is calculated as shown below, where the discharge coefficient is C=0.6, density is assumed to be 0.09 kg/m$^3$, and delta P is 50 Pa. [55]

$$ACH = \frac{Q_{hr}}{V} = \frac{Q_s * 3600}{V}$$

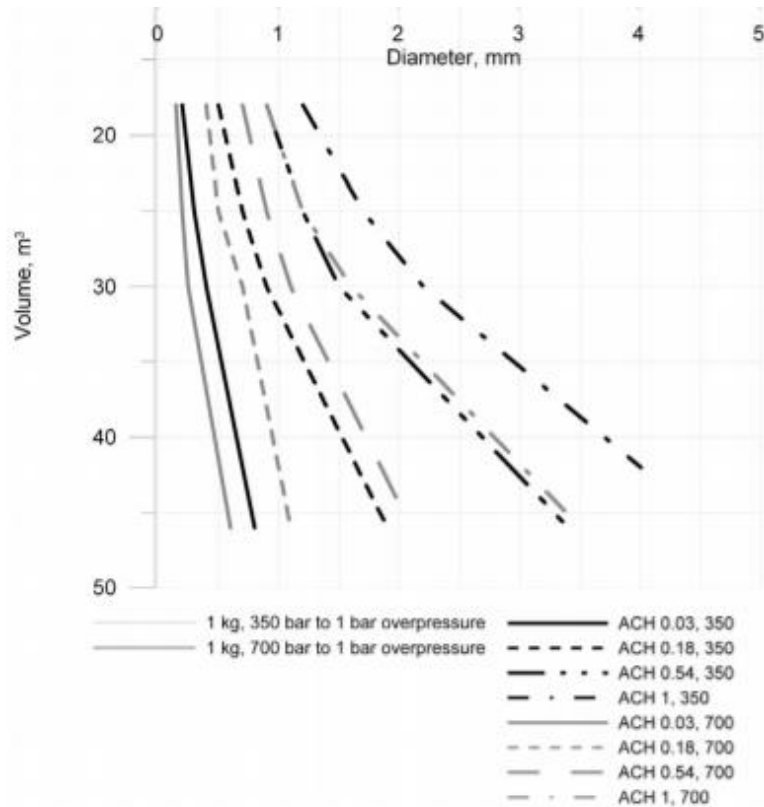$$Q_s = C * A \sqrt{\frac{2 * \Delta P}{\rho}}$$

Figure 68 Nomogram for 1 kg release, 350 and 700 bar [55]

At 700 bar, 1 kg hydrogen blow-down of ACH 0.18 will have a safe PRD diameter of about 0.75mm, considering the threshold limit of 20 kPa. ACH 0.18 is equivalent to vent size 0.000273 $m^2$ at 30 $m^3$ enclosure. When using the same properties as listed above in the MATLAB simulation displayed in chapter 6, max overpressure reaches 19.6 kPa. Taking in consideration the difference in discharge rate, as well as the fact that the study assumes constant mass flow, the values are quite similar for 1 kg hydrogen. [55]

To configure safe TPRD and vent size, the pressure threshold defined in the structural analysis for both the leca and wooden garage is compared with the overpressure results achieved by the MATLAB simulations. Both for unignited and ignited release.
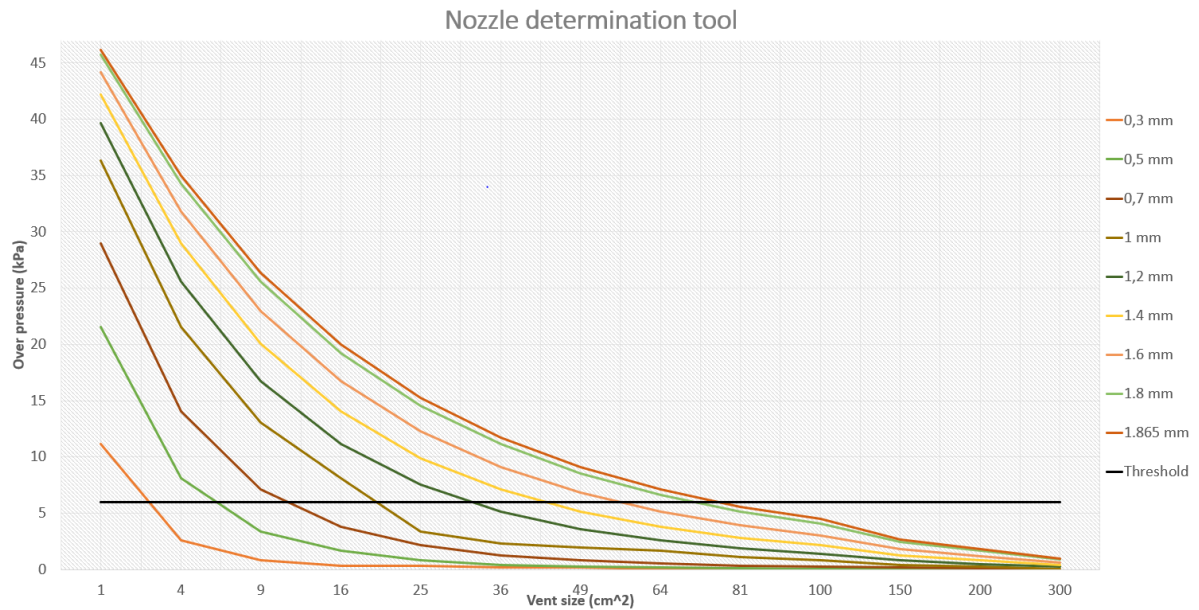
# 8.1 Leca garage



Figure 69 Unignited - 6 kPa threshold

Table 17 Leca garage unignited release results

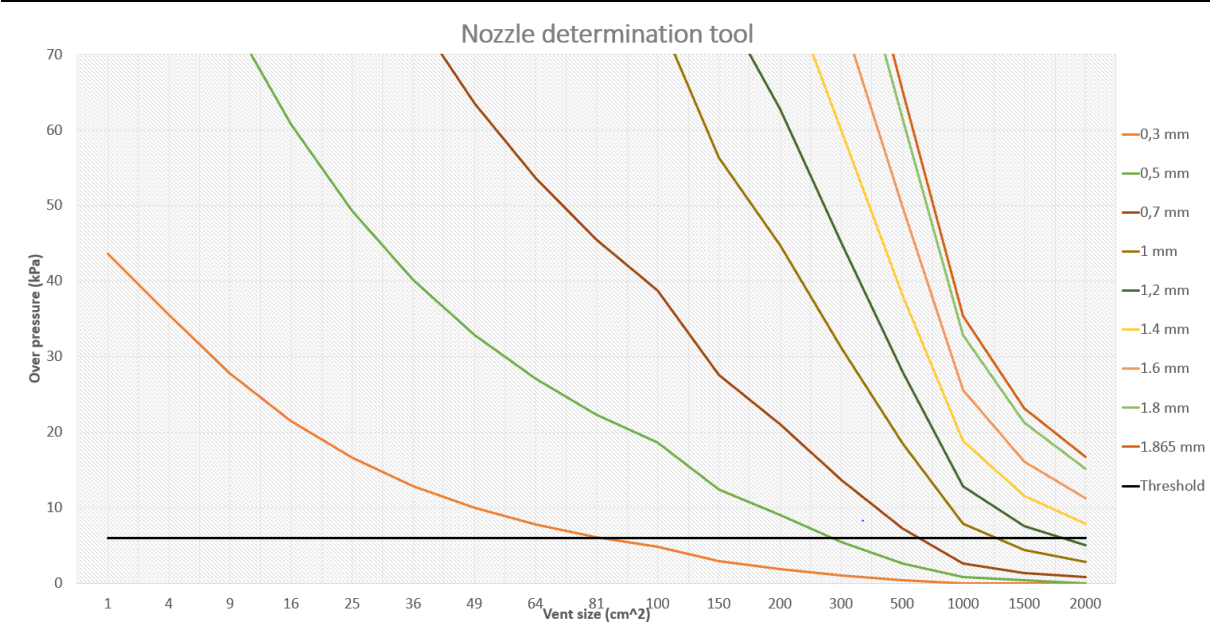| TPRD diameter (mm): | Lowest allowable vent size (cm$^2$): |
|:---:|:---:|
| 0.3 | 4 |
| 0.5 | 9 |
| 0.7 | 16 |
| 1 | 25 |
| 1.2 | 36 |
| 1.4 | 49 |
| 1.6 | 64 |
| 1.8 | 81 |

Figure 70 Ignited - 6 kPa threshold

Table 18 Leca garage ignited results

| TPRD diameter (mm): | Lowest allowable vent size (cm$^2$): |
|---|---|
| 0.3 | 100 |
| 0.5 | 300 |
| 0.7 | 1000 |
| 1 | 1500 |
| 1.2 | 2000 |
| 1.4 | 2500 |
| 1.6 | 3200 |
| 1.8 | 4200 |

When building a garage using leca masonry a vent would normally be a whole leca block or part of one. From the graphs above one can determine the vent size needed for both an unignited- and ignited release. The type of leca block used in the Solidworks simulation would create a vent equal to 1230.06 cm$^2$ if one were to be removed. This would be a vastly oversized vent in terms of overpressures linked to a release. As seen in the graphs above a vent size below 100 cm$^2$ would be sufficient using a TPRD with 0.3 mm diameter in both cases. A vent size of 615.03 cm$^2$ (half a leca block) is an ideal size. This allows the use of TPRD diameters up to 0.7 mm without exceeding the overpressure threshold.

## 8.2 Wood garage



Figure 71 Unignited - 7.8 kPa threshold

Table 19 Wood garage unignited results

| TPRD diameter (mm): | Lowest allowable vent size ($cm^2$): |
|:---:|:---:|
| 0.3 | 4 |
| 0.5 | 9 |
| 0.7 | 9 |
| 1 | 25 |
| 1.2 | 25 |
| 1.4 | 36 |
| 1.6 | 49 |
| 1.8 | 64 |

Given the results above, unignited release will most likely not propose any structural damage to a wooden garage as long as the vent size is of at least 81 $cm^2$.
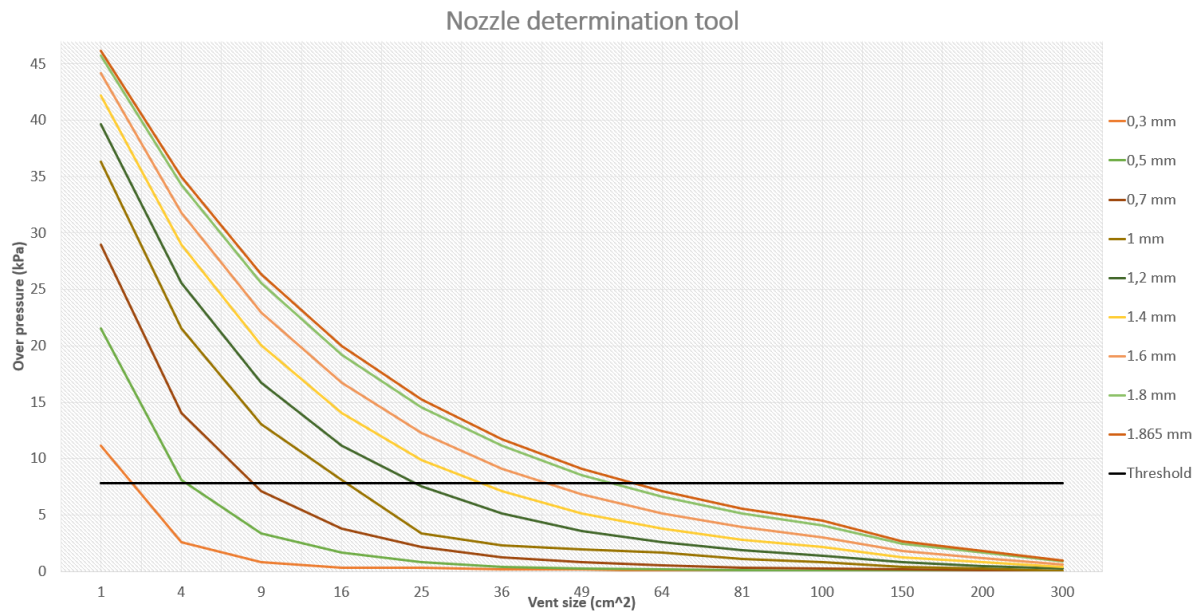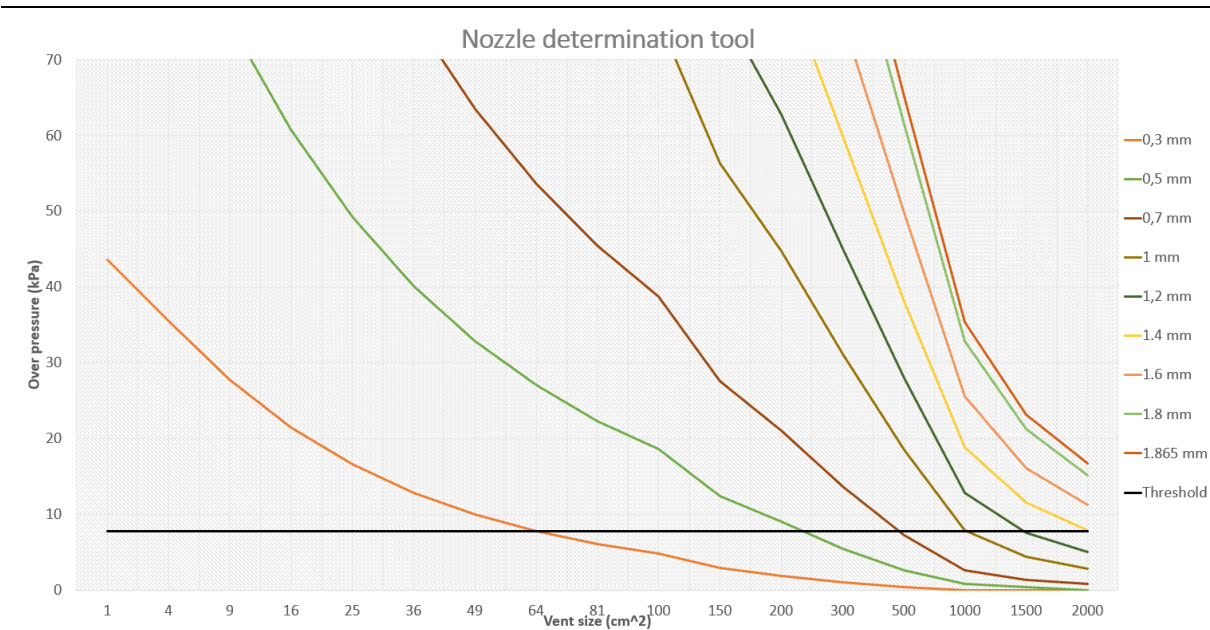
Figure 72 Ignited - 7.8 kPa threshold

Table 20 Wood garage ignited results

| TPRD diameter (mm): | Lowest allowable vent size (cm$^2$): |
|---|---|
| 0.3 | 81 |
| 0.5 | 300 |
| 0.7 | 500 |
| 1 | 1500 |
| 1.2 | 1500 |
| 1.4 | 2100 |
| 1.6 | 2700 |
| 1.8 | 3500 |

The results propose a minimum of 81 cm$^2$ ventilation size for 0.3 mm TPRD. The graph also presents the possibility of use up to 0.7 mm TPRD, any bigger diameter TPRD will need unrealistic large ventilation.

According to TEK10, Norwegian garages must have a minimum volume flow of 3 $m^3$/h per $m^2$ gross area. The garage of 30.42 $m^3$ will then have a necessary ventilation mass flow of 35.1 $m^3$/h. Using the same ACH method presented by Brennan et al. must the vent be minimum of 17.9 $cm^2$. [56] Anything larger than 1000 $cm^2$ will not be a realistic ventilation size in a residential garage. With the upper and lower vent size limit, the results can be narrowed down to the conclusion that TPRD diameter shall not be greater than 0.7mm. Furthermore, with a general safety factor of 2, the combination of vent size and TPRD diameter is displayed below:

Table 21 Final configuration

| TPRD diameter (mm): | Lowest allowable vent size ($cm^2$): | |
| --- | --- | --- |
| | Leca | Wood |
| 0.3 | 150 | 120 |
| 0.5 | 465 | 380 |
| 0.7 | 950 | 790 |

## 8.3 Vent shape and placement

It is worth mentioning that due to extreme buoyancy of hydrogen gas, placement and shape of vent play a big factor in lowering hydrogen concentration to under LFL.

Hajji et al. present a numerical simulation of natural ventilation in a residential garage. Using the software FLUENT, influence of ventilation positioning and vent shape was studied to prevent accumulation of hydrogen. The study first demonstrates the effect of vent positioning running three different simulations with a bottom, middle and top vent. Logically hydrogen will be very buoyant due to low density. The bottom vent was therefore not suitable as stratifications of hydrogen was formed in three layers, where the upper layer has the highest hydrogen concentration. [57]

The study illustrates that if the vent is located higher, the stratification layers decrease thus resulting in a more homogenous mixture as well as lower hydrogen concentration. The shape will also have influence on the hydrogen concentration. Simulation of vents located near the ceiling with circular, triangular, rectangular, and square shapes prove that simple geometries such as square and rectangular are more adaptable. The triangular geometry caused the highest hydrogen concentration, overall about 32% higher than the square vent. [57]

# 9 Conclusion

This bachelor thesis presents the necessary precautions taken when executing an experiment. Support systems of the components have been designed and cooperation with Swagelok has allowed for a final experimental layout for safe hydrogen operation.

With the ASTM G-124 method it is possible to calculate approximately the number of purges required, knowing the final concentration of air and the pressure at which the purge will be performed. With the study carried out to know the conditions inside the tank during the purge, on one hand, it is possible to verify the importance of taking an adequate control volume, which includes the tank walls. On the other hand, with the excel program, it is possible to know what the temperature inside the tank will be based on the pressure, the external conditions, and the mass inflow. The conclusion is therefore that it is possible to purge at 10 bar in 4 cycles in a completely safe way.

After purging the tank, proceed to fill it with hydrogen. The main difference with other studies previously done is that the initial pressure of the tank will be 1 bar instead of 50 or 100 bar. In addition, the working pressure limit is 720 bar. Taking all this into account, in addition to the safety limitations imposed by the tank design itself, it has been seen that multiple filling and cooling stages are necessary. Taking the time necessary to carry out this process up to 5 hours to fill the tank to 98.5%.

This bachelor thesis proves the importance of adequate vent size, as this may lower risk to structural damage substantially. MATLAB simulations and structural analysis has been the foundation of the final configuration considered to be safe.

In the simulations done in this report the leca garage made with 150 mm blocks will not have the mechanical strength to withstand the pressure generated. Even though more investigation needs to be done for the structural analysis, the results in this report shows that a leca garage with 150 mm blocks is not ideal to house hydrogen vehicles. It would be more beneficial and safer to use 300 mm blocks with reinforcement in every joint. This would make the structure stronger and able to withstand more pressure.

From the results of the structural analysis, it is clear that a wooden residential garage may be a stronger alternative when storing hydrogen fuelled vehicles. Wooden garage will likely experience failure to nail constructions before the structural frame is affected. The flexibility of wood also reduces the risk of structural collapse, where the porosity of leca may be a problem. Considering the simple design of the wood garage in the report, will likely most garages of this kind withstand hydrogen release. Provided that the safe vent and nozzle configuration is respected.

It is clear that a hydrogen release in a garage enclosure poses great risk of structural damage. If hydrogen vehicles are to be stored in these kinds of enclosures, new standards of building material, vent sizes and TPRD must be implemented. Further study of the structural response must be carried out in order to give better advice considering building standards of garages that will house hydrogen vehicles.

# 10 Further work

This bachelor thesis bases its primary results of vent size configuration on the results from the structural analysis. The threshold given from the structural analysis defines the strength limit of such residential garages. To further verify the credibility of the results from the structural analysis, experiment should be performed defining the accuracy of the finite element method in such cases.

An attempt was made to find the correct diameter and vent size configuration for a given overpressure and enclosure volume. This bachelor thesis does not consider the temperatures that arise in the enclosure. It is clear that ignited release results in great overpressures which leads to increase in temperature. Further work should include the effect of hydrogen jet fires on structural integrity as well as autoignition of materials such as wood.

Hydrogen concentration should also be taken into account when a vent and diameter configuration is defined. A reduced nozzle diameter which guarantee hydrogen concentration below LFL during release will exclude the possibility of ignition. Such nozzle diameter as well as adequate garage volume should be found to satisfy this criterion.

In the thesis, the pressure loss in the system and the tank filling process have been calculated. Unfortunately, it has not been possible to combine the two results to reach a unified conclusion. It would be interesting to carry out more work trying to find out the increase in stages in the filling process that this loss of pressure would entail, maintaining the same filling percentage. Moreover, during the experiment verification of the temperatures and pressure during filling using thermocouples and pressure gauges to check the accuracy of the method.

# 11 **References**

[1]     EERE Energy efficiency and renewable energy, "energy.gov," Desember 2001.
        [Online]. Available:
        https://www1.eere.energy.gov/hydrogenandfuelcells/tech_validation/pdfs/fcm01r0.pdf.
        [Accessed 3 April 2020].

[2]     A. Zuttel, "Materials for hydrogen storage," *Materialstoday,* pp. 24-33, September
        2003.

[3]     HyTunnel, "Report on hydrogen hazards and risks in tunnels and similar confined
        spaces," HyTunnel, 2019.

[4]     V. Molkov, Fundamentals of Hydrogen Safety Engineering I, Bookboon.com, 2012.

[5]     "Princtermo," [Online]. Available:
        https://sites.google.com/site/princtermo/Home/primera-ley/tablagases.

[6]     "elementos.org," [Online]. Available: https://elementos.org.es/hidrogeno.

[7]     H. Hussein, S. Brennan, V. Shentsov, D. Makarov and V. Molkov, "Numerical
        validation of pressure peaking from an ignited hydrogen release in a labratory-scale
        enclosure and application to a garage scenario," *International Journal of Hydrogen
        Energy,* pp. 17954-17968, 30 April 2018.

[8]     S. Brennan, H. G. Hussein, D. Makarov, V. Shentsov and V. Molkov, "Pressure effects
        of an ignited release from onboard storage in a garage with a single vent,"
        *International Journal of Hydrogen Energy,* pp. 8927-8934, 9 March 2019.

[9]     D. A. Crowl, Chemical process safety, Boston: Pearson, 2019.

[10]    V. Shentsov, M. Kuznetsov and V. Molkov, "The Pressure Peaking Phenomenon:
        Validation for unginited release in laboratory-scale enclosure".*Hydrogen Safety
        Engineering and Research Center (HySAFER).*

[11]    Emerson, "Coriolis flow meters," 2020. [Online]. Available:
        https://www.emerson.com/en-us/automation/measurement-instrumentation/flow-
        measurement/coriolis-flow-meters?fbclid=IwAR2N4uZnjMYuK3hdJDbrJ-
        eS45dcK1nc4gjWQBCH8s0AOxvmg4bhp5OyftE.

[12]    Reinforced Plastics, "Hexagon develops hydrogen cylinder for new Mercedes-Benz,"
        *Reinforced Plastics,* no. 6, p. 340, 2016.

[13]    G. D. S. M. B. A. H. M. Raymond G. Hart MD. MPH, "Prevention of high-pressure
        injection injuries to the hand," Elsevier, Louisville, 2005.

[14]    D. K. H. S. S. H. Toshi Mogi, "Self-ignition and explosion during discharge of high-
        pressure hydrogen," Elsevier, Tsukuba, 2007.

[15] H. X. W. G. Q. W. X. S. L. J. J. S. Qiangling Duan, "An experimental study on shock waves and spontaneous ignition produced by pressurized hydrogen release through a subi into atmosphere," Elsevier, Hefei, 2015.

[16] ICSC Inchem, "Inchem.org," 2014. [Online]. Available: http://www.inchem.org/documents/icsc/icsc/eics0001.htm. [Accessed 12 Mars 2020].

[17] V. Molkov, "Hydrogen jet flames," *International journal of hydrogen energy,* pp. 8141-8158, 2013.

[18] Emerson, "Emerson.com," [Online]. Available: https://www.emerson.com/en-us/automation/measurement-instrumentation/flow-measurement/coriolis-flow-meters. [Accessed 9 Febrero 2020].

[19] airconspares, "airconspares.com," [Online]. Available: https://www.airconspares.com/rubber-lined-pipe-clamp. [Accessed 9 February 2020].

[20] boschrexroth, "boschrexroth.com," [Online]. Available: boschrexroth.com/en/xc/products/product-groups/assembly-technology/basic-mechanic-elements/connection-elements/flange-nut-t-bolt#. [Accessed 9 February 2020].

[21] I. Ø. Bo Lundkvist, Maskin Tegning, Oslo: Gyldendal, 2012.

[22] Y. M. Gordon Rogers, Engineering Thermodynamics Work and heat transfer, Harlow: Pearson education , 1992.

[23] R. T. a. D. F. O.C. Zienkiewicz, The finite element method for solid and structural mechanics, Kidlingtod, Oxford: Elsevier Ltd, 2014.

[24] G. R. K. Jr., "Properly Purge and inert storage vessels," *Chemical Engineering Progress,* pp. 57-61, februar 2001.

[25] AGMcontainer, "agmcontainer .com," [Online]. Available: https://www.agmcontainer.com/blog/neps/nitrogen-purging-theory/. [Accessed 3 April 2020].

[26] K. E. D. S. E. Robbins, "Verification of the ASTM G-124 Purge equation," in *Twelfth International Symposium on Flammability and Sensitivity of Materials in Oxygen Enriched Atmospheres*, berlin, NASA Marshall Space Flight Center, 2009.

[27] P. B. R. C. Jinsheng Xiao, "Estimation of final hydrogen temperature from refueling parameters," *International journal of hydrogen energy ,* no. 47, pp. 7521-7528, 2017.

[28] D. A.Chin, "Conservation of energy," in *Fluid Mechanics for engineers*, Pearson, pp. 307-322.

[29] D. A. Chin, "Conservation of mass," in *Fluid Mechanics for Engineers*.

[30] "engineering toolbox," [Online]. Available: https://www.engineeringtoolbox.com/nitrogen-N2-thermal-conductivity-temperature-pressure-d_2084.html.

[31] U. o. Cambridge, "doitpoms," [Online]. Available: https://www.doitpoms.ac.uk/tlplib/bones/derivation_mixture_rules.php. [Accessed 11 April 2020].

[32] D. H. J.-C. G. S. V. F. N. Juan Pedro Berro Ramirez, "700 bar type IV high pressure hydrogen storage vessel burst - Simulation and experimental validation," *International journal of hydrogen energy,* no. 40, pp. 13183-13192, 2015.

[33] D. Roylance, "web.mit.edu," 24 March 2000. [Online]. Available: http://web.mit.edu/course/3/3.11/www/modules/composites.pdf. [Accessed April 13 2020].

[34] H. N. S. Michael J. Moran, "ENERGY AND THE FIRST PRINCIPLE OF THERMODYNAMICS," in *Fundamentals of Engineering Thermodynamics*, REVERTE, 2004, pp. 68-70.

[35] B. M. Ronald Joven, "Thermal properties of autoclave and out-of-autoclave carbon fiber-epoxy composites with different fiber weave configurations," *Journal of composite materials,* vol. 52, pp. 4075-4085, 2018.

[36] "https://ctherm.com/," [Online]. Available: https://ctherm.com/products/tci_thermal_conductivity/helpful_links_tools/thermal_resistance_thermal_conductance/lang/es/. [Accessed 24 March 2020].

[37] T. H. R. A. H.S. Roh, "Optimization of carbon fiber usage in Type 4 hydrogen storage tanks for fuel cell automobiles," *International journal of hydrogen energy,* no. 38, pp. 12795-12802, 2013.

[38] R. D. A. A. P. R. B. M. R. Joven, "researchgate.net," 28 June 2015. [Online]. Available: https://www.researchgate.net/publication/262007032_Thermal_properties_of_carbon_fiberepoxy_composites_with_different_fabric_weaves. [Accessed 13 April 2020].

[39] W. M. C.J.B. Dicken, "Measured effects of filling time and initial mass on the temperature distribution within a hydrogen cylinder during refuelling," *Journal of power sources,* no. 165, pp. 324-336, 2007.

[40] J. F. S. J. A. E. V. G. A. T. G. M. A. C. Fco. Javier Rey Martínez, Ingeniería Térmica, Valladolid.

[41] T. B. F. B. F. A. D. B. D. M. B. A.-I. D. Z. D. S. D. L. T. Bourgeois, "Optimization of hydrogen vehicle refuelling requirements," *International journal of hydrogen energy,* no. 42, pp. 13789-13809, 2017.

[42] M. M. a. T. S. Md. Tawhidul Islam Khan, "Hydrogen Gas Filling into an Actual Tank at High Pressure and Optimization of its thermal Characteristics," *Journal of Thermal Science,* vol. 18, no. 3, pp. 235-240, 2009.

[43] "PennState college of enegine," [Online]. Available:
https://www.me.psu.edu/cimbala/me433/Links/Table_A_9_CC_Properties_of_Air.pdf.
[Accessed 1 May 2020].

[44] A. T. Eloy Velasco, "Leccion02 Conveccion," in *Apuntes curso ingeniería térmica Universidad de Valladolid*, 2018.

[45] F. F. John C. Dixon Ph.D., "Appendix B," in *The Shock Absorber Handbook*, John Wiley & Sons, 2007.

[46] M. D. M. V. Brennan S, "Dynamics of flammable hydrogen-air mixture formation in an enclosure with single vent," *Proceedings of the Sixth International Seminar on Fire and Explosion Hazards,* pp. 493-503, 1 July 2011.

[47] I. Buckland, "Explosion of gas layers in a room size chamber," *I. Chem. E. Symposium Series No. 58,* pp. 289-304, 1980.

[48] Leca International, "Who are we?," Leca International, 2020. [Online]. Available:
https://www.leca.com/#sustainability. [Accessed 18 04 2020].

[49] Leca Norge AS, "Kapittel 7 - Dimensjonering," in *Leca Teknisk Håndbok*, Rælingen, Leca Norge AS, 2018, p. 56.

[50] T. Kvande, "Investigations of some Material Properties for Stuctural Analysis of LECA Masonry," Tore Kvande ved NTNU, Trondheim, 2001.

[51] Leca Norge AS, "Kapittel 4 - Prosjektering og utførelse av Leca murverk," in *Leca Teknisk Håndbok*, Nordby, Leca Norge AS, 2018, pp. 28-56.

[52] E. S. T. Audun Øvrum, "treteknisk.no," september 2007. [Online]. Available:
http://www.treteknisk.no/resources/filer/publikasjoner/fokus-pa-tre/Fokus-nr-43.pdf.
[Accessed 19 April 2020].

[53] T. Ø. R. Knut Ivar Edvardsen, Trehus, Oslo: SINTEF akademisk forlag, 2015.

[54] Swantec, "Swantec.com," [Online]. Available:
https://www.swantec.com/technology/numerical-simulation/. [Accessed 20 April 2020].

[55] S. Brennan and V. Molkov, "Safety assessment of unignited hydrogen discharge from onboard storage in garages with low level of natural ventilation," *International journal of hydrogen energy,* p. 8159(8), 27 June 2013.

[56] M. M. Sverre Holøs, "Krav til ventilasjon og termisk inneklima i," SINTEF Byggforsk, OSLO, 2016.

[57] Y. Hajji, M. Bouteraa, A. Elcafsi, A. Belghith, P. Bournot and F. Kallel, "Natural ventilation of hydrogen during a leak in a residential garage," *Renewable and Sustainable Energy reviews,* pp. 810-818, 16 April 2015.

[58] Bosch Rexroth, "boschrexroth.com," Engineering products, 27 august 2018. [Online]. Available: https://www.boschrexroth.com/en/xc/products/product-groups/assembly-technology/basic-mechanic-elements/connection-elements/bracket/45-90. [Accessed 9 april 2020].

[59] A. Scott, " Occupational high-pressure injection injuries: Pathogenesis and prevention," in *Occupational high-pressure injection injuries: Pathogenesis and prevention*, 1983, pp. 56-59.

[60] "all3dp," [Online]. Available: https://all3dp.com/2/fused-deposition-modeling-fdm-3d-printing-simply-explained/. [Accessed 10 April 2020].

[61] H. X. W. G. L. G. J. S. Qiangling Duan, "Experimental investigation of spontaneous ignition and flame," Elsevier, Hefei, 2016.

# 12 **Appendices**